



Theses and Dissertations

2023-08-18

Phosphorus Sorption and Kinetics Across the Sediment-Water Interface of Utah Lake, a Shallow Eutrophic Lake

Forrest Fielding Stretch Jarvis Jarvis
Brigham Young University

Follow this and additional works at: <https://scholarsarchive.byu.edu/etd>



Part of the [Physical Sciences and Mathematics Commons](#)

BYU ScholarsArchive Citation

Jarvis, Forrest Fielding Stretch Jarvis, "Phosphorus Sorption and Kinetics Across the Sediment-Water Interface of Utah Lake, a Shallow Eutrophic Lake" (2023). *Theses and Dissertations*. 10499.
<https://scholarsarchive.byu.edu/etd/10499>

This Thesis is brought to you for free and open access by BYU ScholarsArchive. It has been accepted for inclusion in Theses and Dissertations by an authorized administrator of BYU ScholarsArchive. For more information, please contact ellen_amatangelo@byu.edu.

Phosphorus Sorption and Kinetics Across the Sediment-Water Interface of Utah Lake,
a Shallow Eutrophic Lake

Forrest Fielding Streh Jarvis

A thesis submitted to the faculty of
Brigham Young University
in partial fulfillment of the requirements for the degree of
Master of Science

Joshua J. LeMonte, Chair
Gregory T. Carling
Zachary Aanderud
Barry R. Bickmore
Stephen Tracy Nelson

Department of Geological Sciences
Brigham Young University

Copyright © 2023 Forrest Fielding Streh Jarvis
All Rights Reserved

ABSTRACT

Phosphorus Sorption and Kinetics Across the Sediment-Water Interface of Utah Lake, a Shallow Eutrophic Lake

Forrest Fielding Streh Jarvis
Department of Geological Sciences, BYU
Master of Science

Internal sediment phosphorus (P) cycling may regulate harmful algal blooms (HABs) in shallow eutrophic lakes. Utah Lake frequently experiences HABs despite its high alkalinity and P-rich sediment. Phosphorus cycling between the lakebed and the water column is dependent upon stable P-sorption with organic matter (OM) and mineral species, which can vary with substrate availability, P-concentrations, temperature, redox, pH, and microbial activity. A full biogeochemical analysis of the water and sediment across seven sites shows Utah Lake to be spatially well-mixed in terms of composition and sorption, with few exceptions. Sediment P-concentrations (avg. 677 mg-P kg^{-1}) primarily correlate with redox-sensitive iron (avg. $9403 \text{ mg-Fe kg}^{-1}$) and manganese (avg. $295 \text{ mg-Mn kg}^{-1}$) compounds (avg. 13.9%-Total P) and carbonate minerals (avg. 62.6%-Total P). Sorption experiments conducted with sediment from across Utah Lake reveal that as pH increases the favorability of P-sorption also increases, while the maximum number of available P-binding sites decreases. Kinetics experiments highlight nonlinear retention of P and demonstrate how sediments depleted of P generate faster retention rates and initiate early sorption during low aqueous P-concentrations. Ultimately, Utah Lake is a natural system existing in dynamic equilibrium; change one factor, and the lake will respond to maintain its state. Nevertheless, anthropogenic activities can still negatively impact the lake if left unchecked, as we have seen in the past.

Keywords: Utah Lake, phosphorus, cycling, retention, release, binding, sorption, kinetics, batch, stirred-flow, eutrophic, linear, Freundlich, Langmuir, sequential extraction, sediment, partitioning, HABs, mineralogy, carbonate, redox, pH, geochemistry, sediment geochemistry

ACKNOWLEDGMENTS

This research comes through the advisement of trusted professors and the assistance of students belonging to the Environmental Geochemistry Lab. I am grateful for the guidance of my advisor, Dr. Joshua LeMonte, and committee members, doctors Gregory Carling, Zachary Aanderud, Barry Bickmore, and Stephen Nelson. I have immense gratitude for the help of my fellow students, Abidemi Aremu, Adam Norris, Audrey Hughes, Alan Ketring, Austen Lambert, Kara Hunter, Kate Hales, Maliea Holden, Lindy Miller, Mahina Pieno, Mardell Overson, Meagan Boden, Rachel Wilmore, Sierra Stewart, and Shu-yu Chen in completing large-scale laboratory experiments. The acquisition and analysis of thousands of samples without the consistent instruction of Kevin Rey and David Tingey would be impossible. The funds provided by the Department of Geological Sciences at Brigham Young University and the Utah Division of Water Quality (DWQ) have made this research possible. I also want to acknowledge the original heritage of the land where this study was conducted. The lake residues within the indigenous region of the Noochew, commonly known as Ute, people. Finally, I want to thank family. I am grateful for my spouse, Margaret Jarvis, for her continual support and upliftment. I am grateful for my son, Sasha, for his smile and cheery attitude, both of which are very contagious.

TABLE OF CONTENTS

TITLE PAGE.....	i
ABSTRACT	ii
ACKNOWLEDGMENTS.....	iii
TABLE OF CONTENTS	iv
LIST OF TABLES.....	vi
LIST OF FIGURES	vii
1.Introduction.....	1
2. Material and Methods.....	2
2.1 Site Description.....	3
2.2 Field Sampling	4
2.3 Sediment Characterization	5
2.3.1 HCl Digestion of Carbonates	5
2.3.2 NaOCl Digestion of Organic Matter.....	7
2.3.3 Particle Size Distribution	8
2.3.4 Minerals by X-ray Diffraction.....	9
2.3.5 Elements by Acid-digestion	10
2.3.6 Sequential Extractions of Phosphorus	10
2.3.7 DNA Extractions	13
2.4 Water Column Characterization.....	14
2.4.1 Isotopes by Los Gatos Research Liquid Water Isotope Analyzer.....	14
2.4.2 Elements by Inductively Coupled Plasma Optical Emission Spectroscopy	15
2.4.3 Water Quality Parameters Obtained with Utah Lake Data Explorer.....	15
2.5 Sorption Experiments	15
2.6 Kinetics Experiments.....	19
3. Results and Discussion	21
3.1 Sediment Composition	21
3.1.1 Carbonates and Organic Matter.....	21
3.1.2 Particle Size Fractionation	21
3.1.3 Mineralogy	22
3.1.4 Major Elements	24
3.1.5 Phosphorus Fractionation.....	25
3.1.6 Microbiome	28

3.2 Water Column Composition	28
3.2.1 Hydrogen and Oxygen Isotopes	28
3.2.2 Vertical and Horizontal Mixing.....	30
3.2.3 Nutrients and Organics	30
3.3 Sorption Isotherms Fit by Linear, Freundlich, and Langmuir Models.....	31
3.3.1 Y- and X-intercepts.....	31
3.3.2 Partition Coefficients	32
3.3.3 Sorption Maximums and Freundlich Correction Factors.....	34
3.3.4 Impacts of UV-treatment on Partitioning.....	35
3.4 Nonlinear Kinetic Retention Models.....	36
4. Conclusion	37
REFERENCES	41
APPENDIX	48
Tables	48
Figures	53

LIST OF TABLES

Table 1. Physiochemical properties of Utah Lake sediments.....	48
Table 2. Sequential P-fractionation percentages for Utah Lake sediments.....	49
Table 3. Physiochemical properties of Utah Lake column waters	50
Table 4. Coefficient values from Linear, Freundlich, and Langmuir sorption models.....	51
Table 5. Parameters and coefficients for stirred-flow experiments using Utah Lake sediments ..	52

LIST OF FIGURES

Figure 1. A map of Utah Lake showing the location of seven sampling sites	53
Figure 2. A schematic example of a batch sorption isotherm experiment.....	53
Figure 3. Schematic depiction of stirred-flow reaction chamber.....	54
Figure 4. Sediment carbonate and organic matter percentages	54
Figure 5. Particle size distributions across the various locations within Utah Lake	55
Figure 6. Mineral fractions across seven sites in Utah Lake.....	55
Figure 7. Chemical compositions of sediment by acid-digestion.....	56
Figure 8. Sequential P-fractions of Utah Lake sediment	56
Figure 9. Sequences obtained from DNA extractions from lakebed sediments.....	57
Figure 10. A plot of $\delta^2\text{H}$ vs. $\delta^{18}\text{O}$ values from Utah Lake surface waters	58
Figure 11. Average concentrations of P across water depth in Utah Lake	58
Figure 12. Average concentrations of organic compounds in column waters in Utah Lake	59
Figure 13. A plot of Q vs. C_f obtained from a batch sorption isotherm experiment.....	60
Figure 14. Average X, or sorption origin, for each site in Utah Lake	61
Figure 15. Site focused trends of $K_{d,f,l}$ from Linear, Freundlich, and Langmuir models	62
Figure 16. pH focused trends of $K_{d,f,l}$ from Linear, Freundlich, and Langmuir models.....	63
Figure 17. Site focused trends of n and S_{max} from Freundlich and Langmuir models.....	64
Figure 18. pH focused trends of n and S_{max} from Freundlich and Langmuir models.....	65
Figure 19. Site focused trends of $b_{d,f,l}$ from Linear, Freundlich, and Langmuir models.....	66
Figure 20. pH focused trends of $b_{d,f,l}$ from Linear, Freundlich, and Langmuir models.....	67
Figure 21. Changes in $K_{d,f,l}$ following sediment UV-treatment	68
Figure 22. Changes in n and S_{max} following sediment UV-treatment.....	69

Figure 23. Changes in output solution and P-sorption from stirred-flow experiments.....70

Figure 24. Nonlinear retention behavior from stirred-flow experiments.....71

1. Introduction

Internal sediment phosphorus (P) cycling may regulate harmful algal blooms (HABs) in eutrophic lakes. Fueled by nitrogen (N) and P, HABs produce elevated toxins and bacterial growth in water inducing human sickness when consumed (Li et al. 2017). Lakes regulate the amount of bioavailable P within the water column via microbial activity and sorption processes mediated at the sediment-water interface. Microbial activity and sorption processes remove P from the water column, binding P with organic matter (OM) and minerals that deposit on the lakebed (Nowlin et al. 2005). Lakebed sediment P-retention requires stable P-sorption, which can vary with microbial community, substrate availability, and OM grade (Richardson 1985, Reddy et al. 1999, and Adam 2016). Physical, chemical, and biological mechanisms can affect P-release from sediments in lakes. Wave action, boat propellers, and bottom-dwelling fish can significantly drive internal P-release in shallow lakes through re-suspension of sediment (Søndergaard et al. 2013). Changes in pH, temperature, ionic strength, and redox can promote the dissolution of P-retaining minerals or increase diffusion (Moore et al. 1994). Microbes can produce organic acids and metabolize sediment-bound P, which can mobilize P into the water column (Boström et al. 1988). Consequently, lakes that retain elevated levels of P within sediment may experience delayed recovery from remediation efforts (Jeppesen et al. 2015).

Utah Lake is a shallow eutrophic lake that frequently experiences HABs despite its high alkalinity and P-affable sediment. Utah Lake sediments maintain substantial P-concentrations ($> 600 \text{ mg-P kg}^{-1}$), but the influences of sediment P on eutrophication remain unclear (Ogdahl et al. 2014). Studies show that Utah Lake is a well-buffered system with spatially variable sediment and P-loading (Smithson et al. 2020 and Taggart et al. 2021). Phosphorus fractionates mostly with OM, calcite, and iron-hydroxides in the lakebed, helping Utah Lake retain 90% of external

P-loading (Abu-Hmeidan et al. 2018 and Randall et al. 2019). Fluxes of P from sediment, measured in situ, estimate that as much as 1,500 tons of P cycle between the lakebed and water column of Utah Lake per year (Hogsett et al. 2019). Nevertheless, the strength of P-binding to certain minerals, P-partitioning among available sorbents, kinetic rates of P-retention, or the exact parameters surrounding sediment P-cycling in the lake are unknown.

The environmental health of Utah Lake affects the inhabitants of Utah County and the surrounding areas. Without proper stewardship, HABs will continue to impact Utah Lake, which could place increased stress on the limited available water in this semi-arid region. Moreover, extreme seasonal temperature shifts brought on by climate change might increase the likelihood of HABs into the future, especially during the summer. The Utah Division of Water Quality (DWQ) plans to model P-cycling in Utah Lake, thereby promoting proper lake management and helping preserve the lake for years to come. The purpose of this study is to identify, quantify, and parameterize components of P-sorption to create a mechanistic approach for internal P-cycling inside Utah Lake. Specific objectives are to (1) perform a full biogeochemical analysis of sediment and water collected from seven sites across the lake; (2) identify major constituents and mechanisms of P-sorption within sediment; (3) evaluate environmental conditions affecting P-sequestration; (4) quantify spatial variations in P-partitioning and capacities over a range of pH using batch sorption isotherm (sorption) experiments; and (5) scope P-retention kinetics of sediments via kinetics experiments. Our findings will guide the decisions of DWQ when it comes to HABs prevention and lake regulations, including the Utah Lake Water Quality Model, WWTP improvement projects, private development regulations, and sediment remediation approaches.

2. Material and Methods

2.1 Site Description

Utah Lake (Figure 1) is one of the largest natural freshwater lakes west of the Mississippi River (PSOMAS 2007). Residing in the state of Utah near the eastern edge of the Basin and Range Province, Utah Lake sits directly west of the Wasatch Range, directly east of the Lake Mountains, and approximately 48 km southeast of the Great Salt Lake. The lake covers about 375 km² and is shallow, with an average depth of 2.7-3 m during normal lake levels (PSOMAS 2007). Despite its shallow nature, the lake is a major water resource in the area. Utah Lake is utilized for recreation, seven wastewater treatment plants (WWTPs), and industries. The lake also supplies sensitive ecosystems, like the Great Salt Lake via the Jordan River (Mohammed & Tarboton 2012).

The water that flows into Utah Lake primarily originates in the Wasatch and Uinta mountain ranges as snowmelt. Major inflows deliver melt waters into Utah Lake through groundwater, meteoric precipitation, creeks (Hobble and Currant), and rivers (Provo, Spanish Fork, and American Fork). Together these inputs provide more than 925 million m³ of water per year (Zanazzi et al. 2020). The only major outflows for the lake are the Jordan River, groundwater, and evaporation. Evaporation accounts for 43% of the lake's yearly outflow, creating isotopically enriched waters with a residence time of about six months (Zanazzi et al. 2020). Inherent of saturated evaporative waters, sedimentation is mostly comprised of calcium carbonate precipitation, then silicate minerals, and metal hydroxides, with the total sedimentation rate averaging about 1.4 mm yr⁻¹ (Macharia 2012).

Precipitation of carbonates creates a signature milky appearance in the water of Utah Lake. Furthermore, the lake's turbidity enhances the water's milky appearance. Due to the shallow depth of the lake and its large surface area, wind can easily re-suspend lakebed

sediments to form turbid waters. Consequently, Utah Lake is vertically well-mixed and exhibits no discernible thermocline (Zanazzi et al. 2020).

Reports estimate that the population of Utah County increased by 3.51% from 2020 to 2022 (Albers et al. 2022). If this rate of growth continues, the population surrounding Utah Lake will double in size by 2050, increasing the demand for water in the region. Current nutrient loads from agricultural runoff and WWTPs already put pressure on the lake. External P-loading from anthropogenic pressures has contributed to algae blooms, especially in the late summer or early fall. The longevity of Utah Lake is a debated issue and solutions for algal blooms and invasive species have ranged from all over, including from an artificial island building company. Though far from perfect, the health of the lake has improved immensely over the years, though occasional toxic cyano-blooms are still of concern.

2.2 Field Sampling

To capture the spatially variability of Utah Lake, we collected sediment and water across seven sites (Figure 1). Sites were selected due to their proximity to inlets or the outlet of Utah Lake. Names assigned to the seven sites were chosen based on site proximity to prominent features or surrounding municipalities. Names include Provo Bay (PB), Provo (PV), Vineyard (VY), Goshen Bay (GB), Bird Island (BI), Saratoga Springs (SS), and Pelican Point (PP). Changes in environmental deposition within the lake cause slight variations in temperature, pH, redox, conductivity, P-concentration, and sediment composition, all of which can affect P-sorption.

Surface lakebed sediments, or interface sediments, were collected in August 2021 using an AMS Ekman dredge attached to 15 m of cord. The dredge was lowered from a porthole in the center of the pontoon boat and captured about 1-2 L of saturated sediment from the top few

centimeters of the lakebed (< 10cm depth from lakebed surface). Spread thin (1-2 cm thick) onto trays, these sediments were left to air dry at room temperature (~25°C) for one week. After drying, sediments were lightly ground to pass through a 2 mm mesh sieve and stored at 25°C in 1 L HDPE bottles until analyzed or used in sorption or kinetics experiments.

Water column samples were collected in November 2021 from each site using 6 m of 0.19" silicone tubing threaded through a Masterflex Cole-Parmer (model: 70 15-00) peristaltic pump attached to a Milwaukee M12 hand drill. The pump obtained water from the surface, middle, and bottom of the column (~4 cm, ~1-2 m, and ~3-4 m depth from water surface, respectively), filling a 1 L HDPE bottle for each depth. Additionally, a large volume of surface water was collected from Saratoga Springs site (SS) on May 6, 2022, filling four 26 L HDPE containers. The mass collection of water from SS was used in sorption and kinetics experiments for its low P-concentration (~120 $\mu\text{g-P L}^{-1}$). All water collected was immediately placed within an onboard cooler filled with dry ice and later transferred to a -25°C walk-in freezer. Water temperature, pH, conductivity, and ORP were measured in the field, as well as in the lab using a Mettler Toledo Benchtop multi-probe meter. Stored water samples were saved for characterization analyses and use in sorption or kinetics experiments.

2.3 Sediment Characterization

2.3.1 HCl Digestion of Carbonates

To obtain carbonate percentages, we digested interface sediments using 1 M HCl (Dhillon et al. 2015). Prior to digestion, wet sediments were dried for 24 hours at 105°C within a Brooks Rand Labs wireless hot block placed inside a continuous flow (CF) hood. After drying, samples were removed from the hot block and left to cool in the hood for at least 30 minutes. Dry samples were gently ground using an agate mortar and pestle to pass through 250 μm mesh.

Once ground, 1 g of sediment was obtained from each sample, placed within 50 mL centrifuge tube, and the weight recorded (individual sample mass and mass of sample with tube).

In a fume hood, 1-2 mL of 1 M hydrochloric acid (HCl) were added to the sediment contained within the tube to create a slurry. When effervescence had ceased, we added 1 drop of 1 M HCl to the solution. If effervescence resumed, we added an additional 1 mL of 1 M HCl to the solution and agitated the tube vertically on a shaker table set to 200 rpm for 1 hour. This process of testing and adding HCl to the mixture was concluded when no visible or audible effervescence occurred and the pH of the mixture measured < 7, indicating a total digestion of carbonates. After fully digesting the carbonate in the sample, 5 mL of MilliQ were added to the solution, the tube was capped, and subsequently centrifuged at 2500 rpm for 10 minutes.

Once centrifuged, the supernatant was decanted into a designated 50 mL tube. Then the sample was triple rinsed with MilliQ. A single rinse was performed as follows: 10 mL of MilliQ added to the sediment in the tube, tube centrifuged at 2500 rpm for 10 minutes, and the supernatant decanted into a designated tube. Following the triple rinse, the tube holding sediment was dried for 24 hours at 105°C within the hot block placed inside a CF hood. After drying, the sample was removed from the hot block, left to cool in the hood for at least 30 minutes, and the weight recorded (mass of digested sample with tube). After recording the mass, the sample was ground to pass through 250 µm mesh and sent to SIRFER lab at the University of Utah for carbon (C) and N isotope analysis.

Total carbonate percentages for the sediment samples were calculated using the following equation:

$$\frac{M_I - M_F}{M} (100) = C\%$$

where M is the individual mass of the sediment sample before digestion in g ($M = \sim 1.0$ g). M_I is the combined mass of the sediment sample and its respective 50 mL centrifuge tube in g. M_F is the combined mass of the digested sediment sample and its respective tube in g. $C\%$ is the percent mass loss or total carbonate percentage for the digested sediment sample in percent.

2.3.2 NaOCl Digestion of Organic Matter

To obtain sediment organic matter (SOM) percentages, we digested interface sediments using sodium hypochlorite or NaOCl (Anderson 1961). Prior to digestion, wet sediments were dried for 24 hours at 105°C within a Brooks Rand Labs wireless hot block placed inside a CF hood. After drying, samples were removed from the hot block and left to cool in the hood for at least 30 minutes. Dry samples were gently ground using an agate mortar and pestle to pass through 250 µm mesh. Once ground, 1 g of sediment was obtained from each sample, placed within 50 mL centrifuge tube, and the weight recorded (individual sample mass and mass of sample with tube).

In a fume hood, 2 mL of reagent-grade NaOCl (minimum 5.7% available chlorine, pH 9.5) were added to the sediment contained within the tube to create a slurry. In the same fume hood, the open tube was immediately placed onto a hot block set to 105°C for 15 minutes. After heating, 6 mL of MilliQ were added to the tube, being left to cool for at least 5 minutes. The cool tube was then centrifuged at 3000 rpm for 15 minutes and the supernatant decanted into a separate 50 mL centrifuge tube designated for ICP-OES analysis. This process of adding NaOCl, heating the slurry, and centrifuging to remove the supernatant was repeated for a total of three treatments.

Following the NaOCl triple treatment, the sediment within the tube was triple rinsed with MilliQ. A single rinse was performed as follows: 6 mL of MilliQ added to the sediment in the

tube, tube centrifuged at 3000 rpm for 15 minutes, and the supernatant decanted into its designated tube. Following the triple rinse, the tube holding sediment was dried for 24 hours at 105°C within the hot block placed inside a CF hood. After drying, the sample was removed from the hot block, left to cool in the hood for at least 30 minutes, and the weight recorded (mass of digested sample with tube). After recording the mass, the sample was pulverized within a tungsten ball-mill for 5 minutes and sent to SIRFER for C and oxygen (O) isotope analysis. Total SOM percentages for sediment samples were calculated using the same equation used to calculate carbonate percentages in the previous section.

2.3.3 Particle Size Distribution

Particle size distributions were evaluated via physical separation of sediment sands, silts, and clays (Kettler et al. 2001). Sediment-particles were dispersed using 90 mL of sodium hexametaphosphate (HMP; 0.5% w/v) mixed with 30 g of sediment and placed onto a shaker table set to 120 rpm for 16 hours. After shaking, the slurry mixture was sieved through nested standard 0.5-mm mesh (no. 35) and 0.053-mm mesh (no. 270). Collected sand particles (> 0.053 mm) were gathered into an aluminum dish of known dry weight and placed into an oven set to 55°C for 24 hours or till constant weight. After drying, the dry mass of the sand particulate was recorded, then immediately placed into a muffle furnace set to 450°C for 4 hours, and the mass recorded again. Silt and clay particles passed through the sieves mentioned above were collected into a 1 L beaker. The mixture of silt, clay, and water were stirred to achieve active suspension of all particles. While stirring, we subsampled 45 mL of solution using a serological pipette, transferring the solution to a 50 mL centrifuge tube, shaking the new tube, and then allowing the solution to settled in a vertical position, undisturbed at room temperature (18-24°C), for at least 90 minutes but < 6 hours to allow silt particles to settle. After settling, the solution containing the

suspended clay was decanted into a pre-weighed aluminum dish, the silt particles were rinsed into another pre-weighed aluminum dish, both were dried at 105°C for 24 hours or until constant weight, and the dry mass recorded.

Particulate mass percentages were calculated using the following equations:

$$Sand\% = \frac{dry\ sand\ mass}{original\ sample\ mass} \times 100$$

$$(Silt + Clay)\% = 100 - Sand\%$$

$$Silt\% = \left(\frac{dry\ silt\ mass_{sub}}{dry\ silt\ mass_{sub} + dry\ clay\ mass_{sub}} \right) \times (Silt + Clay)\%$$

$$Clay\% = 100 - (Sand\% + Silt\%)$$

where *original sample mass* is the dry mass of the sediment originally mixed with HMP in g (~30 g). *dry sand mass* is the mass of the sand (> 0.053 mm) collected in the sieves mentioned above and dried at 55°C in g. *Sand%* is the percentage of sand in the original sediment sample. *(Silt + Clay)%* is the percentage of silt and clay in the original sediment sample based on calculated percent sand of the same sample. *dry silt mass_{sub}* is the mass of the silt collected from the subsample and dried at 105°C in g. *dry clay mass_{sub}* is the mass of the clay collected from the subsample and dried at 105°C in g. *Silt%* is the percentage of silt in the original sediment sample, and *Clay%* is the percentage of clay in the original sediment sample.

2.3.4 Minerals by X-ray Diffraction

Mineral identities and percentages were classified for interface sediments using Rietveld refinement via the application PDXL2. Peaks analyzed in PDXL2 were originally obtained from sediments ran on a Rigaku MiniFlex 600 X-ray diffractometer (XRD) over a range of 5-65 2θ.

Sediments prepared for XRD analysis were gently ground using an agate mortar and pestle to pass through 250 µm mesh. The ground sediment was then side-packed into shallow aluminum sample wells and immediately placed into the XRD for analysis.

2.3.5 Elements by Acid-digestion

Interface sediments were analyzed for their elemental content via acid digestion. Following EPA Method 3051A, we digested 0.5 g of sediment with 6 mL nitric acid (HNO_3 ; 67-70% w/w, trace-metal grade) and 6 mL HCl (34-37% w/w, trace-metal grade) for 30 minutes using a CEM Mars 6 microwave (U.S. EPA 2007). After digestion, the supernatant was separated via centrifugation, decanted into a separate 15 mL centrifuge tube, and filled to 15 mL mark using MilliQ water. Dilutions (50-100x) created from these 15 mL centrifuge tubes were analyzed using a Thermo Scientific iCAP 7400 Duo inductively coupled plasma optical emission spectrometer (ICP-OES) attached to a Teledyne ASX-560 autosampler.

Results obtained from ICP-OES were dilution corrected and converted back into mg kg^{-1} using the following equation:

$$\frac{C_1(V)}{M} = C_0$$

where C_1 is the concentration of the ion in the centrifuge tube in mg L^{-1} . V is the total volume of the solution in the tube before dilution in L ($V = 0.015 \text{ L}$). M is the dry mass of sediment digested in kg ($M = \sim 0.0005 \text{ kg}$). C_0 is the concentration of the element for the sediment in mg kg^{-1} .

2.3.6 Sequential Extractions of Phosphorus

Sediment is composed of mineral and organic fractions that are associated with variable amounts of P. The reversibility or strength of P-binding with these sediment fractions is

dependent upon fraction type and the environment of bonding. Using a sequential extraction method developed for calcite rich lakes by Hupfer et al. 2009 and Gu et al. 2020, modified after Psenner et al. 1984, we can classify sediment bound P into five fractions: P in pore water and loosely adsorbed P (NH_4Cl), redox-sensitive P mainly bound to iron (Fe) and manganese (Mn) compounds (BD), P exchangeable against OH- ions or bound in OM (NaOH), carbonate mineral P (HCl), and refractory organic P and non-extractable mineral P (Residual). Each fraction of the extraction described above was performed as a distinct step of the extraction sequence.

To determine the loosely bound P, 10 mL of deoxygenated 1 M NH_4Cl were added to 1 g of sediment contained within 50 mL centrifuge tubes in an anaerobic COY glovebox equipped with an anaerobic gas infuser, two catalyst boxes, and an airlock transfer chamber. After adding NH_4Cl , the tubes were capped and sealed with parafilm and then transferred to an Eberbach digital shaker table set to 100 rpm for 30 minutes. After shaking, the tubes were centrifuged at 3000 rpm for 10 minutes and transferred back into the glovebox. In the glovebox, the supernatant was decanted into a 50 mL centrifuge tube designated for Step 1. The sediment remaining in the tubes was then double rinsed with NH_4Cl . A single NH_4Cl rinse was performed as follows: within the glovebox 10 mL of deoxygenated 1 M NH_4Cl were added to the sediment remaining in the tubes, the tubes were capped and sealed, the tubes were transferred to a centrifuge set to 3000 rpm for 10 minutes, the tubes were transferred back into the glovebox, and the supernatant collected. Removed from the glovebox, collected supernatants were filtered using 0.45-micron filter, acidified with 0.6 mL of HNO_3 (67-70% w/w, trace-metal grade), filled to the 50 mL mark using 2% v/v HNO_3 , and analyzed using ICP-OES.

Step 2 (redox-sensitive P mainly bound to Fe and Mn compounds) was performed on the same day as Step 1, immediately following. Within the glovebox, 10 mL of deoxygenated 0.11

M Na₂O₄S₂ (BD; sodium hydrosulfite or sodium dithionite) buffered to pH 7 using 0.11 M NaHCO₃ (sodium bicarbonate) were added to the sediment treated in Step 1. After adding the BD (bicarbonate/dithionite) solution, the tubes were capped and sealed with parafilm and transferred to a shaker table set to 100 rpm for 1 hour. After shaking, the tubes were centrifuged at 3000 rpm for 10 minutes, transferred back into the glovebox, and the supernatant decanted into a 50 mL centrifuge tube designated for Step 2. The sediment remaining in the tubes was then rinsed twice, once with BD and once with NH₄Cl. Rinses were performed in the same manner as Step 1. Collected supernatants were prepared for ICP-OES analysis in the same manner as Step 1.

Step 3 (P exchangeable against OH- ions or bound in OM) immediately following Step 2 the sediment was removed from the glovebox and 10 mL of 1 M NaOH were added under normal laboratory atmospheric conditions. The tubes containing sediment were then placed onto a shaker table set to 100 rpm for 16 hours. After shaking, the tubes were centrifuged at 3000 rpm for 10 minutes and the supernatant decanted into a 50 mL centrifuge tube designated for Step 3. The sediment remaining in the tubes was then rinsed twice, once with NaOH and once with NH₄Cl. Rinses were performed in the same manner as Step 1, excluding sealing and transfers in or out of the glovebox. Collected supernatants were prepared for ICP-OES analysis in the same manner as Step 1.

Step 4 (carbonate mineral P), 10 mL of 1 M HCl were added to the sediment treated in Step 3. After adding HCl, the tubes were capped and placed onto a shaker table set to 100 rpm for 16 hours. After shaking, the tubes were centrifuged at 3000 rpm for 10 minutes and the supernatant decanted into a 50 mL centrifuge tube designated for Step 4. The sediment remaining in the tubes was then rinsed twice, once with HCl and once with NH₄Cl. Rinses were performed in the

same manner as Step 3. Collected supernatants were prepared for ICP-OES analysis in the same manner as Step 1.

Step 5 (refractory organic P and non-extractable mineral P), immediately following Step 4 the tubes containing sediment were transferred to 20 mL aluminum weighing dishes of known mass and dried within a Lindberg Blue M laboratory mechanical oven set to 105°C for at least 24 hours. After drying, the dishes were placed inside a desiccator to cool for at least 30 minutes. After cooling, the dishes were weighed, and the mass recorded. The dishes were then placed into a muffle furnace set to 550°C for 2 hours. After 2 hours, the dishes were removed from the muffle furnace and placed into desiccators for at least 30 minutes to cool. Once cooled, the dishes were weighed, and the mass recorded. After weighing, the remaining sediment from each dish and digested using EPA Method 3051A.

The concentration of P associated with each fraction of the extraction was calculated using the following equation:

$$\frac{C_i(V_i)}{M} = C_{frac}$$

Where M is the mass of the dry sediment in kg ($M = \sim 0.001$ kg). C_i is the P-concentration of the supernatant collected from a single step in mg L⁻¹. V_i is the total volume contained within the supernatant tube in L ($V_i = 0.05$ L). C_{frac} is the P-concentration of the dry sediment associated with the step performed in mg kg⁻¹.

2.3.7 DNA Extractions

Sequences were obtained from DNA extractions from lakebed sediments collected near VY, PB, BI, and PP sites. Members of Dr. Zach Aanderud's lab performed DNA extractions via

gel electrophoresis. DNA sequences were analyzed using Qiime2 for microbiome richness and taxonomy.

2.4 Water Column Characterization

2.4.1 Isotopes by Los Gatos Research Liquid Water Isotope Analyzer

Stable isotopes of O and hydrogen (H) found in lakes help us to measure the evaporative evolution of their waters and calculate the $\delta^{18}\text{O}_{\text{VPDB}}$ signature of calcite precipitated from the water column. Using unfiltered surficial waters collected from four sites (PB, PV, VY, and PP) on November 15, 2021, we analyzed for $\delta^2\text{H}_{\text{VSMOW}}$ and $\delta^{18}\text{O}_{\text{VSMOW}}$ using a Los Gatos Research (LGR) cavity ring-down Liquid Water Isotope Analyzer (model: 908-0008).

Predictions of potential $\delta^{18}\text{O}_{\text{SMOW}}$ composition of authigenic carbonates formed in Utah Lake were made using the following equation (Sharp 2007):

$$\delta^{18}\text{O}_{\text{VSMOW}}^{\text{calcite}} = \alpha_{\text{calcite-water}}(1000 + \delta^{18}\text{O}_{\text{VSMOW}}^{\text{water}}) - 1000$$

where $\alpha_{\text{calcite-water}}$ is the isotopic fractionation between calcite and water (O’Neil et al. 1969). Calculated values of $\delta^{18}\text{O}_{\text{VSMOW}}^{\text{calcite}}$ show the potential isotopic O signature of authigenic Utah Lake calcite given the mineral is formed under near equilibrium conditions and outside of the ‘vital effect’ (Sharp 2007).

VSMOW can be converted to the VPDB reference frame through the following equation (Sharp 2007):

$$\delta^{18}\text{O}_{\text{VPDB}} = \frac{\delta^{18}\text{O}_{\text{SMOW}} - 30.91}{1.03091}$$

2.4.2 Elements by Inductively Coupled Plasma Optical Emission Spectroscopy

Column waters collected from the field were analyzed for their elemental content using ICP-OES. Before ICP-OES analysis, column waters were thawed and filtered using a nylon 0.45-micron syringe filter. After filtering, the waters were acidified to 2% v/v HNO₃, diluted, and placed onto the instrument for analysis. Cation concentrations obtained from the instrument were corrected according to the dilution of the sample.

2.4.3 Water Quality Parameters Obtained with Utah Lake Data Explorer

To discuss the effects of water composition on P-cycling in Utah Lake, we need to review numerous parameters which would be difficult for any one study to obtain. Consequently, water quality parameters within Utah Lake were supplemented using the Utah Lake Data Explorer (ULDE) developed by the DWQ (<https://udwq.shinyapps.io/UtahLakeDataExplorer/>). Measurements taken in August 2021 were matched to the sites outlined in this study, averaged, and given 95% confidence bounds (degrees of freedom, $df > 1$). Supplemented values were labeled with the superscript of DWQ (Table 3).

2.5 Sorption Experiments

P-sorption is dependent upon a myriad of factors, including sediment composition, water composition, microbiome, pH, temperature, and redox. Sorption experiments allow us to observe the effects of a single factor affecting P-sorption in a system by keeping all other factors constant. For P-sorption across the sediment-water interface of Utah Lake, we wanted to observe the effect of four individual factors: sediment composition, pH, aqueous P-concentration, and biological activity. To achieve this goal, we performed five major batch sorption isotherm (BSI) experiments: (1) at pH 7.5, we reacted interface sediments collected from PB and PM with water collected from SS spiked with various amounts of P (0, 50, 100, 250, and 500 mg-P L⁻¹-water);

(2-3) at pH 8.0 and 9.0, we reacted interface sediments collected from each site with water collected from SS spiked with various amounts of P (0, 50, 100, 250, and 500 mg-P L⁻¹-water); (4) at pH 8.5, we reacted interface sediments collected from each site with water collected from SS spiked with various amounts of P (0, 0.5, 1, 3, 10, 50, 76, 100, 152, 250, 381, 500, and 762 mg-P L⁻¹-water); and (5) at pH 8.5, we utilized UV-treated interface sediments collected from each site to react with UV-treated water collected from SS spiked with various amounts of P (0, 50, 100, 250, and 500 mg-P L⁻¹-water). All BSI experiments were performed for 24 hours at ~25°C, the temperature of Utah Lake water in the summer when algal blooms are most likely to occur (Søndergaard et al. 2013).

BSI experiments are performed by mixing water and sediment until equilibrium and measuring the change in aqueous P (Figure 2). For each P-spiking level, we weighed 4 g of sediment from each site into 50 mL centrifuge tubes in triplicate. After weighing, we added 4 mL of 0.5 M HEPES or CHES (zwitterionic buffers; buffered to the desired pH using 10 M NaOH), 0-1 mL of 20,000 ppm-P or 400 ppm-P stock (made from dissolved KH₂PO₄ and buffered to the desired pH using 10 M NaOH), and 35-36 mL of lake water (collected from SS on May 6, 2022 and buffered to the desired pH using 10 M NaOH) depending on the required volume of P-stock (Total water volume = 40 mL). After the reagents were added, the pH, conductivity, ORP, and temperature of the sediment-water mixture inside each tube was measured using a Mettler Toledo probe. The tubes were then placed onto a shaker table set to 100 rpm for 24 hours. After shaking, the tubes were measured for pH, conducting, ORP and temperature again. After measuring, the tubes were centrifuged at 3000 rpm for 15 minutes and the supernatant decanted into a separate tube. The remaining sediment was immediately stored in a walk-in freezer at -25°C and the supernatant was filtered through a PES 0.45-micron syringe filter. The filtered

supernatant from each tube was prepared for ICP-OES and IC analysis as previously described. Post-reaction or post-sorption sediments from BSI experiments performed at pH 8.5 (spike-level: 1 mg-P L⁻¹) were sent to SIRFER for isotopes of C, N, and O. Post-sorption sediments from BSI experiments performed at pH 8.5 (spike-level: 3 mg-P L⁻¹) were analyzed using sequential extractions for changes in P-fractionation.

The isotherms derived from sorption experiments were fitted for Linear, Freundlich, and Langmuir models using MATLAB 2022b. Values of R^2 for fitted models across all batch sorption experiments performed were greater than 0.73 with the mean value being 0.98. Batch sorption isotherms only apply to systems operating under the same environmental conditions as the experiment. BSI experiments do not account for advective flow in systems and, therefore, cannot quantify sorption rates (Sparks 2003). Since Utah Lake sediment has clearly been exposed to P-contamination before experimentation we have decided to include a y-intercept, $b_{df,l}$, into our sorption models (Chappell et al. 2020). The amount of P-sorption/desorption occurring in each tube of the sorption experiment was calculated using the following equation:

$$Q = \frac{C_0(V_0) - C_f(V_f)}{M}$$

where Q is the amount of P that sorbed to or desorbed from the sediment in mg kg⁻¹. M is the mass of sediment contained within the 50 mL centrifuge tube in kg ($M = \sim 0.004$ kg). C_0 is the initial concentration of aqueous P in mg L⁻¹ ($C_0 = \sim 0.25\text{-}762$ mg-P L⁻¹). C_f is the final concentration of aqueous P after shaking in mg L⁻¹. V_0 is the initial volume of water contained within the tube in L ($V_0 = \sim 0.04$ L). V_f is the final volume of water contained within the tube after shaking in L ($V_f = \sim 0.04$ L).

Linear models help to quantify P-partitioning at lower, more environmentally relevant, aqueous P-concentrations for a given system. The Linear fit employed to model P-sorption for a given site within an experiment is as follows:

$$Q = K_d(C_f) + b_d$$

where Q is the amount of P that sorbed to or desorbed from the sediment in mg kg^{-1} . C_f is the final concentration of aqueous P after shaking in mg L^{-1} . K_d is the Linear P-partitioning coefficient for the system in L kg^{-1} . b_d is the y-intercept, a shifting factor for the model used to find the true x-intercept for the system, in mg L^{-1} , and $b_{d,f,l}$ is relevant when utilizing sediments previously exposed to P. Though $b_{d,f,l}$ by itself is more theoretical in nature, the x-intercept or sorption origin it provides for the system has real-world applications, representing the predicted aqueous-P concentration at which sorption phenomena in the system switches from sediment P-sequestration to sediment P-release.

Freundlich models help to quantify P-partitioning across low and high aqueous P-concentrations for a given system. The Freundlich fit employed to model P-sorption for a given site within an experiment is as follows:

$$Q = (K_f)C_f^{(1/n)} + b_f$$

where Q is the amount of P that sorbed to or desorbed from the sediment in mg kg^{-1} . C_f is the final concentration of aqueous P after shaking in mg L^{-1} . K_f is the Freundlich P-partitioning coefficient for the system in L kg^{-1} . n is the Freundlich correction factor and is unitless, and b_f is the y-intercept, a shifting factor for the model used to find the true x-intercept for the system, in mg L^{-1} .

Langmuir models define the maximum amount and relative affinity of P-binding in a system. The Langmuir fit employed to model P-sorption for a given site within an experiment is as follows:

$$Q = \frac{K_l(C_f)S_{max}}{1 + K_l(C_f)} + b_l$$

where Q is the amount of P that sorbed to or desorbed from the sediment in mg kg⁻¹. C_f is the final concentration of aqueous P after shaking in mg L⁻¹. K_l is the Langmuir relative binding strength for the system and is unitless. S_{max} is the P-sorption limit or maximum for the sediment in the system in mg kg⁻¹. b_l is the y-intercept, a shifting factor for the model used to find the true x-intercept for the system, in mg L⁻¹.

2.6 Kinetics Experiments

Kinetics experiments control pH, temperature, redox, flow, time, sediment composition, and water composition to determine kinetic P-retention rates. The stirred-flow (SF) method is particularly useful because the sorbent is exposed to a greater number of ions than in a static batch system (Sparks 2003). Also, the flowing solution removes any desorbed/unsorbed species, helping prevent secondary precipitation and quantify the advective flow of P through the system. The enhanced temporal resolution associated with SF is more representative of natural system evolution.

Kinetics experiments were performed in triplicate for each site using three SF reactors (Figure 3). For the reaction we flowed lake water containing 1.1 mg-P L⁻¹, pH 8.5, into each reactor holding 0.32 g of sediment, creating a 1:50 ratio of sediment to water inside the reaction chamber. Water flowed through the reactor at 1 mL min⁻¹, entering from the side of the reactor and exiting out the top via a 0.45-micron filter. Two main kinetics experiments were conducted,

one using sediment from site PB and the other using sediment from site PV. These two experiments were performed for 16 hours, despite it only taking 120 minutes for the systems to reach equilibrium. Effluent from the reactor was collected every 10 minutes using a Teledyne ISCO Foxy R2 autosampler. The solution extracted from the SF reactor was analyzed using ICP-OES (stored at 4°C and analyzed within 90 days) and IC (stored at -25°C and analyzed within 28 days).

Sorbed concentrations of total-P were calculated via mass balance from the following equation (Padilla & Selim 2021):

$$S_n = \frac{q[\sum_{k=1}^n \Delta t_k (C_0 - C_k)] - V(C_n)}{M}$$

where q is the volumetric flow rate in L min⁻¹ ($q = 1$ mL min⁻¹). Δt_k is the time interval between measurements $k-1$ and k in min ($\Delta t_k = 10$ min). C_0 is the input or influent concentration in mg-P L⁻¹ ($C_0 \approx 1.1$ mg-P L⁻¹). C_k is the measured effluent concentration at sampling interval k in mg-P L⁻¹. C_n is the measured concentration at the present sampling interval in mg-P L⁻¹. V is the effective reactor volume in L ($V \approx 16$ mL), and M is the mass of soil or sediment contained within the reactor in g or kg ($M \approx 0.32$ g).

Sediment P-retention kinetic rates were calculated using the following nonlinear kinetic equation (Selim 2014):

$$\frac{\partial S}{\partial t} = k_f \left(\frac{\theta}{\rho} \right) C^b - k_b(S)$$

where b is dimensionless and represents the order of the retention reaction, illustrating the heterogeneity of sorption processes. $\frac{\partial S}{\partial t}$ is the change in P-sorbed over time in mg-P kg⁻¹ min⁻¹. k_f

and k_b are the forward and backward rates of reactions for the retention mechanism, respectively, in min^{-1} . C is the change in effluent concentration in mg-P L^{-1} . S is the change in P-sorbed in mg-P kg^{-1} . θ is the volumetric water content of the soil or sediment in L L^{-1} , and ρ is the bulk density of the soil or sediment in kg L^{-1} .

3. Results and Discussion

3.1 Sediment Composition

3.1.1 Carbonates and Organic Matter

Carbonate percentages as determined by HCl digestion show PB to be significantly ($p < 0.05$) carbonate-depleted when compared to all other locations (Table 1; Figure 4). Provo Bay averages 24.9%-Carbonate and the rest of the lake ranges from 54.5-57.3%-Carbonate. Organic matter percentages as determined by NaOCl digestion show PP to be significantly depleted when compared to all other locations (Table 1; Figure 4). Pelican Point averages 6.59%-SOM while the rest of the lake ranges from 7.67-9.63%-SOM, excluding PB. Provo Bay has the highest average amount of SOM at 11.4%. As supported by Figures 5 and 6, the low percentage of carbonate and relatively high percentage of OM in PB can attributed to the bay's shallow nature as a major inlet into the lake, making it an ideal location for early deposition of allochthonous detritus and quartz grains. Low organic matter percentages in PP are likely due to the absence of an inlet or outlet in the area and longshore drift, reducing the amount of allochthonous OM received into the area. Despite the role of allochthonous OM in P-sorption, the majority of OM found in Utah Lake is authigenic and produced from algae (Williams et al. 2023).

3.1.2 Particle Size Fractionation

Sediment texture and clay content often affect sorption by influencing mineral surface area and substrate availability (Schweizer et al. 2021). Thus, variations in particle size amongst

differing locations could explain deviations in P-sorption. In the case of Utah Lake, particle size distributions across the various locations follow a similar trend (Figure 5). Each site has comparable amounts of silt and clay, averaging 69.7% and 28.6% respectively. Deviations in size fractions are only apparent in PB and PP where the sand fraction is 3.5 times greater than the rest of the lake. The average at PB and PP is 3.54%-Sand, while the rest of the lake averages of 1.02%-Sand. The divergent sand fractions in PB are easily explained when considering the bay's shallow water depth and the fact that it is a major inlet for the lake, creating ideal conditions for sand particles to settle out and be deposited before entering the lake proper. Sand fractions in PP are explained by longshore drift, which creates a shallow northward propagating shelf protruding into the lake and is unlike other locations. As the fetch of Utah Lake delivers sand into the shallow point, current velocities increase and filter clay sized particles and OM from the area. Ultimately, PP receives a less mature influx of sediment compared to other main lake sites, leaving it with the lowest clay sized fraction (25.9%) and OM content (6.59%).

3.1.3 Mineralogy

Mineral identification and quantification help us evaluate how sediment composition may influence P-sorption. For instance, following experimentation we observed that sediments deficient in a critical bonding component—all other factors being equal—exhibit decreased P-sorption. The difference in P-sorption between the sediments indicates that the component in question (calcite, clay, OM, or metal hydroxides) accounts for a certain amount of P-binding in the system.

Mineral fractions across Utah Lake proper appear to be spatially consistent (Figure 6), excluding a significant enrichment of quartz found in PP. Provo Bay also significantly diverges from Utah Lake proper in terms of quartz and calcite content, being enriched with quartz but

depleted of calcite. Quartz percentages in PB average 53.0%-Mineral Mass (MM), while Utah Lake proper averages 12.1%-MM, excluding PP where the average is 19.7%-MM. Quartz enters the lake via stream flow carrying eroded sands from the surrounding mountains. Calcite percentages in PB average 25.6%-MM, however percentages in the main body of the lake average 58.7%-MM. Though calcite percentages show little statistical variation from site-to-site inside Utah Lake proper, PP does have the lowest average at 49.7%-MM. Given the lake's high alkalinity, most calcite found in the lakebed should originate from authigenic precipitation (Randall et al. 2019). However, without C and O isotope measurements from the sediment a specific amount of authigenic vs. allochthonous calcite cannot be estimated.

Other detectable minerals, including dolomite, oligoclase, and clay, do not statistically vary from site-to-site for the entirety of the lake and are detrital in origin. Dolomite averages around 3.62%-MM and is eroded into the lake from the surrounding mountains, which are rich in carbonate strata like the Oquirrh Group (Konopka & Dott 1982). Feldspar percentages, identified as oligoclase, are highly variable but do not significantly differ across sites, averaging 7.23%-MM for the whole of the lake. Feldspar, or oligoclase, is delivered into Utah Lake through intermittent stream flow and the American Fork River. The oligoclase found in these flows is sourced from silicic and plutonic igneous rocks found in the Tintic, Oquirrh, and Traverse Mountains, as well as the Little Cottonwood Stock (Moore 1973, Harbor et al. 2009, and Jensen et al. 2022). Total clay content (avg. 16.2%-MM) is also highly variable but does not statistically vary across the lake, including at PB. Like quartz, clays are delivered into the lake via stream flow containing weathered sediments from the surrounding mountain ranges. Additionally, Utah Lake sediment might contain authigenic metal hydroxides, however low concentrations yield the secondary minerals imperceptible using XRD.

Trends found in mineral fractions identified by XRD follow the trends identified by particle size distributions and carbonate/OM digestions. In fact, carbonate percentages determined by HCl digestion and calcite percentages determined by XRD were within 3.8% of each other when averaging across all locations. The uncertainty of oligoclase and clay percentages is likely due to variable grain size and orientation associated with sample prep. Furthermore, specific species of clays are difficult to distinguish without glycolating samples just prior to XRD analysis (Schultz 1964). Thus, clays here are identified into two broad categories: 2:1 clays with edges and interlayers capable of P-binding and 1:1 clays with only edges capable of P-binding. Again, PB is a shallow inlet for Utah Lake, creating an ideal location for allochthonous sediment (quartz) and detritus (OM) deposition before it has a chance to enter the main lake. Longshore drift forms PP, leading to deposition of less mature sediment enriched with quartz but slightly depleted of finer particulates (calcite, clay, and OM).

3.1.4 Major Elements

An elemental analysis of the sediment from Utah Lake allows us to evaluate current P-concentrations and associations. When comparing sorption potential across sites, higher levels of associated P help us make certain assumptions or possibilities. First, it suggests that a large portion of the sediment's available sites for P may be already occupied, hindering the degree of future sorption. Secondly, it could indicate that the sediment's composition and/or its environment is more favorable for P-binding, exhibiting enhanced sorption upon experimentation. Lastly, the location where the sediment resides may receive a greater influx of P, therefore sequestering more P due to greater exposure.

Chemical compositions as determined by acid-digestion of Utah Lake sediment do not vary greatly from site to site except for in a few notable instances (Figure 7). One, PB has

significantly less calcium (118 g-Ca kg^{-1}) and Mn ($190 \text{ mg-Mn kg}^{-1}$) when compared to main lake averages (190 g-Ca kg^{-1} ; $313 \text{ mg-Mn kg}^{-1}$). Two, PP holds significantly less P on average (612 mg-P kg^{-1}), when compared with GB, BI, and SS, which average 689 mg-P kg^{-1} . The relative absence of Ca in PB concurs with XRD and carbonate digestions which reveal the region to be depleted in calcite. Low sediment P-content in PP could be due to low organic matter percentages within the sediment (Figure 4). This assumption seems especially reasonable when considering that PB has the highest average of sediment P-content (723 mg-P kg^{-1}) and organic matter content (11.4%) while PP has the lowest of both (612 mg-P kg^{-1} ; 6.59%). Mn depletion in PB might be explained by the amount of discharge into the area, which is greater than other area in the lake (Zanazzi et al. 2020), receiving directly from Hobble creek and proximally from Spanish Fork and Provo River. Incoming waters may introduce more Mn to PB in total but the concentration of Mn in the sediment is diluted with quartz particles delivered by the same waters. This assumption is also supported by the fact PB has the lowest average of aluminum ($6.55 \text{ g-Al kg}^{-1}$) and Fe ($7.81 \text{ g-Fe kg}^{-1}$) when compared to averages in the main body of Utah Lake, though the difference is not statistically significant in most instances.

3.1.5 Phosphorus Fractionation

P-fraction amounts obtained through sequential extractions of Utah Lake sediment (Table 1) show no statistical variation across sites either before or after sorption experimentation. Sediment P-concentrations found in the lake (Total; avg. 677 mg-P kg^{-1}) are divided among carbonate minerals (HCl; avg. 424 mg-P kg^{-1}), redox-sensitive Fe and Mn compounds (BD; avg. $94.1 \text{ mg-P kg}^{-1}$), hyper-stable minerals and refractory OM (Residual; avg. $88.0 \text{ mg-P kg}^{-1}$), OM and OH- exchangeable compounds (NaOH; avg. $53.5 \text{ mg-P kg}^{-1}$), and loosely binding compounds (NH₄Cl; avg. $17.7 \text{ mg-P kg}^{-1}$).

P-fraction percentages derived from P-fraction amounts from each location reveal that lakebed-P is primarily held by carbonate minerals (avg. 62.6%-Total P, Table 2). Following carbonate minerals, lakebed-P is associated with redox-sensitive Fe and Mn compounds (avg. 13.9%-Total P), non-extractable minerals and refractory OM (avg. 13.0%-Total P), OM and OH-exchangeable compounds (avg. 7.87%-Total P), and loosely binding compounds (avg. 2.61%-Total P).

Individual P-fraction percentages (Figure 8A) do not significantly vary from site-to-site, except for in a few select instances. Redox-sensitive associated P is significantly higher in VY (15.4%-Total P) and PB (16.5%-Total P) when compared to GB (12.22%-Total P) and PP (12.39%-Total P). OM and OH- exchangeable associated P is significantly higher in PB (9.44%-Total P) when compared to VY (5.92%-Total P) and BI (6.77%-Total P). Also, OM and OH-exchangeable associated P is significantly less in VY (5.92%-Total P) when compared to PP (7.95%-Total P). Hyper-stable minerals and refractory OM associated P is statically lower in PB (8.75%-Total P) when compared with GB, SS, PP, and VY (avg. 13.9%-Total P). Higher percentages of P associated with OM and OH- exchangeable compounds found in PB are attributed to higher percentages of organic matter found in PB sediment (Figure 4).

Like unreacted sediments, individual P-fraction percentages (Figure 8B) do not significantly vary from site-to-site following sorption experimentation except for in a few instances, which are not particularly notable. However, non-extractable minerals and refractory OM associated P is statistically lower in PB following experimentation (7.81%-Total P) when compared to every other site (avg. 13.3%-Total P).

Sediment P-fraction amounts and percentages for an individual site indicate that P is sorbing to loosely binding and redox-sensitive Fe/Mn compounds. The other P-fractions do not

significantly increase following sorption experimentation, indicating little changed for them in terms of their P-content. Sediment P-fraction amounts associated with loosely binding compounds significantly increase for BI, GB, PV, PP, and SS following experimentation (avg. 36.5 mg-P kg⁻¹). Amounts associated with redox-sensitive bound P significantly increase for BI (86.4 vs. 127 mg-P kg⁻¹) and SS (92.4 vs. 134 mg-P kg⁻¹) after experimentation. Sediment P-fraction percentages associated with loosely binding compounds significantly increase (2x) for every site following experimentation minus PB (avg. 4.45%-Total P). Percentages associated with redox-sensitive bound P remain constant for every site after experimentation, except for SS (13.8 vs. 16.1%-Total P).

In summary, the most significant changes in P-fractionation for post-sorption sediments occur in the loosely bound (NH₄Cl) and redox-sensitive bound (BD) portions of P. In fact, the average increase for the loosely bound associated P is 19.8 mg-P kg⁻¹ when accounting for all sites. Sorption experiments that were conducted with these sediments reacted for 24 hours at pH 8.5, 25°C, and with solutions initially spiked to 3 mg-P L⁻¹. After 24 hours, the actual amount of P-sorption was observed and recorded for each batch system. An average of all the sites estimates that about 23.0 mg-P kg⁻¹ were sorbed following sorption experimentation. At 95% confidence, there is no statistical difference between the increase of loosely adsorbed P observed with iterative sequential extractions—19.8 (17.8, 21.7) mg-P kg⁻¹—and the amount of sorbed P observed during sorption experiments—23.0 (21.4, 24.7) mg-P kg⁻¹. All-in-all, we have statistical standing to assume that at pH 8.5 and temperatures near 25°C, Utah Lake sediments sorb P majorly with loosely binding compounds and minorly with redox-sensitive Fe and Mn compounds. The loosely bound fractions of sorbed P are adsorbed to surfaces as hydrated outer-sphere complexations. Given PB has the highest average of loosely bound associated P, OM may

be a critical component of loosely binding substrates in Utah Lake. The redox-sensitive fraction of sorbed P is complexed with Fe and Mn compounds, which are dominated by Fe compounds given the low concentration of Mn associated with lakebed sediments in Utah Lake (Randall et al. 2019). Note, P-sorption to loosely binding and redox-sensitive binding compounds in Utah Lake is not indefinite. As evident in extraction data, once binding sites for these substrates have been filled, P binds itself to carbonate minerals to make up the bulk of sequestered P in Utah Lake.

3.1.6 Microbiome

Sequences obtained from DNA extractions from lakebed sediments collected near VY, PB, BI, and PP reveal the microbiome of Utah Lake sediment to be taxonomically diverse (Figure 9). The microbiome of Utah Lake sediment is dominated by bacterial species in the proteobacteria, actinobacteria, chloroflexi, and firmicutes kingdoms. Despite the diversity of species housed within Utah Lake sediment, an emperor analysis of the sequences from each site suggests statistical microbiome uniformity across the lake.

3.2 Water Column Composition

3.2.1 Hydrogen and Oxygen Isotopes

$\delta^2\text{H}_{\text{VSMOW}}$ and $\delta^{18}\text{O}_{\text{VSMOW}}$ values of main lake water collected on November 15, 2021, average -50.7‰ and -4.5‰, respectively. Unlike the other sites, $\delta^2\text{H}_{\text{VSMOW}}$ and $\delta^{18}\text{O}_{\text{VSMOW}}$ values of lake water collected from PB on the same date average -116.6‰ and -15‰, respectively. $\delta^2\text{H}$ vs. $\delta^{18}\text{O}$ values from surface waters collected from the main body of Utah Lake (PV, VY, and PP) follow the local evaporation line (LEL) for Utah Lake, proposed by Zanazzi et al. 2020, by demonstrating significant enrichment from evaporation (Figure 10). Samples collected from PB plot at the intersection of the local meteoric water line (LMWL) and LEL,

showing PB to be an inlet point from which local meteoric waters enter the lake and subsequently evolve into enriched evaporated waters (Zanazzi et al. 2020). $\delta^2\text{H}_{\text{vSMOW}}$ and $\delta^{18}\text{O}_{\text{vSMOW}}$ for waters collected from Zanazzi et al. 2020 agree with measurements found in this study, which exhibit significant enrichment towards the later end of the water year in September. During melt periods the waters of Utah Lake tend to be more depleted. Given our observations, we estimate $\delta^{18}\text{O}_{\text{VPDB}}$ of authigenic carbonates to range from $-1.09\text{\textperthousand}$ to $-14.3\text{\textperthousand}$ depending on the temperature and season of water collection, more enriched towards the later end of the water year and more depleted during melt periods of the water year. Note, since the solubility of calcium carbonate decreases with increasing temperature, authigenic carbonate precipitation should increase in the summer for Utah Lake. Increased carbonate precipitation from evaporated waters in the summer would enrich $\delta^{18}\text{O}_{\text{VPDB}}$ values, therefore narrowing our estimates of $\delta^{18}\text{O}_{\text{VPDB}}$ in authigenic carbonates closer to $-1.09\text{\textperthousand}$.

The values of $\delta^{18}\text{O}_{\text{VPDB}}$ are relevant to sediment P-sorption by influencing the strength and the extent of P-binding with a substrate. Substrates of differing authigenic, allogeic, biotic, or abiotic origin will exhibit unique qualities for P-binding. For instance, if the primary driver of P-sorption is allogeic carbonates eroded from limestones and delivered through rivers into Utah Lake we could postulate that P-sorption varies greatly with river discharge and likely adsorbs to the surface of those minerals (i.e. limited sorption capacity and greater reversibility when compared to absorbed P precipitated out of the water column with calcite). The stable isotopes of C, N, and O found within sediment carbonates and OM will help us understand whether sediment fractions in Utah Lake are inorganically or organically derived, if calcite is mostly delivered to or indeed precipitated out of the lake, the temperature at which carbonates form, and the biota that dominate the C/P cycles. Given Utah Lake's high alkalinity, relatively warm

temperature, and sediment composition we predict P is primarily bound with authigenic carbonates generated from inorganic (precipitation) and organic processes (photoautotrophic metabolism) at temperatures $\sim 25^{\circ}\text{C}$. However, this hypothesis can only be verified after results for SIRFER have been received.

3.2.2 Vertical and Horizontal Mixing

An elemental analysis of the water from Utah Lake allows us to evaluate how much total P is available for bonding (Table 3; Figure 11). The P-concentration of water often controls the rate, extent, and direction of sorption/desorption for a given system. The overall ionic composition of water also dictates P-sorption by influencing ionic competition, mineral precipitation, pH, and conductivity.

Concentrations of P and other elements found in the column water of an individual site do not significantly differ across depth in almost all instances, suggesting Utah Lake to be well mixed vertically (Zanazzi et al., 2020). A notable exception to this rule is PB, which has poor vertical mixing. Furthermore, most sites share similar water-column P-concentrations, excluding PV and PB. Water-column P-concentrations in PB and PV are more like each other (avg. 61.9 $\mu\text{g-P L}^{-1}$) than to other sites in the lake (avg. 18.5 $\mu\text{g-P L}^{-1}$). Elevated P-concentrations found in the column water of PB are tied to increased sediment P-concentrations and enhanced P-mobility in the area due to microbial activity (Figure 10).

3.2.3 Nutrients and Organics

Concentrations of nutrients and organic compounds found in the water column of Utah Lake appear to be horizontally consistent across the lake from site-to-site (Figure 12). However, the mean concentration of N, ammonia, C_{org} , orthophosphate, chlorophyll-a, and pheophytin-a is clearly greatest in PB (Table 3). Elevated mean concentrations of organics, chlorophyll-a, and

pheophytin-a in PB suggest enhanced microbial activity in the area. Increased microbial activity could engender increased organic matter percentages in PB. Vice versa, increased organic matter percentages found in the sediment of PB could engender increased microbial activity in the water column.

3.3 Sorption Isotherms Fit by Linear, Freundlich, and Langmuir Models

3.3.1 Y- and X-intercepts

The application of a y-intercept into Linear (b_d), Freundlich (b_f), and Langmuir (b_l) models (Figure 13) only has precedence if the soil or sediment considered has been previously exposed to the contaminant of study (Chappell et al. 2020). For Utah Lake, we know without question that the sediment of the lake has been heavily exposed to P contamination prior to examination. However, a potential downside of using $b_{d,f,l}$ in models comparing sorption trends from different locations is that if $b_{d,f,l}$ greatly differs from location-to-location one cannot make meaningful comparisons of contaminant partition coefficients ($K_{d,f,l}$). Luckily, $b_{d,f,l}$ values for Utah Lake sorption models do not significantly vary across sites for a given pH (Figure 19). There is only one exception, which exists for b_d at pH 8.5 between PB with VY and GB, however at 97.2% confidence the intervals of these locations do overlap. Additionally, b_d values do significantly vary across pH for a given location and exceptions to this are negligible (Figure 20). Values of b_l do not significantly vary across pH for a given site. Values of b_f across pH do not significantly vary from b_f values observed at pH 8.5 for a given site, excluding for PB at pH 7.5 and for VY at pH 8.

Considering all these trends exhibited by $b_{d,f,l}$, it would be interesting to take an average of all $b_{d,f,l}$ values to create a single constant y-intercept value for Linear (avg. $b_d = -24.2 \text{ mg-P kg}^{-1}$), Freundlich (avg. $b_f = -400 \text{ mg-P kg}^{-1}$), and Langmuir (avg. $b_l = -7.57 \text{ mg-P kg}^{-1}$) models.

These singular values of $b_{d,f,l}$ would be applied to every site in the lake for all pH scenarios.

Using these constant $b_{d,f,l}$ values, we would recalculate $K_{d,f,l}$ values for each site and pH scenario.

Given the wide 95% confidence bounds of current $K_{d,f,l}$ values, most changes in calculated partition coefficients would not be significant and should not severely reduce R^2 fitting values.

However, the incorporation of a single constant y-intercept value for the lake would further solidify our claims for using $b_{d,f,l}$ in our Linear, Freundlich, and Langmuir models and enhance our ability to make meaningful mathematical comparisons of contaminant partition coefficients across sites and pH.

Sorption origin, or X , represents the x-intercept of Linear, Freundlich, and Langmuir models. It is the minimum concentration of total dissolved P (TDP) required in the water column above a given lakebed sediment before P-sorption behavior can be observed (Figure 14).

Aqueous TDP-concentrations below X tend to cause desorption behavior instead of sorption behavior for a given sediment. Sorption origin values calculated for each site using $b_{d,f,l}$ are constant across pH, thus the X values in Figure 14 represent the average X from all models for a given location. Average X values do not significantly differ from site-to-site except between PV (0.81 mg-P L⁻¹) and PP (0.30 mg-P L⁻¹). Pelican Point has the lowest average X of any site as well as the lowest average sediment P-content (612 mg-P kg⁻¹). Lower concentrations of P found in the sediment of PP may assist P-sorption at lower concentrations of aqueous-P by increasing the number of sites available for P-binding (i.e., less P currently bound to sediment = more vacant P-binding sites).

3.3.2 Partition Coefficients

The partitioning coefficients K_d , K_f , and K_l , from Linear, Freundlich, and Langmuir models, respectively, all significantly increase from pH 8 to 9 for all locations taken from Utah

Lake (Figure 16). The tight confidence intervals of K_d suggest sorption behavior to be more site-specific (Figure 15). Therefore, when using K_d in models, it is advisable to use site-specific K_d values for most cases. However, groups may be formed to simplify the lake's geochemical behavior when the 95% confidence intervals of K_d overlap between sites (Table 4). K_f values differ from K_d values in that they are statistically more uniform across sites. When compared to Linear models, Freundlich models cover a broader range of concentrations in a sorption system for a given pH, redox, and temperature. Consequently, it may not be so that odd K_f appears more generalized for sediments of similar composition like Utah Lake. However, at pH 8.5 we do observe that VY exhibits significantly increased sorption when compared directly with GB, SS, and PP (see Table 4). Looking at Tables 1 and 3, we can see that there are no apparent differences in composition between these sites. Therefore, the deviation of partitioning of VY to these sites at pH 8.5 may be related to optimal binding conditions for differing redox species, including Fe (II, III) and Mn (II, III, IV).

K_l is a mix of K_f and K_d in terms of variation across sites. At pH 7.5, PB and PV have similar sorption trends. At pH 8.0, all sites exhibit similar sorption partitioning to PB. At pH 8.5, all sites exhibit similar sorption behavior to each other except for VY, which shows increased sorption to all other sites. At pH 9.0, all sites exhibit similar sorption partitioning to PV.

Overall, it is advisable to use partition values ($K_{d,f,l}$) in accordance with the pH from which they were obtained. However, exceptions may apply where adjacent pH values may not show significant differences in $K_{d,f,l}$, like when transitioning from pH 8.0 to 8.5 or 8.5 to 9. Nevertheless, it is best to exercise caution as some sites still exhibit significant variations at those pH jumps. Therefore, when using K_d it is recommended to utilize individual values for corresponding sites and pH. When using K_f , most sites can be treated as uniform, except for VY

at pH 8.5. As for K_l , one can either average values for most situations or compare them to specific references, such as PB at pH 8 and PV at pH 9.

3.3.3 Sorption Maximums and Freundlich Correction Factors

Values of n calculated from Freundlich models highlight two important trends. One, like K_f , n values significantly increase for an individual site from pH 8 to 9 (Figure 18). Two, also like K_f , n values do not statistically vary from site-to-site for a given pH, excluding VY which has a higher n (5.92) at pH 8.5 (Table 4; Figure 17). Higher values of n for VY at pH 8.5 can be explained by the same reason K_f values are higher for VY at pH 8.5.

The values of S_{max} calculated from Langmuir models also highlight two interesting trends for Utah Lake sediment. One, S_{max} values observed at pH 9 for a given location are statistically lower than S_{max} values observed at pH's 7.5, 8, or 8.5 in at least one circumstance for each site. Two, S_{max} appears to be consistent from site-to-site for a given pH in most instances. There are three exceptions to this rule: (1) at pH 8, S_{max} for PV is significantly lower than every other site minus SS, averaging 2099 mg-P kg⁻¹ for PV plus SS vs. 2598 mg-P kg⁻¹ for the rest of the lake; (2) at pH 8.5, S_{max} for VY is significantly lower than any other site at 1976 mg-P kg⁻¹ compared to an average 2580 mg-P kg⁻¹ for the other sites; and (3) at pH 9, S_{max} for SS is statistically lower than PB, VY, and GB, while PP is lower than PB, PV, VY, and GB. Together PP and SS have an average S_{max} of 1839 mg-P kg⁻¹ and the other parts of the lake average 2141 mg-P kg⁻¹. Variations in S_{max} across pH and sites are difficult to explain. It could be the case that slight variations in composition between sites might require varying conditions for maximal P-sorption. In general, lower pHs generate higher values of S_{max} for each location.

3.3.4 Impacts of UV-treatment on Partitioning

UV-treatment of Utah Lake sediments significantly decreases K_d for every site (Figure 21). Despite this, K_f and K_l do not statistically decrease for a given location following UV-treatment (excluding K_l for VY). For UV-treated sediments, K_d for VY averages 32.4 L kg^{-1} while the rest of the lake averages 18.2 L kg^{-1} . For UV-treated sediments, K_f does not significantly differ across sites, including VY, creating an average of 199 L kg^{-1} . For UV-treated sediments, K_l for VY averages 0.016 L kg^{-1} while the rest of the lake averages 0.009 L kg^{-1} . Given these trends, UV-treatment of Utah Lake sediments tends to homogenize sediment compositions or characteristics which contribute to P-sorption between sites. Originally performed to control microbial activity among different sites, UV-treatment of sediments could easily degrade organic matter (Li et al. 2015). Consequently, the removal of organic matter from Utah Lake sediments could homogenize sorption trends from site-to-site, as seen in PB (11.4%-SOM) and PP (6.59%-SOM) which significantly differed in K_d before treatment. Again, the elevated values of $K_{d,f,l}$ in VY sediments following UV-treatment can be attributed to something other than organic matter. Redox-sensitive Fe and Mn compounds in VY could maintain elevated partitioning the area, which seems probable given that VY reported the highest percentage of BD associated P following batch experimentation. These redox-sensitive Fe and Mn compounds could have been deposited during the time of Geneva Steel, a company which heavily contaminated the area with iron production by-products and was immediately east of the VY site (Hogsett et al. 2019).

UV-treatment of Utah Lake sediments does not appear to significantly change values of n or S_{max} for most locations (Figure 22). For VY, UV-treated sediments yielded a significant decrease in n (2.90^{UV} vs. $5.92^{\text{pH8.5}}$) and a significant increase in S_{max} (2628^{UV} vs. $1976 \text{ mg-P kg}^{-1}$)

$\text{pH}^{8.5}$). For PP, UV-treated sediments yielded a significant decrease in S_{max} (1921^{UV} vs. $2586 \text{ mg-P kg}^{-1}$ $\text{pH}^{8.5}$). Values of n do not significantly differ from site-to-site following UV-treatment. Meanwhile, S_{max} does not differ from site-to-site following UV-treatment, except PP ($1921 \text{ mg-P kg}^{-1}$) is significantly less than PV, VY, and BI (avg. $2577 \text{ mg-P kg}^{-1}$). Trends in n and S_{max} following UV-treatment of Utah Lake sediments uphold previously made assertions. Exposure to UV can degrade SOM, which can homogenize sediment compositions or characteristics which contribute to P-sorption (Li et al. 2015). PP reports the lowest percentage of SOM (6.59%-SOM) of any site in Utah Lake, which might mean PP suffers greater losses of SOM during UV exposure. PP might suffer greater losses of SOM following UV-treatment precisely because it has less, which is an issue for some sediments where loss on ignition (LOI) is performed (Heiri et al. 2001). However, the changes in S_{max} for VY following treatment may complicate this assertion. If UV exposure degrades SOM, a major component of P-retention in sediment, why does S_{max} significantly increase for VY following treatment? The answer might have to do with VY's suspected unique composition of redox-sensitive compounds. Perhaps, the loss of SOM in VY decreases competition for redox-sensitive P-binding sites which are inherently more stable than loosely binding sites associated with SOM, leading to more effective P-sequestration.

3.4 Nonlinear Kinetic Retention Models

Changes in the rate of sorption indicate that as experimental effluent P-concentrations trend toward influent P-concentrations the rate of P-sorption slows for PV and PB sediments (Figure 23). This slowing indicates saturation of P-binding sites. P-sorption increases with time for both locations, reaching peak sorption between 80-100 min. Averages for peak sorption are $37.8 \text{ mg-P kg}^{-1}$ for PV and $30.3 \text{ mg-P kg}^{-1}$ for PB. After reaching peak sorption, P seems to exchange evenly

between sediment and solution phases. Effluent P-concentrations (C) reach influent concentrations (C_0) at about 80-100 min and with comparable paces between PV and PB.

Kinetics experiments highlight nonlinear retention kinetics of P-sorption for PV and PB sediments (Figure 24). For PV ($b = -4.52$), b suggests more heterogeneity of sorption processes than PB ($b = -2.96$). Forward (k_f ; $^{PV}0.78 \text{ min}^{-1}$ vs. $^{PB}0.48 \text{ min}^{-1}$) and backward (k_b ; $^{PV}0.003 \text{ min}^{-1}$ vs. $^{PB}0.003 \text{ min}^{-1}$) retention rates suggest that PV experiences faster initial P-retention than PB, however as time progresses the retention maintained at both sites is comparable. Initially faster rates of P-retention in PV might be explained by the differences in sediment P-concentrations found between PB and PV. With initially lower sediment P-concentration, PV has more sites available for P-binding relative to PB. However, these vacant sites quickly fill and ultimately PV and PB retain the same amount of P.

4. Conclusion

Our biogeochemical analysis of sediment and water shows Utah Lake to be spatially well-mixed in terms of composition, with PB and PP being the most divergent. Low Fe, Mn, Al, and carbonate content vs. high organic matter, chlorophyll-a, and pheophytin-a content found in PB can be attributed to the bay's shallow nature as a major inlet into the lake, making it an ideal location for increased microbial activity and early deposition of allochthonous detritus and quartz grains which dilute the concentration of calcite and metals found in the sediment. Low organic matter and clay content vs. high quartz content in PP is likely due to longshore drift, reducing the maturity and OM content of eroded sediments received into the area.

Sediment P-concentrations (avg. 677 mg-P kg^{-1}) primarily fractionate with carbonate minerals (avg. 62.6%-Total P), followed by redox-sensitive Fe and Mn compounds (avg. 13.9%-

Total P), hyper-stable minerals and refractory OM (13.0%-Total P), OM and OH- exchangeable compounds (avg. 7.87%-Total P), and loosely binding compounds (avg. 2.61%-Total P). Low P-content in PP (612 mg-P kg^{-1}) is due to less SOM (6.59%) while high P-content in PB (723 mg-P kg^{-1}) is due to more SOM (11.4%). Sorption experiments performed with UV-treated sediments exhibit SOM degradation, which emphasizes the role of SOM in P-sorption. Sediments treated with UV have more similar compositions to each other due to SOM loss via degradation and therefore have homogeneous P-sorption behaviors, like in the case of PB and PP which demonstrated significantly differing K_d before treatment but similar K_d after treatment.

Sequential P-extractions performed prior to and following sorption experimentation suggest that near pH 8.5 and 25°C sediments in Utah Lake sorb newly introduced P to loosely binding and redox-sensitive compounds. However, this sorbing of P with loosely binding and redox-sensitive compounds is not indefinite, as evident by the sediment's high percentage of P associated with carbonate minerals. After initially sorbing to more labile components, P deposited on the lakebed will mobilize into porewater and column water under more anoxic conditions, or simply diffuse deeper into the sediment or back into the water column where P-concentrations are less (Williams et al. 2023). Despite remobilization, we propose that P can again be removed from solution, this time via absorption with carbonate minerals precipitated from saturated porewater and column water. Note, we have yet to calculate entropy values for these reactions, saturation indices of porewater and column water, nor have we observed crystallization re-growth of calcite minerals in sediment samples. Once P has formed stable bounds with carbonate minerals it is unlikely to reenter the water column (Richardson 1985 and Søndergaard et al. 2001). Nevertheless, P-desorption from sediment can occur especially when aqueous P-concentrations are low.

Sorption experiments confirm the P-sequestering capabilities of Utah Lake sediment when conditions are primed. Remember, in most cases sorption behavior is comparable, especially for the main body of the lake. Nevertheless, deviations in sorption behavior do occur and should be accounted for when applicable, like increased partitioning for VY at pH 8.5. As a general trend for sediment across the lake, P-partitioning increases while maximum P-sorption decreases with pH. Averaging from all sites: $K_d = {}^{pH\ 7.5}13.4$, ${}^{pH\ 8.0}17.0$, ${}^{pH\ 8.5}38.5$, & ${}^{pH\ 9.0}77.2\text{ L kg}^{-1}$; $K_f = {}^{pH\ 7.5}63.0$, ${}^{pH\ 8.0}134$, ${}^{pH\ 8.5}419$, & ${}^{pH\ 9.0}911\text{ L kg}^{-1}$; $n = {}^{pH\ 7.5}\ 1.71$, ${}^{pH\ 8.0}\ 2.19$, ${}^{pH\ 8.5}\ 3.36$, & ${}^{pH\ 9.0}\ 5.18$; $K_l = {}^{pH\ 7.5}4.12$, ${}^{pH\ 8.0}7.64$, ${}^{pH\ 8.5}15.1$, & ${}^{pH\ 9.0}41.7\text{ mL kg}^{-1}$; and $S_{max} = {}^{pH\ 7.5}\ 3097$, ${}^{pH\ 8.0}\ 2455$, ${}^{pH\ 8.5}\ 2494$, & ${}^{pH\ 9.0}\ 2055\text{ mg-P kg}^{-1}$. Increasing P-partition coefficients are associated with enhanced carbonate precipitation at more alkaline pHs. Decreasing P-sorption maximums are associated with increasing pH and shifts in-and-out of optimal bonding conditions for a particular substrate. In general, substrates, excluding carbonate, appear to decrease in the number of sites available for P-binding as pH increases.

Kinetics experiments highlight nonlinear retention of P for PV and PB sediments. The center-lake sediments of PV experience faster initial P-retention than PB ($k_f = {}^{PV}\ 0.78$ vs. ${}^{PB}\ 0.48\text{ min}^{-1}$; $k_b = {}^{PV}\ 0.003$ vs. ${}^{PB}\ 0.003\text{ min}^{-1}$). However, as time progresses the retention maintained at both sites is comparable (${}^{PV}\ 37.8$ vs. ${}^{PB}\ 30.3\text{ mg-P kg}^{-1}$). Initially faster rates of retention in PV are assisted by lower concentrations of sediment P-content. Lower P-content in sediments can imply the presence of more sites available for P-binding, which may also assist in early sorption during low aqueous P-concentrations, like with PP ($X = 0.3\text{ mg-P L}^{-1}$). According to b (${}^{PV}\ -4.52$ vs. ${}^{PB}\ -2.96$), PV has more heterogeneity of sorption processes when compared to PB. Enhanced heterogeneity in PV could be due to differences in SOM content between the two sites. SOM is a highly competitive substrate for contaminants in soil and sediment (Sparks 2003). Consequently,

higher concentrations of SOM could increase competition for P-binding with carbonates, clays, and hydroxides found in PB, making SOM the initial primary destination for newly introduced P, and decreasing the overall heterogeneity of the sorption system.

Our findings emphasize that Utah Lake is a natural system existing in dynamic equilibrium. Several processes and mechanisms govern P-sorption behavior between the lakebed and water column; change one factor, and the lake will respond to maintain its state. Nevertheless, anthropogenic activities can still negatively impact the lake if left unchecked, as we have seen in the past. In short, benefits from remediation efforts surrounding input reduction of contaminants, including P, into Utah Lake may take several years to take effect (Markovic et al. 2019).

REFERENCES

- Abu-Hmeidan, H., Williams, G., & Miller, A. (2018). Characterizing total phosphorus in current and geologic Utah Lake sediments: Implications for water quality management issues. *Hydrology*, 5(1), 8. <https://doi.org/10.3390/hydrology5010008>
- Adam, N. (2016). Phosphate speciation under organic-acid-promoted dissolution of phosphorus-sorbed Ferrihydrite–Boehmite mixtures: Implications for soil phosphorus. *Soil Science Society of America Journal*, 80(4), 900–910. <https://doi.org/10.2136/sssaj2016.02.0024>
- AGRC (2016) Statewide 10-meter hillshade base map, Utah (WMTS). AGRC, Utah Automated Geographic Reference Center, Available online: <https://www.arcgis.com/home/item.html?id=10baf68f84784d4883d0d13d8e0a5b46> (accessed on 10 August 2023)
- Albers, E., Bateman, M., & Harris E. (2022). State and County Population Estimates for Utah: 2022. Kem C. Gardner Policy Institute of the University of Utah. Informed Decisions, Dec2022
- Amundson, R., Austin, A.T., Schuur, E.A.G., Yoo, K., Matzek, V., Kendall, C., Uebersax, A., Brenner, D. and Baisden, W.T. (2003). Global patterns of the isotopic composition of soil and plant nitrogen. *Biological Abstracts* Vol. 95, Iss. 3, Ref. 30880. 17, doi:10.1029/2002GB00190.
- Anderson, J.U. (1961). An Improved Pretreatment for Mineralogical analysis of Samples Containing Organic Matter. *Clays Clay Miner.* 10, 380–388. <https://doi.org/10.1346/CCMN.1961.0100134>
- Boström, B., Andersen, J.M., Fleischer, S., Jansson, M., (1998). Exchange of phosphorus across the sediment–water interface. *Hydrobiologia*, 170, 229–244.
- Brand, W. A., Coplen, T. B., Vogl, J., Rosner, M., & Prohaska, T. (2014). Assessment of international reference materials for isotope-ratio analysis (IUPAC Technical Report). *Pure and Applied Chemistry*. 86 (3): 425–467. doi:10.1515/pac-2013-1023. hdl:11858/00-001M-0000-0023-C6D8-8. S2CID 98812517.
- Chappell, M. A., Seiter, J., M., West, H., M., Miller, L., F., Negrete, M., E., LeMonte, J., J., Porter, B., E., Price, C., L., & Middleton, M., A. (2020). Organic contaminant sorption parameters should only be compared across a consistent system of linear functions. *Heliyon*. Mar 26;6(3):e03511. doi: 10.1016/j.heliyon.2020.e03511. PMID: 32258452; PMCID: PMC7109627.
- Chen, M., Ding, S., Wu, Y., Fan, X., Jin, Z., Tsang, D. C. W., Wang, Y., & Zhang, C. (2019). Phosphorus mobilization in lake sediments: Experimental evidence of strong control by iron and negligible influences of manganese redox reactions. *Environmental Pollution*, 246, 472–481. <https://doi.org/10.1016/j.envpol.2018.12.031>
- Clark, I. D., & Fritz, P. (1997). Environmental isotopes in hydrogeology. Lewis.
- Clarkson, M. O., Poulton, S. W., Guilbaud, R., & Wood, R. A. (2014). Assessing the utility of Fe/Al and Fe-speciation to record water column redox conditions in carbonate-rich

- sediments. *Chemical Geology*, 382, 111–122.
<https://doi.org/10.1016/j.chemgeo.2014.05.031>
- Coplen, T.B. (2007). Calibration of the calcite-water oxygen-isotope geothermometer at Devils Hole, Nevada, a natural laboratory. *Geochimica et Cosmochimica Acta*, 71, 3948-3957.
- Craig, H. (1961). Isotopic variations in meteoric waters. *Science*, 133, 1702–1703.
- Dhillon, G. S., Amichev, B. Y., Freitas, R., & Rees, K. V. (2015). Accurate and Precise Measurement of Organic Carbon Content in Carbonate-Rich Soils. *Communications in Soil Science and Plant Analysis*, Philadelphia, 46(21).
<https://doi.org/10.1080/00103624.2015.1089271>
- Epstein, S., Buchsbaum, R., Lowenstam, H.A. and Urey, H.C. (1953). Revised carbonate-water isotopic temperature scale. *Geological Society of America Bulletin* 64, 1315-1326.
- Gächter, R., & Müller, B. (2003). Why the phosphorus retention of lakes does not necessarily depend on the oxygen supply to their sediment surface. *Limnology and Oceanography*, 48(2), 929–933. <https://doi.org/10.4319/lo.2003.48.2.0929>
- Grady, J. K., Chasteen, N. D., and Harris, D. C. (1988). Radicals from “Good's” buffers. *Analytical Biochemistry*, Volume 173, Issue 1, Pages 111-115, 0003-2697, DOI: 10.1016/0003-2697(88)90167-4.
- Gu, C., Dam, T., Hart S. C., Turner B. L., Chadwick, O. A., Berhe, A. A., Hu, Y., & Zhu, M. (2020). Quantifying Uncertainties in Sequential Chemical Extraction of Soil Phosphorus Using XANES Spectroscopy. *Environmental Science & Technology*, 54(4), 2257-2267. DOI: 10.1021/acs.est.9b05278
- Harbor, R. L., Christiansen, E. H., Kowallis, B., McKean, A. (2009) Mid and late Cenozoic volcanism in northern east Tintic Mountains, west-central Utah. *Geological Society of America*, 41(6), 43-44
- Harper, C. (2015). User Guide for GoldBio Buffers. Gold Biotechnology, St. Louis, MO, Rev. 2. Retrieved:
<https://www.goldbio.com/documents/3581/User+Guide+for+GoldBio+Buffers.pdf>
- Heiri, O., Lotter, A. F., & Lemcke, G. (2001). Loss on ignition as a method for estimating organic and carbonate content in sediments: reproducibility and comparability of results. *Journal of Paleolimnology*, 25, 101-110.
- Herczeg, A. L., & Fairbanks, R. G. (1987). Anomalous carbon isotope fractionation between atmospheric CO₂ and dissolved inorganic carbon induced by intense photosynthesis. *Geochimica et Cosmochimica Acta*, 51, 895–899.
- Hesslein, R. H. (1976). An in-situ sampler for close interval pore water studies 1. *Limnology and oceanography*, 21(6), 912-914.
- Hogsett, M., Li, H., & Goel, R. (2019). The Role of Internal Nutrient Cycling in a Freshwater Shallow Alkaline Lake. Mary Ann Liebert, Inc. *Environmental Engineering Science*, 36(5). <https://doi.org/10.1089/ees.2018.0422>

- Hupfer, M., Zak, D., Roßberg, R., Herzog, C., & Pöthig, R. (2009). Evaluation of a well-established sequential phosphorus fractionation technique for use in calcite-rich lake sediments: identification and prevention of artifacts due to apatite formation. *Limnology and Oceanography: Methods*, 7(6), 399-410.
- Jensen, C. G., Christiansen, E. H., & Keith, J. D. (2022) Multi-stage construction of the Little Cottonwood Stock, Utah, USA; origin, intrusion, venting, mineralization, and mass movement. *Geological Society of America, Geosphere*, 18(4), 1264-1296, DOI: 10.1130/GES02369.1
- Jeppesen, E., Søndergaard, M., Jensen, J. P., Havens, K. E., Anneville, O., & Carvalho, L. (2005). Lake responses to reduced nutrient loading—an analysis of contemporary long-term data from 35 case studies. *Freshwater Biology*, 50(10):1747–71.
- Julia M Otte, Nia Blackwell, Viktoria Soos, Saskia Rughöft, Markus Maisch, Andreas Kappler, Sara Kleindienst, Caroline Schmidt, Sterilization impacts on marine sediment---Are we able to inactivate microorganisms in environmental samples? *FEMS Microbiology Ecology*, Volume 94, Issue 12, December 2018, fiy189, <https://doi.org/10.1093/femsec/fiy189>
- Kettler, T. A., Doran, J. W., & Gilbert, T. L. (2001). Simplified method for soil particle-size determination to accompany soil-quality analyses. *Soil Science Society of America Journal*, 65, 849-852. DOI: 10.2136/sssaj2001.653849x.
- Klamt, A.M., Hilt, S., Moros, M. et al. The effect of a shift from macrophyte to phytoplankton dominance on phosphorus forms and burial in the sediments of a shallow hard-water lake. *Biogeochemistry*, 143, 371–385 (2019). <https://doi.org/10.1007/s10533-019-00567-4>
- Konopka, E. H. & Dott, R. H. Jr. (1982) Stratigraphy and sedimentology, lower part of the Butterfield Peaks Formation (Middle Pennsylvanian), Oquirrh Group, at Mt. Timpanogos, Utah. *Utah Geological Association*, 10, 215-234
- Lafferty, B. J., Ginder-Vogel, M., and Sparks, D. L. (2010). Arsenite Oxidation by a Poorly Crystalline Manganese-Oxide 1. Stirred-Flow Experiments. *Environmental Science & Technology*, 44 (22), 8460-8466. DOI: 10.1021/es102013p
- Li, F., Pan, B., Zhang, D., Yang, X., Li, H., Liao, S., Ghaffar, A., Peng, H., & Xing, B. (2015). Organic matter source and degradation as revealed by molecular biomarkers in agricultural soils of Yuanyang terrace. *Scientific Reports*, 5, 11074. DOI: 10.1038/srep11074
- Li, J., Reardon, P., McKinley, J. P., Joshi, S. R., Bai, Y., Bear, K., & Jaisi, D. P. (2017). Water column particulate matter: A key contributor to phosphorus regeneration in a coastal eutrophic environment, the Chesapeake Bay. *Journal of Geophysical Research: Biogeosciences*, 122(4), 737–752. <https://doi.org/10.1002/2016jg003572>
- Li, Q. M., Zhang, W., Wang, X.-X., Zhou, Y.-Y., Yang, H., & Ji, G.-L. (2007). Phosphorus in interstitial water induced by redox potential in sediment of Dianchi Lake, China. *Pedosphere*, 17(6), 739–746. [https://doi.org/10.1016/s1002-0160\(07\)60089-7](https://doi.org/10.1016/s1002-0160(07)60089-7)

- Macharia, A. N. (2012). Reconstructing Paleoenvironments Using a Mass-Energy Flux Frameworks. (Doctor of Philosophy), University of Utah, Salt Lake City, UT.
- Markovic, S., Liang, A., Watson, S. B., Depew, D., Zastepa, A., Surana, P., Byllaardt, J. V., Arhonditsis, G., & Dittrich, M. (2019). Reduction of industrial iron pollution promotes phosphorus internal loading in eutrophic Hamilton Harbour, Lake Ontario, Canada. *Environmental Pollution*, 252, 697–705. <https://doi.org/10.1016/j.envpol.2019.05.124>
- McKenzie, J.A. (1985). Carbon isotopes and productivity in the lacustrine and marine environment, in: Stumm, W. (Ed.), *Chemical processes in lakes*. Wiley Interscience, New York, pp. 99-118.
- McKenzie, J. A., & Hollander, D. J. (1993). Oxygen-isotope record in Recent carbonate sediments from Lake Greifen, Switzerland (1750-1986); application of continental isotopic indicator for evaluation of changes in climate and atmospheric circulation patterns, in: Swart, P.K., Lohmann, K.C., McKenzie, J.A., Savin, S. (Eds.), *Climate Change in Continental Isotopic Records*. American Geophysical Union, Washington, D.C., pp. 101-111.
- Meyers, P.A. (1994). Preservation of elemental and isotopic source identification in sedimentary organic matter. *Chemical Geology* 114, 289-302.
- Mohammed, I. N., & Tarboton, D. G. (2012). An examination of the sensitivity of the Great Salt Lake to changes in inputs. *Water Resources Research*, 48(11). <https://doi.org/10.1029/2012WR011908>
- Moore, P. A. & Reddy, K. R. (1994). Role of Eh and pH on phosphorus geochemistry in sediments of Lake Okeechobee, Florida. *J. Environ. Qual.*, 23(5), 955–964.
- Moore, W. J. (1973) A Summary of Radiometric Ages of Igneous Rocks in the Oquirrh Mountains, North-Central Utah. *Economic Geology Publishing Company*, 68(1), 97-101
- Nowlin, W. H., Evarts, J. L., & Vanni, M. J. (2005). Release rates and potential fates of nitrogen and phosphorus from sediments in a eutrophic reservoir. *Freshwater Biology*, 50(2), 301–322. <https://doi.org/10.1111/j.1365-2427.2004.01316.x>
- Ogdahl, M. E., Steinman, A. D., & Weinert, M. E. (2014). Laboratory-determined phosphorus flux from lake sediments as a measure of internal phosphorus loading. *Journal of Visualized Experiments*, (85). <https://doi.org/10.3791/51617>
- O'Neil, J. R., Clayton, R. N. and Mayeda, T. K. (1969). Oxygen isotope fractionation in divalent metal carbonates. *Journal of Chemical Physics*, 51, 5547-5558.
- Padilla, J. T., & Selim, H. M. (2021). Modeling the kinetics of competitive sorption and desorption of Zn(II), Ni(II), and Pb (II) in an acidic soil: Stirred-flow experiments. *Soil Science Society of America Journal*, 85, 560–573. <https://doi.org/10.1002/saj2.20220>
- Parsons, C. T., Rezanezhad, F., O'Connell, D. W., & Van Cappellen, P. (2017). Sediment phosphorus speciation and mobility under dynamic redox conditions. *Biogeosciences*, 14(14), 3585–3602. <https://doi.org/10.5194/bg-14-3585-2017>

- Pecher, K., Haderlein, S. B., and Schwarzenbach R. P. (2002). Reduction of Polyhalogenated Methanes by Surface-Bound Fe(II) in Aqueous Suspensions of Iron Oxides. *Environmental Science & Technology*, 36 (8), 1734-1741. DOI: 10.1021/es011191o
- Perrin, D. D. and Dempsey, B. (1974). Buffers for pH and Metal Ion Control. Chapman and Hall Ltd, London, 1974. (26)
- Psenner, R. V., Pucsko, R., & Sager, M. (1984). Die Fraktionierung organischer und anorganischer Phosphorverbindungen von Sedimenten—Versuch einer Definition ökologisch wichtiger Fraktionen. *Arch. Hydrobiol. Suppl.*, 70(1), 111-155.
- PSOMAS. (2007). Utah Lake TMDL: Pollutant Loading Assessment & Designated Beneficial Use Impairment Assessment.
- Randall, M. C., Carling, G. T., Dastrup, D. B., Miller, T., Nelson, S. T., Rey, K. A., Hansen, N. C., Bickmore, B. R., & Aanderud, Z. T. (2019). Sediment potentially controls in-lake phosphorus cycling and harmful cyanobacteria in shallow, eutrophic Utah Lake. *PLOS ONE*, 14(2). <https://doi.org/10.1371/journal.pone.0212238>
- Reddy, K. R., Newman, S., Osborne, T. Z., White, J. R., & Fitz, H. C. (2011). Phosphorous cycling in the Greater Everglades Ecosystem: Legacy phosphorous implications for management and restoration. *Critical Reviews in Environmental Science and Technology*, 41(sup1), 149–186. <https://doi.org/10.1080/10643389.2010.530932>
- Richardson, C. J. (1985). Mechanisms controlling phosphorus retention capacity in freshwater wetlands. *Science*, 228(4706), 1424–1427. <https://doi.org/10.1126/science.228.4706.1424>
- Ruffino, B., & Zanetti, M. (2009). Adsorption study of several hydrophobic organic contaminants on an aquifer Material. *Am. J. Environ. Sci.*, 2009;5
- Sampei, Y., & Matsumoto, E. (2001). C/N ratios in a sediment core from Nakaumi Lagoon, southwest Japan—Usefulness as an organic source indicator. *Geochemical Journal*, 35, 189–205.
- Schweizer, S., A., Mueller, C., W., Höschen, C., Ivanov, P., & Kögel-Knabner, I. (2021). The role of clay content and mineral surface area for soil organic carbon storage in an arable toposequence. *Biogeochemistry*, 156, 401–420. <https://doi.org/10.1007/s10533-021-00850-3>
- Selim, H. Magdi. (1992). Modeling the Transport and Retention of Inorganics in Soils. *Adv. Agron.*, 47, 331-384.
- Selim, H. Magdi. (2014). *Transport and Fate of Chemicals in Soils: Principles and Applications*. Taylor & Francis Group (pp. 35-60). ProQuest Ebook Central. <https://ebookcentral.proquest.com/lib/byu/detail.action?docID=1659652>.
- Selim, H. Magdi. (2016). *Transport & fate of chemicals in Soils: Principles & applications*. CRC Press.
- Sharp, Z. (2007). *Principles of stable isotope geochemistry*. Pearson Education.

- Shiraishi, H., Kataoka, M., Morita, Y., and Umemoto, J. (1993) Interactions of Hydroxyl Radicals with Tris (Hydroxymethyl) Aminomethane and Good's Buffers Containing Hydroxymethyl or Hydroxyethyl Residues Produce Formaldehyde, Free Radical Research Communications, 19:5, 315-321, DOI: 10.3109/10715769309056520
- Smithson, S. M. (2020). Dynamics of internal phosphorus cycling in a highly eutrophic, shallow, fresh water lake in Utah lake state park, Utah, USA (Order No. 28810097). Available from ProQuest Dissertations & Theses Global. (2598955747). Retrieved from: <http://erl.lib.byu.edu/login/?url=https://www.proquest.com/dissertations-theses/dynamics-internal-phosphorus-cycling-highly/docview/2598955747/se-2?accountid=4488>
- Søndergaard, M., Jensen, P. J., & Jeppesen, E. (2001). Retention and internal loading of phosphorus in shallow, Eutrophic Lakes. The Scientific World JOURNAL, 1, 427–442. <https://doi.org/10.1100/tsw.2001.72>
- Sparks, D. L. (2003). Environmental Soil Chemistry, Second Edition. New York: Academic Press.
- Sundman, A., Karlsson, T., Sjöberg, S., & Persson, P. (2016). Impact of iron–organic matter complexes on aqueous phosphate concentrations. Chemical Geology, 426, 109–117. <https://doi.org/10.1016/j.chemgeo.2016.02.008>
- Taggart, J. B. (2021) INORGANIC PHOSPHORUS CHEMISTRY OF UTAH LAKE'S EFFLUENT MIXING ZONES. Available from ProQuest Dissertations & Theses Global. Retrieved from: http://wfwqc.org/wp-content/uploads/2021/04/Inorganic-Phosphorus-Chemistry-Utah-Lake-Mixing-Zones-Taggart_2021.pdf
- Tanner, K. B., Cardall, A. C., & Williams, G. P. (2022). A Spatial Long-Term Trend Analysis of Estimated Chlorophyll-a Concentrations in Utah Lake Using Earth Observation Data. Remote Sens., 14, 3664. <https://doi.org/10.3390/rs14153664>
- U.S. EPA. 2007. “Method 3051A (SW-846): Microwave Assisted Acid Digestion of Sediments, Sludges, Soils, and Oils,” Revision 1
- Utah Department of Water Quality. (2023). Utah Lake Data Explorer. <https://udwq.shinyapps.io/UtahLakeDataExplorer/>
- Wawro, P. R. (2011) Utah Lake Bathymetric Contour Lines. Available online: <https://www.arcgis.com/home/item.html?id=03c0d9b15175479594acca6c6527fad4> (accessed on 27 July 2023)
- Wielinga, B., Mizuba, M. M., Hansel, C. M., and Fendorf S. (2001). Iron Promoted Reduction of Chromate by Dissimilatory Iron-Reducing Bacteria. Environmental Science & Technology, 35 (3), 522-527. DOI: 10.1021/es001457b
- Williams, R., Nelson, S., Rushforth, S. Rey, K., Carling, G., Bickmore, B., Heathcote, A., Miller, T., & Meyers, L. (2023). Human-driven trophic changes in a large, shallow urban lake: Changes in Utah Lake, Utah from pre-European settlement to the present. Water Air Soil Pollution, 234:218. <https://doi.org/10.1007/s11270-023-06228-5>

Zanazzi, A., Wang, W., Peterson, H., & Emerman, S. H. (2020). Using stable isotopes to determine the water balance of Utah Lake (Utah, USA). *Hydrology*, 7(4), 88.
<https://doi.org/10.3390/hydrology7040088>

APPENDIX

Tables

Table 1. Physiochemical properties of Utah Lake sediment gathered using an Ekman dredge from the top 10 cm of the lakebed. Sediments were collected from 7 locations across the lake in August 2021.

Location Site ID	Provo Bay PB	Provo PV	Vineyard VY	Bird Island BI	Goshen Bay GB	Saratoga Springs SS	Pelican Point PP
Latitude, ^{WGS-84} °N	40.1846	40.2357	40.3002	40.1654	40.0906	40.337	40.2703
Longitude, ^{WGS-84} °W	-111.7162	-111.7668	-111.8020	-111.7788	-111.8915	-111.8687	-111.8364
ρ , ^a g cm ⁻³	0.69 (0.53 , 0.85)	0.78 (0.74 , 0.82)	0.79 (0.76 , 0.82)	0.61 (0.57 , 0.64)	0.56 (0.51 , 0.62)	0.45 (0.42 , 0.49)	0.48 (0.45 , 0.52)
θ , ^a L L ⁻¹	0.74 (0.68 , 0.80)	0.72 (0.70 , 0.74)	0.71 (0.69 , 0.74)	0.83 (0.79 , 0.87)	0.79 (0.75 , 0.83)	0.89 (0.82 , 0.96)	0.83 (0.80 , 0.85)
pH	7.69	7.89	7.94	7.94	7.99	8.02	8.04
ORP, rel. mV	131	132	131	133	126	128	127
Conductivity, $\mu\text{S cm}^{-1}$	1589	2476	2273	2640	2438	2186	1876
Sediment Composition, %							
_Organic Matter ^b	11.4 (8.80 , 14.0)	9.63 (8.59 , 10.7)	8.49 (8.05 , 8.93)	9.14 (8.26 , 10.0)	9.28 (8.40 , 10.2)	7.67 (7.09 , 8.26)	6.59 (6.47 , 6.70)
_Carbonates ^c	24.9 (20.1 , 29.7)	57.3 (56.1 , 58.5)	57.3 (56.3 , 58.2)	57.0 (55.3 , 58.7)	56.6 (50.4 , 62.8)	55.7 (48.1 , 63.3)	54.5 (52.3 , 56.7)
Particle Size Distribution,^d %							
_Sand	3.23	1.60	0.62	1.45	1.01	0.40	3.85
_Coarse Sand->0.5mm, % of Sand	1.04	0.15	8.25	6.46	0.03	3.09	0.38
_Fine Sand-<0.053mm, % of Sand	93.3	93.0	81.0	87.1	90.6	89.7	95.6
_POM, % of Sand	5.63	6.89	10.8	6.48	9.37	7.19	3.99
_Silt	66.2	69.8	71.6	68.7	71.9	69.5	70.2
_Clay	30.6	28.6	27.8	29.9	27.1	30.1	25.9
Mineralogy,^e % of mineral mass							
_Quartz	53.0 (32.6 , 73.4)	12.9 (10.9 , 14.8)	11.7 (10.2 , 13.3)	11.6 (9.23 , 14.0)	15.5 (11.4 , 19.7)	8.66 (5.72 , 11.6)	19.7 (18.8 , 20.5)
_Calcite	25.6 (15.6 , 35.6)	62.4 (56.5 , 68.4)	59.5 (53.2 , 65.9)	58.6 (48.1 , 69.1)	55.3 (45.7 , 64.9)	66.7 (49.7 , 83.8)	49.7 (48.0 , 51.3)
_Dolomite	2.56 (1.57 , 3.54)	3.73 (3.11 , 4.36)	3.28 (2.29 , 4.27)	3.57 (1.08 , 6.06)	4.63 (2.70 , 6.56)	3.44 (2.51 , 4.36)	4.15 (3.44 , 4.86)
_Oligoclase	11.6 (0.00 , 28.4)	6.30 (3.07 , 9.53)	8.02 (3.82 , 12.2)	3.80 (0.00 , 9.51)	6.23 (0.00 , 14.5)	3.97 (2.10 , 5.83)	10.7 (5.07 , 16.3)
_2:1 Clays ^f	5.29 (0.00 , 11.5)	10.6 (0.00 , 23.6)	14.2 (8.52 , 19.8)	18.2 (1.22 , 35.2)	12.3 (0.00 , 26.6)	13.1 (0.00 , 28.9)	12.1 (4.23 , 19.9)
_1:1 Clays ^f	2.10 (0.00 , 5.35)	3.90 (0.00 , 9.35)	3.20 (0.94 , 5.46)	4.37 (2.68 , 6.06)	6.00 (5.01 , 6.99)	4.13 (0.00 , 9.04)	3.72 (1.42 , 6.03)
Chemical Composition,^g mg kg⁻¹							
_Ca, 10 ⁵	1.18 (1.07 , 1.29)	1.88 (1.61 , 2.15)	1.94 (1.82 , 2.05)	1.91 (1.84 , 1.98)	1.83 (1.62 , 2.04)	2.18 (2.14 , 2.21)	1.65 (1.45 , 1.85)
_Al, 10 ³	6.55 (5.27 , 7.83)	7.07 (6.62 , 7.51)	7.98 (6.73 , 9.24)	10.0 (8.86 , 11.1)	7.40 (4.54 , 10.3)	7.04 (5.64 , 8.44)	7.35 (4.69 , 10.0)
_Fe, 10 ³	7.81 (6.41 , 9.20)	9.80 (8.83 , 10.8)	9.33 (8.83 , 9.84)	10.8 (10.2 , 11.5)	10.3 (8.30 , 12.4)	8.84 (8.36 , 9.31)	8.89 (8.23 , 9.55)
_Mn	190 (162 , 217)	324 (280 , 369)	304 (288 , 320)	333 (318 , 348)	323 (288 , 359)	330 (324 , 336)	264 (236 , 292)
Sequential P-fractions,^h mg-P kg⁻¹							
_NH ₄ Cl	22.5 (6.4 , 45.0)	15.3 (12.1 , 18.7)	19.3 (14.5 , 24.5)	15.2 (12.3 , 18.3)	16.5 (14.2 , 18.9)	17.8 (14.5 , 21.1)	17.3 (13.6 , 21.4)
BS	44.2 (36.3 , 52.8)	34.8 (22.8 , 48.8)	35.9 (24.2 , 49.5)	36.9 (32.0 , 42.0)	33.9 (25.1 , 43.5)	39.5 (32.3 , 47.3)	37.2 (23.7 , 53.5)
_BD	119 (77.6 , 169)	88.0 (76.2 , 101)	100 (88.9 , 112)	86.4 (62.3 , 113)	87.1 (70.1 , 106)	92.4 (84.5 , 100)	86.8 (70.3 , 103)
BS	174 (138 , 213)	115 (84.4 , 150)	121 (81.0 , 168)	127 (114 , 142)	126 (91.4 , 164)	134 (113 , 156)	137 (34.9 , 287)
_NaOH	68.2 (43.5 , 98.4)	49.9 (39.9 , 60.7)	38.4 (28.3 , 49.3)	46.1 (39.2 , 53.6)	63.5 (44.9 , 84.6)	53.2 (46.4 , 59.9)	55.1 (45.5 , 65.5)
BS	65.4 (44.8 , 89.3)	58.7 (37.6 , 83.5)	48.3 (28.6 , 73.2)	64.0 (47.8 , 82.2)	67.4 (51.8 , 83.5)	54.8 (30.4 , 83.7)	40.7 (6.00 , 92.8)
_HCl	450 (319 , 598)	374 (317 , 436)	407 (384 , 431)	444 (400 , 490)	445 (371 , 526)	406 (375 , 438)	441 (376 , 510)
BS	579 (479 , 689)	463 (346 , 598)	476 (331 , 639)	492 (430 , 558)	510 (384 , 644)	486 (413 , 564)	509 (331 , 719)
_Residual	63.2 (36.2 , 97.6)	84.9 (56.4 , 116)	83.8 (76.2 , 91.8)	90.1 (62.7 , 120)	100 (75.9 , 128)	101 (87.2 , 114)	92.8 (74.4 , 113)
BS	73.1 (43.6 , 108)	102 (64.7 , 145)	108 (73.8 , 147)	116 (98.0 , 136)	112 (79.7 , 149)	116 (91.3 , 143)	99.2 (64.7 , 140)
_Total	723 (558 , 887)	692 (613 , 772)	649 (621 , 677)	682 (648 , 715)	713 (651 , 774)	671 (668 , 673)	612 (577 , 648)
BS	935 (832 , 1038)	824 (606 , 1042)	789 (593 , 985)	837 (755 , 918)	849 (665 , 1033)	830 (740 , 919)	773 (686 , 861)

Notes: () = 95% Confidence Interval; WGS-84 = World Geodetic System 1984 datum; ρ = Bulk density; θ = Volumetric Water Content; ORP = Oxidation-Reduction Potential; POM = Particulate Organic Matter; > 0.5mm = Sand particles larger than 0.5 mm; > 0.053mm = sand particles larger than 0.053 mm but smaller than 0.5 mm; Ca = Calcium; Al = Aluminum; Fe = Iron; Mn = Manganese; P = Phosphorus; NH₄Cl = Ammonium Chloride extracted P, loosely adsorbed P; BD = Bicarbonate/Dithionite extracted P, redox-sensitive P bound to Fe and Mn compounds; NaOH = Sodium Hydroxide extracted P, P exchangeable against OH- ions and bound in organic matter; HCl = Hydrochloric-acid extracted P, carbonate bound P; Residual = Acid-Digestion extracted P, refractory organic P and hyper-stable mineral P; Total = Sum total of P collected from each sequential fraction; BS = Rows are sediment values following a batch sorption isotherm experiment conducted at pH 8.5, 25°C, and an initial aqueous concentration of 3 mg-P L⁻¹; ^a Syringe method determined Bulk Density or VWC, average of top 10 cm of lakebed (Richwine et al. 2015); ^b Sodium-Hypochlorite removal of organic matter (Anderson 1961); ^c Hydrochloric-Acid removal of carbonates (Dhillon et al. 2015); ^d Particle-Size Determination of soil/sediment (Kettler et al. 2001); ^e Mineralogy by X-ray Diffraction and Rietveld fitting method (Bish & Post, 1993); ^f Non-glycolated clays by X-ray Diffraction, percentages represent relative abundances (Schultz 1964); ^g Chemical Composition by Acid-Digestion of Sediments (EPA 2007); ^h Sequential P-fractionation in sediments (Hupfer et al. 2009 and Gu et al. 2020)

Table 2. Sequential P-fractionation percentages for sediment collected using an Ekman dredge from the top 10 cm of the lakebed. Sediments were collected from 7 locations across the lake in August 2021. Rows labeled with BS are percentages obtained from sediments following a BSI experiment conducted at pH 8.5, 25°C, and an initial aqueous concentration of 3 mg-P L⁻¹.

Location Site ID	Provo Bay PB	Provo PV	Vineyard VY	Bird Island BI	Goshen Bay GB	Saratoga Springs SS	Pelican Point PP
Latitude, ^{WGS-84} °N	40.1846	40.2357	40.3002	40.1654	40.0906	40.337	40.2703
Longitude, ^{WGS-84} °W	-111.7162	-111.7668	-111.8020	-111.7788	-111.8915	-111.8687	-111.8364
Sequential P-fractions, ^a %							
_NH ₄ Cl	3.11 (1.15 , 5.07) BS 4.72 (4.36 , 5.08)	2.49 (2.10 , 2.89) 4.50 (3.33 , 5.67)	2.98 (2.34 , 3.62) 4.55 (4.07 , 5.03)	2.23 (1.90 , 2.56) 4.40 (4.24 , 4.57)	2.32 (2.19 , 2.45) 3.99 (3.77 , 4.21)	2.65 (2.18 , 3.13) 4.76 (4.37 , 5.15)	2.50 (2.23 , 2.77) 4.52 (3.91 , 5.13)
_BD	16.5 (13.9 , 19.0) BS 18.5 (16.6 , 20.5)	14.4 (13.2 , 15.5) 14.8 (12.3 , 17.4)	15.4 (14.3 , 16.5) 15.4 (13.7 , 17.1)	12.7 (9.61 , 15.7) 15.2 (15.0 , 15.4)	12.2 (10.8 , 13.7) 14.8 (13.7 , 15.9)	13.8 (12.7 , 14.9) 16.1 (15.2 , 17.0)	12.4 (11.5 , 13.3) 16.7 (5.76 , 27.6)
_NaOH	9.44 (7.79 , 11.1) BS 6.99 (5.39 , 8.60)	8.14 (6.91 , 9.38) 7.59 (5.49 , 9.70)	5.92 (4.56 , 7.28) 6.13 (4.82 , 7.43)	6.77 (6.04 , 7.49) 7.64 (6.33 , 8.95)	8.91 (6.89 , 10.9) 7.94 (7.79 , 8.09)	7.93 (6.95 , 8.90) 6.61 (4.11 , 9.11)	7.95 (7.42 , 8.49) 4.95 (0.98 , 8.91)
_HCl	62.2 (57.1 , 67.4) BS 61.9 (57.5 , 66.3)	61.1 (55.0 , 67.3) 59.9 (50.4 , 69.4)	62.8 (61.9 , 63.7) 60.3 (55.7 , 64.9)	65.1 (61.7 , 68.5) 58.8 (57.0 , 60.7)	62.5 (56.9 , 68.0) 60.1 (57.8 , 62.4)	60.6 (56.1 , 65.1) 58.6 (55.8 , 61.4)	63.8 (61.5 , 66.1) 61.8 (54.6 , 69.0)
_Residual	8.75 (6.49 , 11.0) BS 7.81 (5.23 , 10.4)	13.9 (9.76 , 18.0) 13.1 (9.43 , 16.9)	12.9 (12.3 , 13.6) 13.7 (12.4 , 14.9)	13.2 (9.68 , 16.8) 13.9 (13.0 , 14.8)	14.1 (11.7 , 16.5) 13.2 (12.0 , 14.4)	15.0 (13.1 , 17.0) 13.9 (12.3 , 15.5)	13.4 (12.2 , 14.7) 12.0 (10.7 , 13.4)

Notes: () = 95% Confidence Interval; WGS-84 = World Geodetic System 1984 datum; P = Phosphorus; NH₄Cl = Ammonium Chloride extracted P, loosely adsorbed P; BD = Bicarbonate/Dithionite extracted P, redox-sensitive P bound to Fe and Mn compounds; NaOH = Sodium Hydroxide extracted P, P exchangeable against OH- ions and bound in organic matter; HCl = Hydrochloric-acid extracted P, carbonate bound P; Residual = Acid-Digestion extracted P, refractory organic P and hyper-stable mineral P; ^a Sequential P-fractionation in sediments (Hupfer et al. 2009 and Gu et al. 2020)

Table 3. Physiochemical properties of Utah Lake column waters gathered using a peristaltic pump attached to a hand drill. Waters were collected from 7 locations across the lake in Fall 2021.

Location Site ID	Provo Bay PB	Provo PV	Vineyard VY	Bird Island BI	Goshen Bay GB	Saratoga Springs SS	Pelican Point PP
Latitude, ^{WGS-84} °N	40.1846	40.2357	40.3002	40.1654	40.0906	40.337	40.2703
Longitude, ^{WGS-84} °W	-111.7162	-111.7668	-111.8020	-111.7788	-111.8915	-111.8687	-111.8364
Temperature, ^{DWQ} °C	23.0 (20.6 , 25.5)	24.6 (24.5 , 24.7)	24.1 (24.1 , 24.2)	26.5 (26.4 , 26.7)	20.9 (20.9 , 21.0)	25.1 (25.1 , 25.1)	25.2 (25.0 , 25.4)
Conductivity, ^{DWQ} $\mu\text{S cm}^{-1}$	1442 (982 , 1902)	2418 (2405 , 2431)	2399 (2395 , 2402)	2380 (2373 , 2387)	2746 (2741 , 2751)	2424 (2422 , 2425)	2342 (2318 , 2365)
pH ^{DWQ}	8.48 (6.39 , 10.58)	8.88 (8.87 , 8.88)	8.85 (8.84 , 8.86)	8.89 (8.89 , 8.90)	8.21 (8.15 , 8.28)	8.74 (8.73 , 8.75)	8.75 (8.73 , 8.77)
ORP, rel. mV	201 (154 , 248)	250 (213 , 288)	255 (231 , 279)	245 (124 , 365)	212 (187 , 238)	287 (268 , 306)	132 (108 , 155)
Alkalinity, ^{DWQ} mg L ⁻¹	176	182	172	169	195	170	175
Turbidity, ^{DWQ} NTU	56.2	39.8	27.1	21.6	38.2	24.6	33.3
Solids, mg L ⁻¹							
_Total Dissolved Solids ^{DWQ}	914	1420	1410	1430	1730	1450	1370
_Total Suspended Solids ^{DWQ}	132	53	55	42	93	69	53
_Total Volatile Solids ^{DWQ}	36	17	17	15	20	23	17
Isotopes, ^a %							
_δ ² H _{VSMOW}	-117 (-119 , -114)	-50.5 (-54.5 , -46.6)	-49.7 (-50.5 , -48.9)				-51.7 (-52.1 , -51.3)
_δ ¹⁸ O _{VSMOW}	-15.0 (-15.3 , -14.7)	-4.27 (-5.05 , -3.50)	-4.33 (-4.40 , -4.26)				-4.90 (-5.21 , -4.59)
Nutrients & Organics, mg L ⁻¹							
_N ^{DWQ}	2.41 (0.00 , 4.94)	0.78 (0.18 , 1.38)	0.85 (0.70 , 1.00)	0.89 (0.00 , 2.04)	1.29 (0.21 , 2.38)	0.79 (0.78 , 0.80)	0.75 (0.29 , 1.20)
_NH ₃ ^{DWQ}	0.0379	0.0085	0.0085	0.0085	0.0085	0.0085	0.0085
_Organic-C ^{DWQ}	23.1 (0.34 , 45.8)	8.90 (7.50 , 10.3)	10.6 (6.53 , 14.6)	10.9 (0.00 , 38.8)	14.1 (0.00 , 53.5)	8.84 (5.72 , 12.0)	8.46 (8.27 , 8.66)
_Dissolved-O ^{DWQ}	7.15 (0.00 , 24.8)	7.90 (7.74 , 8.06)	7.88 (7.77 , 7.98)	8.77 (8.70 , 8.84)	5.66 (5.59 , 5.72)	9.49 (9.47 , 9.52)	7.63 (7.35 , 7.90)
_Dissolved-O Saturation, ^{DWQ} %	98.0 (0.00 , 321)	113 (111 , 115)	111 (110 , 113)	130 (129 , 130)	75.8 (74.3 , 77.2)	137 (137 , 137)	110 (106 , 114)
_Chlorophyll-a, ^{DWQ} µg L ⁻¹	183 (0.00 , 385)	51.6 (0.00 , 118)	59.7 (0.00 , 125)	54.4 (0.00 , 121)	72.5 (0.00 , 171)	84.2 (0.00 , 189)	52.6 (0.00 , 121)
_Pheophytin-a, ^{DWQ} µg L ⁻¹	8.25	1.98	4.44	1.98	4.61	2.47	2.47
Cations, ^b mg L ⁻¹							
_Ca	sur 47.9 (45.9 , 49.8)	54.1 (46.0 , 62.1)	15.6 (12.7 , 18.4)	19.5 (15.1 , 23.9)	9.42 (5.47 , 13.4)	15.9 (3.06 , 28.7)	21.1 (19.8 , 22.3)
	mid 51.4 (49.3 , 53.5)	53.2 (50.5 , 55.9)	19.1 (10.6 , 27.7)	22.1 (15.6 , 28.5)	10.7 (6.16 , 15.2)	14.8 (3.17 , 26.4)	16.9 (15.4 , 18.3)
	bot 55.8 (50.1 , 61.5)	49.2 (31.8 , 66.6)	13.5 (1.48 , 25.4)	16.7 (16.3 , 17.1)	17.0 (14.0 , 19.9)	16.3 (7.13 , 25.4)	24.8 (22.4 , 27.1)
_K	sur 14.4 (14.1 , 14.7)	27.1 (23.7 , 30.4)	12.9 (11.7 , 14.0)	14.7 (12.4 , 17.0)	10.7 (7.53 , 13.9)	12.6 (6.17 , 19.0)	17.1 (16.1 , 18.1)
	mid 15.6 (15.0 , 16.2)	28.2 (27.0 , 29.4)	14.1 (10.5 , 17.8)	16.0 (13.0 , 19.1)	11.0 (8.30 , 13.7)	11.8 (5.84 , 17.7)	13.2 (12.6 , 13.9)
	bot 16.8 (15.6 , 17.9)	25.4 (19.1 , 31.7)	11.6 (5.84 , 17.3)	13.5 (13.0 , 14.0)	10.9 (9.37 , 12.3)	12.4 (7.40 , 17.5)	15.1 (14.0 , 16.3)
_Mg	sur 49.3 (47.4 , 51.2)	80.5 (71.6 , 89.4)	27.8 (22.6 , 33.1)	32.9 (25.1 , 40.6)	16.5 (9.24 , 23.7)	27.7 (4.74 , 50.7)	44.2 (39.4 , 49.0)
	mid 56.1 (54.1 , 58.2)	83.7 (80.4 , 87.0)	33.3 (18.0 , 48.7)	36.9 (25.7 , 48.1)	16.9 (9.40 , 24.5)	26.1 (5.02 , 47.1)	29.6 (26.8 , 32.4)
	bot 58.1 (51.8 , 64.5)	72.5 (48.1 , 97.0)	21.4 (1.42 , 41.4)	27.4 (26.6 , 28.2)	16.4 (13.8 , 18.9)	28.7 (12.7 , 44.7)	37.3 (35.0 , 39.5)
_Na	sur 139 (135 , 144)	290 (268 , 311)	127 (111 , 144)	150 (122 , 179)	104 (69.4 , 139)	126 (49.2 , 204)	179 (171 , 186)
	mid 161 (154 , 168)	294 (274 , 315)	144 (99.5 , 189)	164 (129 , 199)	108 (76.1 , 139)	118 (48.4 , 189)	133 (124 , 143)
	bot 172 (160 , 184)	264 (213 , 315)	111 (43.3 , 179)	135 (131 , 138)	104 (87.9 , 120)	127 (69.8 , 183)	156 (144 , 167)
_Fe, 10 ⁻³	sur 60.3 (56.5 , 64.1)	68.3 (60.3 , 76.3)	19.7 (0.00 , 82.8)	9.00 (0.00 , 26.2)	5.00 (0.00 , 11.6)	6.00 (0.00 , 19.1)	11.3 (0.00 , 32.2)
	mid 30.3 (18.1 , 42.6)	65.0 (62.5 , 67.5)	13.7 (7.41 , 19.9)	18.0 (0.00 , 65.4)	28.0 (0.00 , 61.4)	7.33 (0.00 , 26.1)	8.33 (6.90 , 9.77)
	bot 99.3 (83.2 , 116)	86.0 (42.9 , 129)	15.3 (0.99 , 29.7)	89.7 (0.00 , 347)	151 (0.00 , 351)	4.00 (0.00 , 10.6)	10.7 (0.00 , 22.9)
_P, 10 ⁻³	sur 65.3 (62.5 , 68.2)	54.3 (41.8 , 66.8)	14.0 (9.03 , 19.0)	13.0 (12.9 , 13.2)	10.3 (7.46 , 13.2)	11.7 (2.94 , 20.4)	15.3 (12.5 , 18.2)
	mid 40.3 (36.5 , 44.1)	47.3 (41.1 , 53.6)	19.7 (5.98 , 33.3)	13.0 (8.70 , 17.3)	21.3 (11.0 , 31.7)	10.7 (2.68 , 18.7)	11.7 (10.2 , 13.1)
	bot 107 (95.5 , 118)	57.3 (42.8 , 71.9)	17.0 (6.17 , 27.8)	10.7 (6.87 , 14.5)	55.7 (49.4 , 61.9)	12.0 (9.52 , 14.5)	19.3 (13.6 , 25.1)
Anions, mg L ⁻¹							
_Cl ⁻ ^{DWQ}	236	453	435	433	545	458	442
_NO ₃ ⁻ + NO ₂ ⁻ ^{DWQ}	0.0115	0.0115	0.0115	0.0115	0.0115	0.0115	0.0115
_SO ₄ ²⁻ ^{DWQ}	281	367	365	369	434	373	355
_PO ₄ ³⁻ ^{DWQ}	0.0823	0.0682	0.0648	0.0651	0.0658	0.0618	0.0691

Notes: () = 95% Confidence Interval; WGS-84 = World Geodetic System 1984 datum; DWQ = Data derived using the Utah Department of Water Quality (DWQ) Utah Lake Data Explorer (ULDE) for August 2021; ORP = Oxidation-Reduction Potential; VSMOW = Vienna Standard Mean Ocean Water; sur = Waters in row collected from ~4 cm below water surface; mid = Waters in row collected from ~1-2 m below water surface; bot = Waters in row collected from ~3-4 m below water surface; C = Carbon; Ca = Calcium; Cl⁻ = Chloride; Fe = Iron; H = Hydrogen; K = Potassium; O = Oxygen; Mg = Magnesium; N = Nitrogen; Na = Sodium; NH₃ = Ammonia; NO₃⁻ + NO₂⁻ = Nitrate and Nitrite; SO₄²⁻ = Sulfate; P = Phosphorus; PO₄³⁻ = Orthophosphate; ^a Waters collected on November 15, 2021 and analyzed using a Los Gatos Research cavity ring-down Liquid Water Isotope Analyzer; ^b Waters collected on August 20, 2021, filtered (0.45 microns), acidified, and analyzed using Inductively Coupled Plasma Optical Emission spectroscopy

Table 4. Coefficient values from Linear, Freundlich, and Langmuir sorption models fitted to Q (sediment sorbed P, mg-P kg⁻¹) vs. C_f (equilibrium aqueous-P concentration, mg-P L⁻¹) trends. Data obtained from BSI experiments which reacted Utah Lake sediment and water collected from 7 locations across the lake. Experiments were performed at approximately 25°C with pH intervals at 7.5, 8.0, 8.5, and 9.0 for 24 hours. Initial aqueous-P concentrations for batch experiments ranged from 0 to 760 mg-P L⁻¹.

Location Site ID	Provo Bay PB	Provo PV	Vineyard VY	Bird Island BI	Goshen Bay GB	Saratoga Springs SS	Pelican Point PP	
Latitude, ^{WGS-84} °N	40.1846	40.2357	40.3002	40.1654	40.0906	40.337	40.2703	
Longitude, ^{WGS-84} °W	-111.7162	-111.7668	-111.8020	-111.7788	-111.8915	-111.8687	-111.8364	
X, ^a mg-P L ⁻¹	1.07 (0.42 , 1.72)	0.81 (0.51 , 1.11)	0.40 (0.18 , 0.62)	0.70 (0.28 , 1.13)	0.50 (0.25 , 0.75)	0.36 (0.15 , 0.56)	0.30 (0.16 , 0.44)	
Linear: Q = K _d ·(C _f) + b _d								
_K _d , L kg ⁻¹	pH 7.5 pH 8.0 pH 8.5-A pH 8.5 pH 9.0	11.7 (10.8 , 12.5) 14.0 (6.47 , 21.5) 18.8 (15.2 , 22.4) 41.7 (37.1 , 46.3) 145 (126 , 165)	15.2 (13.2 , 17.1) 18.5 (17.5 , 19.5) 17.9 (15.9 , 19.9) 34.2 (31.5 , 37.0) 63.5 (60.6 , 66.4)	18.7 (17.9 , 19.5) 19.0 (17.5 , 20.4) 32.4 (24.6 , 40.2) 56.7 (52.7 , 60.7) 74.3 (56.8 , 91.7)	16.2 (15.2 , 17.3) 18.1 (16.4 , 19.7) 19.6 (16.4 , 22.8) 38.0 (34.2 , 41.7) 74.3 (69.6 , 79.1)	18.8 (17.6 , 20.1) 17.2 (14.3 , 20.1) 17.4 (15.6 , 19.2) 33.3 (31.0 , 35.6) 58.9 (55.1 , 62.7)	13.9 (13.4 , 14.5) 40.337 32.6 (30.2 , 34.9) 33.1 (30.6 , 35.6) 50.8 (49.4 , 52.2) 73.5 (69.4 , 77.6)	
_b _d , mg-P kg ⁻¹	pH 7.5 pH 8.0 pH 8.5-A pH 8.5 pH 9.0	-8.72 (-23.4 , 0.00) -51.7 (-268 , 0.00) -13.8 (-60.0 , 0.00) -63.9 (-101 , -26.8) -58.7 (-109 , -8.44)	-10.3 (-38.5 , 0.00) -16.8 (-29.8 , -3.87) -18.7 (-66.8 , 0.00) -16.2 (-38.6 , 0.00) -49.5 (-65.2 , -33.8)	-6.67 (-17.3 , 0.00) -14.0 (-32.8 , 0.00) -24.0 (-97.8 , 0.00) -19.8 (-48.1 , 0.00) -79.0 (-165.1 , 0.00)	-13.3 (-28.3 , 0.00) -12.7 (-28.9 , 0.00) -10.7 (-32.7 , 0.00) -3.84 (-26.5 , 0.00) -15.7 (-36.4 , 0.00)	-12.7 (-28.9 , 0.00) -5.46 (-29.3 , 0.00) -3.98 (-74.7 , 0.00) -7.30 (-28.2 , 0.00) -45.0 (-66.4 , -23.6)	-6.35 (-14.4 , 0.00) -10.0 (-29.9 , 0.00) -19.5 (-37.7 , -1.30) -26.4 (-35.0 , -17.8) -19.5 (-37.7 , -1.30)	
_R ²	pH 7.5 pH 8.0 pH 8.5-A pH 8.5 pH 9.0	0.9972 0.7345 0.9815 0.9591 0.9907	0.9918 0.9985 0.9850 0.9728 0.9989	0.9990 0.9969 0.9323 0.9803 0.9722	0.9969 0.9978 0.9676 0.9592 0.9979	0.9978 0.9977 0.9956 0.9865 0.9979	0.9977 0.9993 0.9660 0.9753 0.9996	0.9993 0.9946 0.9773 0.9984
Freundlich: Q = K _f ·(C _f) ^(1/n) + b _f								
_K _f , L kg ⁻¹	pH 7.5 pH 8.0 pH 8.5-A pH 8.5 pH 9.0	56.5 (37.9 , 75.1) 99.1 (-19.1 , 217) 165 (77.5 , 252) 379 (202 , 555) 1000 (307 , 1693)	69.5 (48.0 , 90.9) 214 (105 , 323) 272 (71.2 , 474) 331 (86.8 , 574) 1000 (395 , 1605)	118 (76.8 , 160) 113 (33.4 , 192) 240 (31.2 , 449) 380 (173 , 586) 1000 (432 , 1568)	133 (75.0 , 190) 133 (75.0 , 190) 157 (68.4 , 246) 298 (142 , 453) 965 (370 , 1560)	169 (97.2 , 241) 128 (54.9 , 201) 267 (123 , 410) 712 (520 , 904) 712 (520 , 904)	91.1 (61.0 , 121) 165 (-15.2 , 346) 276 (169 , 384) 702 (424 , 979) 1000 (148 , 1852)	
_b _f , mg-P kg ⁻¹	pH 7.5 pH 8.0 pH 8.5-A pH 8.5 pH 9.0	-57.4 (-116 , 0.00) -145 (-440 , 0.00) -155 (-305 , -4.07) -403 (-640 , -165) -766 (-1499 , -33.5)	-66.2 (-128 , -4.26) -219 (-386 , -51.7) -343 (-652 , -33.2) -289 (-602 , 0.00) -952 (-1607 , -297)	-90.2 (-175 , -4.98) -109 (-283 , 0.00) -305 (-671 , 0.00) -855 (-1346 , -364) -981 (-1606 , -356)	-109 (-283 , 0.00) -136 (-249 , -23.7) -302 (-649 , 0.00) -339 (-596 , -81.7) -769 (-1386 , -152)	-136 (-249 , -23.7) -157 (-279 , -36.0) -150 (-310 , 0.00) -258 (-486 , -30.8) -678 (-897 , -458)	-157 (-279 , -36.0) -72.0 (-140 , -4.40) -110 (-258 , 0.00) -207 (-399 , -14.9) -621 (-926 , -315)	-132 (-423 , 0.00) -223 (-366 , -79.6) -802 (-1682 , 0.00)
_n	pH 7.5 pH 8.0 pH 8.5-A pH 8.5 pH 9.0	1.69 (1.53 , 1.84) 1.92 (1.22 , 2.62) 2.40 (1.94 , 2.87) 3.11 (2.48 , 3.73) 5.07 (2.93 , 7.22)	1.74 (1.58 , 1.89) 2.72 (2.16 , 3.27) 2.77 (1.94 , 3.61) 3.00 (2.04 , 3.96) 5.32 (3.34 , 7.29)	2.09 (1.84 , 2.33) 2.00 (1.55 , 2.44) 2.90 (1.95 , 3.85) 5.92 (4.04 , 7.81) 5.12 (3.39 , 6.85)	2.00 (1.55 , 2.44) 2.20 (1.87 , 2.53) 2.52 (1.69 , 3.36) 3.14 (2.38 , 3.91) 5.59 (3.37 , 7.81)	2.20 (1.87 , 2.53) 2.45 (2.06 , 2.84) 2.33 (1.85 , 2.80) 2.82 (2.22 , 3.42) 4.29 (3.66 , 4.92)	2.45 (2.06 , 2.84) 2.00 (1.79 , 2.20) 2.11 (1.71 , 2.51) 2.74 (2.14 , 3.35) 4.72 (3.64 , 5.80)	2.00 (1.79 , 2.20) 2.54 (1.47 , 3.60) 2.79 (2.34 , 3.23) 6.12 (2.67 , 9.57)
_R ²	pH 7.5 pH 8.0 pH 8.5-A pH 8.5 pH 9.0	0.9970 0.9544 0.9902 0.9796 0.9872	0.9973 0.9899 0.9950 0.9822 0.9907	0.9950 0.9835 0.9744 0.9820 0.9920	0.9835 0.9930 0.9877 0.9633 0.9852	0.9930 0.9928 0.9879 0.9731 0.9978	0.9928 0.9959 0.9500 0.9615 0.9946	0.9959 0.9500 0.9790
Langmuir: Q = (S _{max} ·K _l ·C _f)·(1 + K _l ·C _f) ⁻¹ + b _l								
_K _l , 10 ⁻³ L kg ⁻¹	pH 7.5 pH 8.0 pH 8.5-A pH 8.5 pH 9.0	3.89 (3.06 , 4.71) 6.00 (2.40 , 9.70) 9.26 (6.26 , 12.3) 11.2 (7.83 , 14.6) 71.2 (38.1 , 104)	4.36 (3.46 , 5.26) 10.8 (9.73 , 11.8) 10.7 (8.70 , 12.7) 13.4 (7.72 , 19.1) 36.1 (27.1 , 45.1)	7.37 (6.55 , 8.19) 6.27 (4.18 , 8.35) 20.0 (10.8 , 21.1) 30.0 (24.7 , 41.0) 29.8 (19.9 , 39.7)	7.45 (6.80 , 8.09) 7.45 (6.80 , 8.09) 10.2 (6.78 , 13.6) 14.0 (9.32 , 18.6) 46.5 (36.2 , 56.8)	9.00 (8.07 , 10.5) 7.51 (5.39 , 9.64) 10.0 (7.56 , 14.7) 11.7 (7.55 , 15.8) 24.1 (16.3 , 32.0)	6.31 (5.19 , 7.43) 10.3 (5.20 , 15.4) 11.2 (8.10 , 14.2) 28.8 (23.1 , 34.6) 55.6 (43.3 , 67.8)	
_b _l , mg-P kg ⁻¹	pH 7.5 pH 8.0 pH 8.5-A pH 8.5 pH 9.0	0.00 (0.00 , 0.00) -58.7 (-221 , 0.00) 0.00 (0.00 , 0.00) 0.00 (0.00 , 0.00) -22.0 (-212 , 0.00)	0.00 (0.00 , 0.00) -13.0 (-38.1 , 0.00) -13.8 (-129 , 0.00) 0.00 (0.00 , 0.00) -35.4 (-125 , 0.00)	0.00 (0.00 , 0.00) 0.00 (0.00 , 0.00) -52.3 (-161 , 0.00) 0.00 (0.00 , 0.00) -11.6 (-131 , 0.00)	-5.13 (-26.8 , 0.00) 0.00 (0.00 , 0.00) 0.00 (0.00 , 0.00) 0.00 (0.00 , 0.00) -5.76 (-86.2 , 0.00)	0.00 (0.00 , 0.00) 0.00 (0.00 , 0.00)	0.00 (0.00 , 0.00) 0.00 (0.00 , 0.00) 0.00 (0.00 , 0.00) 0.00 (0.00 , 0.00) -22.6 (-102 , 0.00)	
_S _{max} , mg-P kg ⁻¹	pH 7.5 pH 8.0 pH 8.5-A pH 8.5 pH 9.0	3019 (2681 , 3356) 2886 (2264 , 3507) 2191 (1923 , 2460) 2643 (2382 , 2904) 2200 (2000 , 2444)	3176 (2840 , 3511) 2034 (1980 , 2088) 2406 (2279 , 2533) 2470 (2147 , 2793) 2072 (1951 , 2194)	2525 (2407 , 2643) 2839 (2415 , 3264) 2628 (2408 , 2847) 1976 (1873 , 2079) 2218 (2061 , 2376)	2399 (2331 , 2467) 2164 (2057 , 2271) 2342 (2159 , 2525) 2542 (2283 , 2802) 1973 (1870 , 2076)	2164 (2057 , 2271) 2342 (2160 , 2523) 2600 (2000 , 2902) 2555 (2262 , 2848) 2220 (2057 , 2382)	2342 (2160 , 2523) 1921 (1577 , 2265) 2586 (2353 , 2819) 2555 (2262 , 2848) 1881 (1780 , 1983)	1797 (1699 , 1895)
_R ²	pH 7.5 pH 8.0 pH 8.5-A pH 8.5 pH 9.0	0.9951 0.9693 0.9813 0.9576 0.9757	0.9951 0.9990 0.9961 0.9137 0.9925	0.9980 0.9842 0.9882 0.9796 0.9881	0.9993 0.9993 0.9930 0.9451 0.9932	0.9993 0.9968 0.9870 0.9416 0.9883	0.9968 0.9951 0.9529 0.9637 0.9904	0.9951 0.9

Table 5. Parameters and coefficients for kinetics experiments using Provo (PV) and Provo Bay (PB) sediment. For experiments, an input solution with a phosphorus (P) concentration of ~1.1 mg L⁻¹ in a lake water (pH 8.5, 24°C) background solution was pumped into a reaction chamber (~16 mL) agitated with a triangular stir-bar (100 rpm) at 1 mL min⁻¹ for 120 min. A 4.0 cm diameter filter membrane with a 0.45-μm pore size was used to retain the sediment in the chamber. A fraction collector was used to collect effluent samples at a 10 min interval. Sorption experiments were not followed by desorption experiments, which is not standard for kinetic adsorption testing (Sun & Selim 2019). Therefore, the results outlined here should be classified as scope or initial observations of kinetic behaviors between PV and PB sediment.

Location Site ID	Provo Bay PB	Provo PV
Latitude, ^{WGS-84} °N	40.1846	40.2357
Longitude, ^{WGS-84} °W	-111.7162	-111.7668
pH	8.46	8.46
Temperature, °C	24.4	24.4
ORP, rel. mV	221.4	221.4
Conductivity, μS cm ⁻¹	2435	2435
C ₀ , mg-P L ⁻¹	1.091	1.091
θ, L L ⁻¹	0.74	0.72
ρ, kg L ⁻¹	0.69	0.78
q, mL min ⁻¹	1.00	1.00
Nonlinear Kinetic Model: dS / dt = k _f *(θ / ρ)*C ^b - k _b *S		
b	-2.96 (-3.59, -2.32)	-4.52 (-5.49, -3.54)
k _f , min ⁻¹	0.482 (0.378, 0.587)	0.779 (0.514, 1.044)
k _b , min ⁻¹	0.003 (-0.001, 0.007)	0.003 (-0.003, 0.009)
R ²	0.7996	0.9640
Reactor		
	1	2
V _R , mL	16.28	16.04
M, g	0.322	0.320
	1	2

Notes: () = 95% Confidence Interval; WGS-84 = World Geodetic System 1984 datum; ρ = Bulk density; θ = Volumetric Water Content; ORP = Oxidation-Reduction Potential; C₀ = Influent P-concentration to stirred-flow reactor; q = rate of flow; b = order of retention; k_f = Forward retention rate; k_b = Backward retention rate; V_R = volume of stirred-flow reaction chamber; M = mass of sediment in reaction chamber; dS/dt = P-sorption over time; C = Effluent P-concentration from reactor; S = P sorbed to sediment in reactor

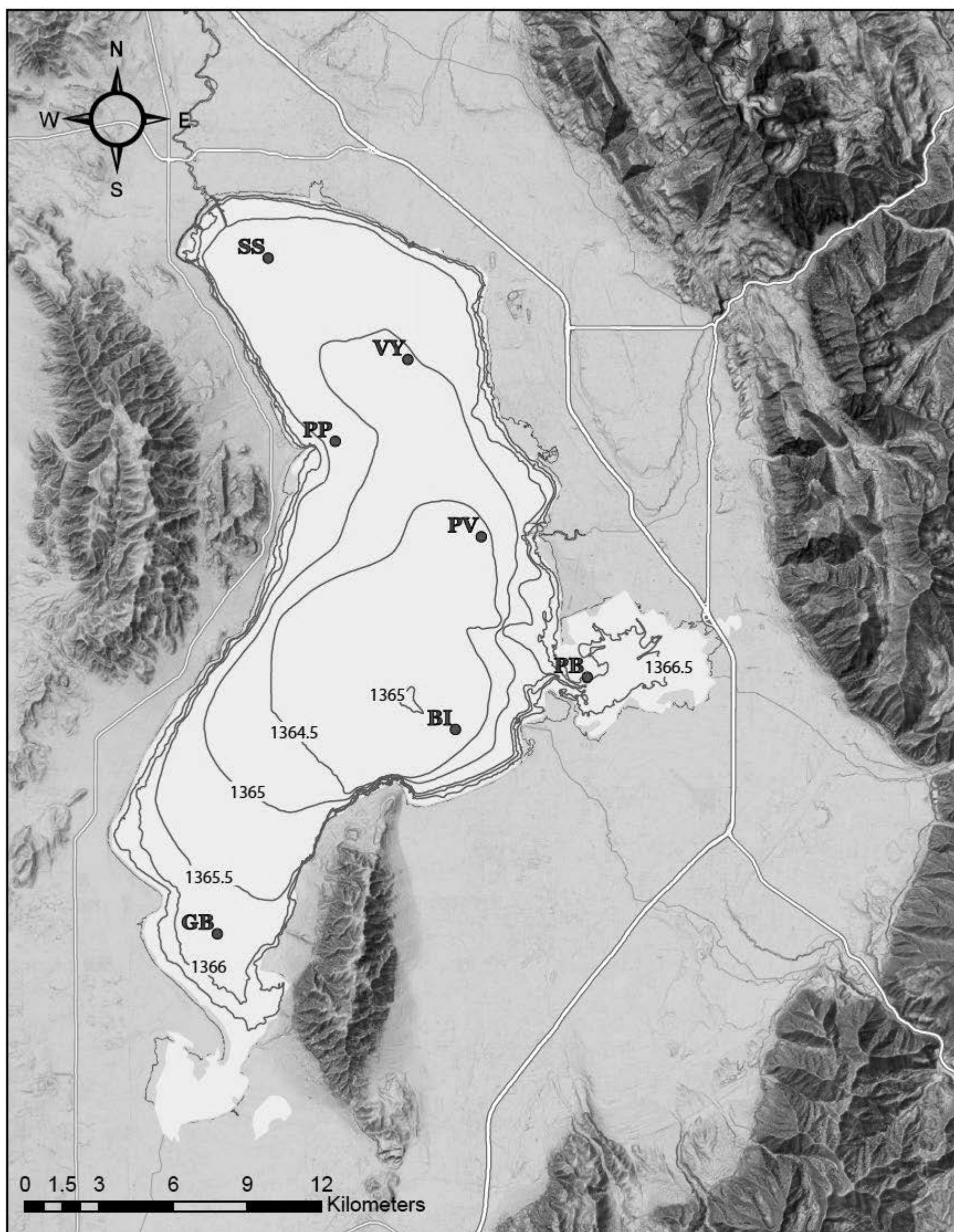


Figure 1. A map of Utah Lake showing the location of seven sampling sites: PB (Provo Bay), PV (Provo), VY (Vineyard), BI (Bird Island), GB (Goshen Bay), SS (Saratoga Springs), and PP (Pelican Point). Blue lines represent half-meter incremented bathymetric contour lines (m above sea-level) generated from depth measurements through surface ice in 1960 by the Bureau of Reclamation (Wawro 2011). The statewide 10 m hillshade (WMTS) used in this map is courtesy of the state of Utah and the Utah Automated Geographic Reference Center (AGRC 2016).

Notes: BSI = Batch sorption Isotherm; ppm = mg L⁻¹

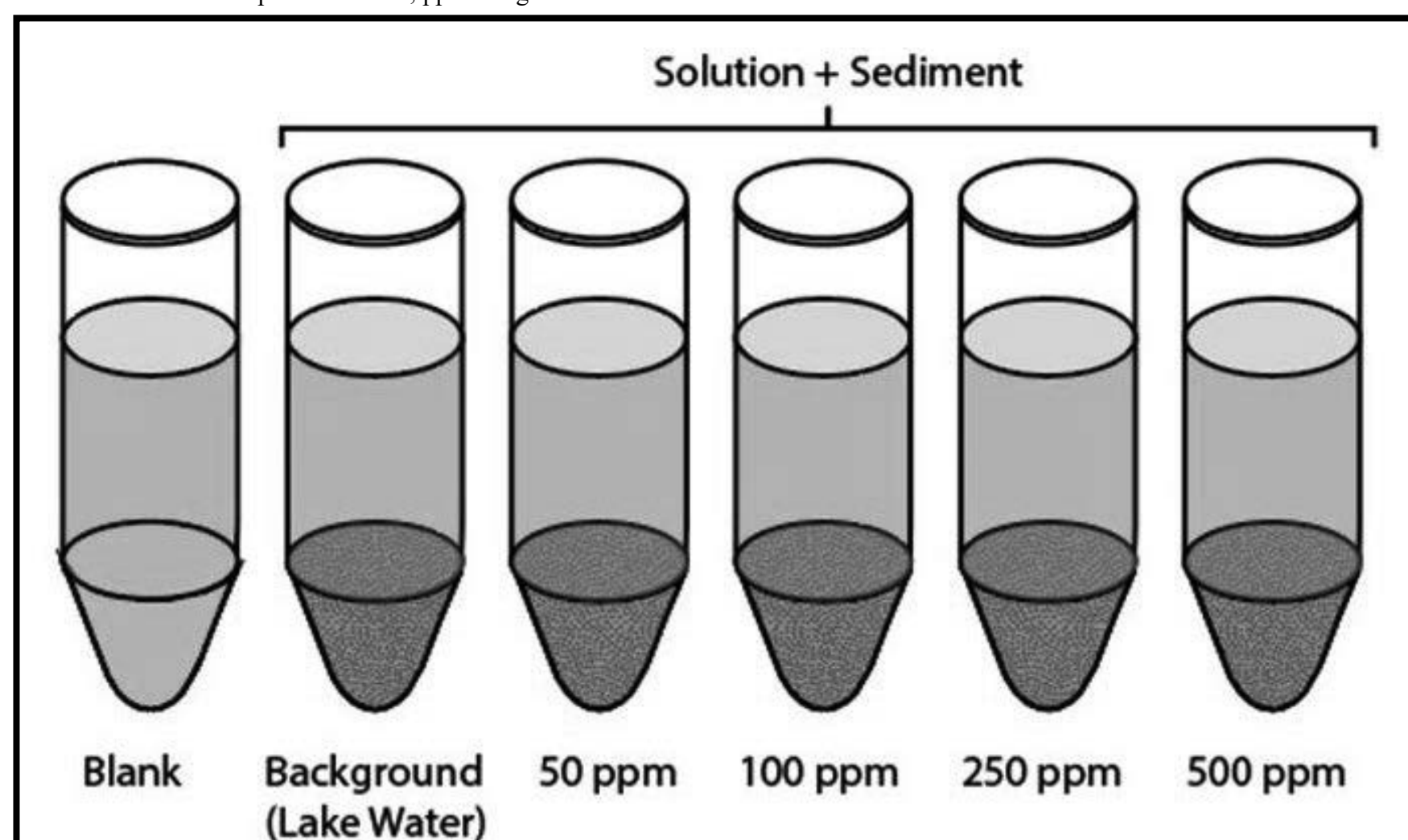


Figure 2. A schematic example of a BSI experiment in which sediment from a specific location or group is reacted with lake water spiked to a desired contaminant concentration.

Notes: SF = Stirred-flow

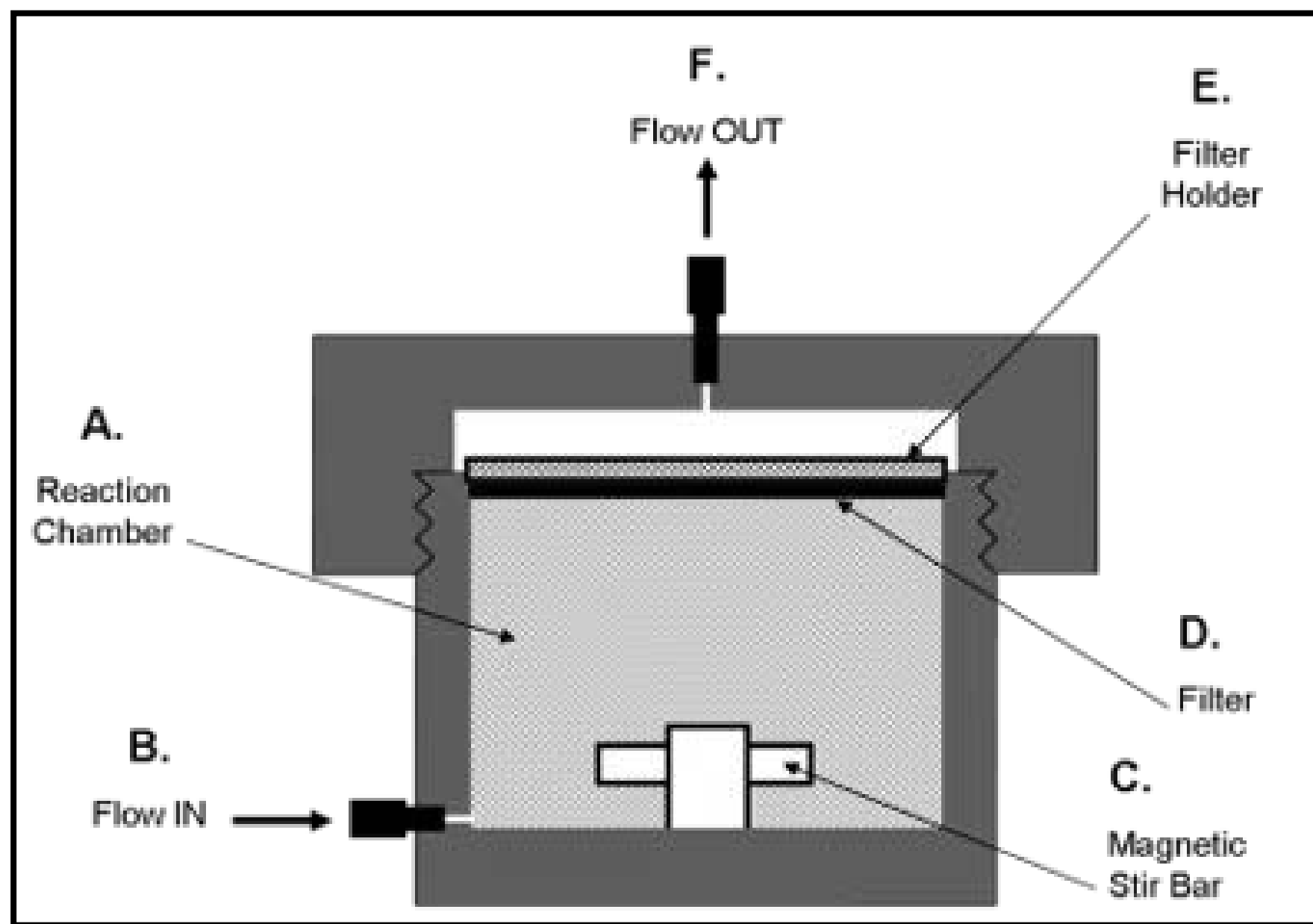


Figure 3. Schematic depiction of SF reaction chamber. Courtesy of Dr. Josh LeMonte.

Notes: PB = Provo Bay; PV = Provo; VY = Vineyard; BI = Bird Island; GB = Goshen Bay; SS = Saratoga Springs; PP = Pelican Point; OM = Organic matter; ^a = Hydrochloric-Acid removal of carbonates (Dhillon et al. 2015); ^b = Sodium-Hypochlorite or Bleach removal of organic matter (Anderson 1961)

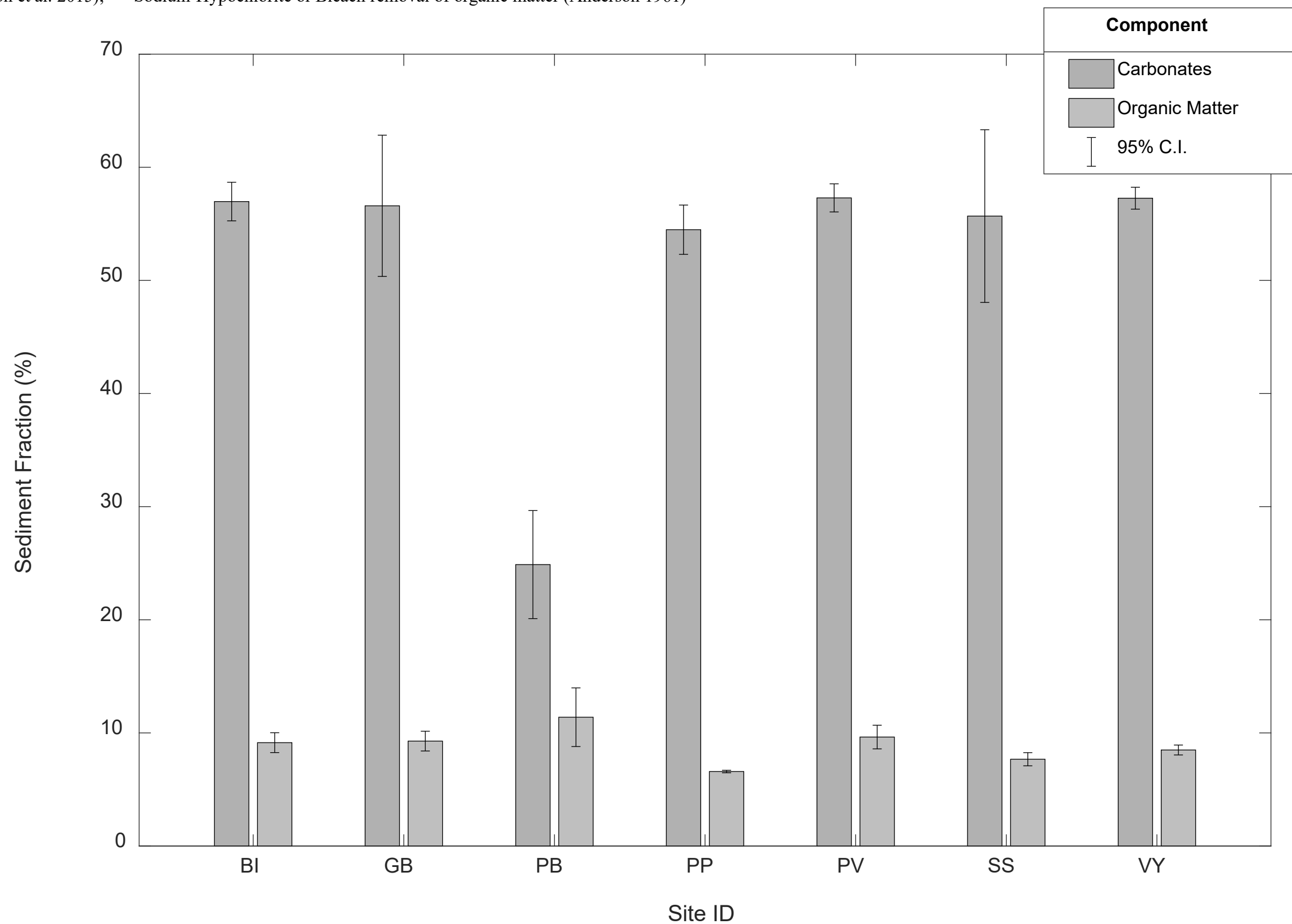


Figure 4. Carbonate percentages with their respective 95% confidence intervals as determined by ^aHCl digestion show PB to be significantly depleted when compared to all other locations. OM percentages with their respective 95% confidence intervals as determined by ^bNaOCl digestion show PP to be significantly depleted when compared to all other locations.

Notes: ^a = Particle-Size Determination of soil/sediment (Kettler et al. 2001); PB = Provo Bay; PV = Provo; VY = Vineyard; BI = Bird Island; GB = Goshen Bay; SS = Saratoga Springs; PP = Pelican Point

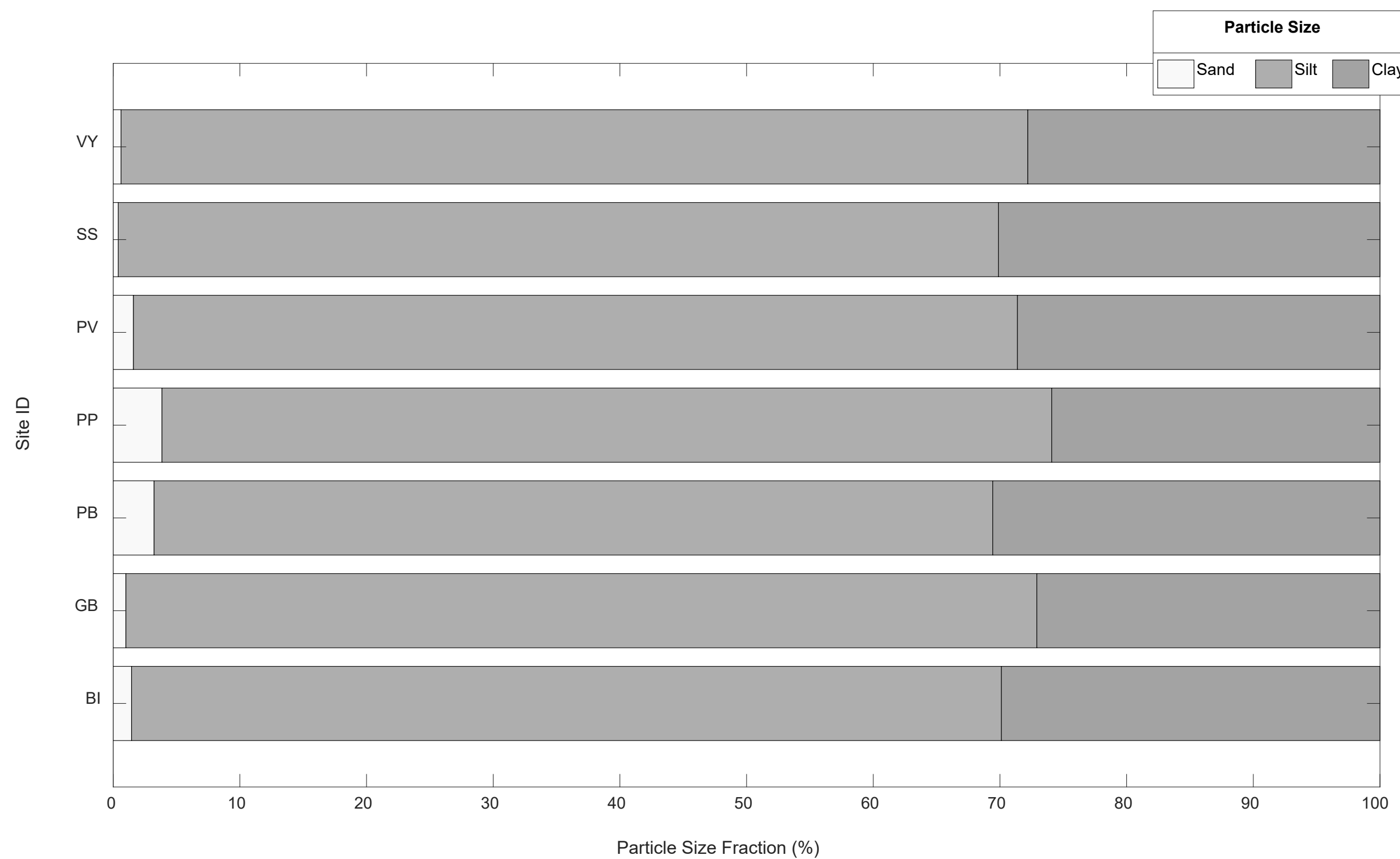


Figure 5. ^aParticle size distributions across the various locations within Utah Lake follow a similar trend. Each site has comparable amounts of silt and clay. Deviations in size fractions are only apparent in PB and PP where the sand fraction is 3.5 times greater than the rest of the lake.

Notes: C = carbon; O = Oxygen; PB = Provo Bay; PV = Provo; VY = Vineyard; BI = Bird Island; GB = Goshen Bay; SS = Saratoga Springs; PP = Pelican Point; OM = Organic matter; ^a = Mineralogy by X-ray Diffraction and Rietveld fitting method (Bish & Post, 1993)

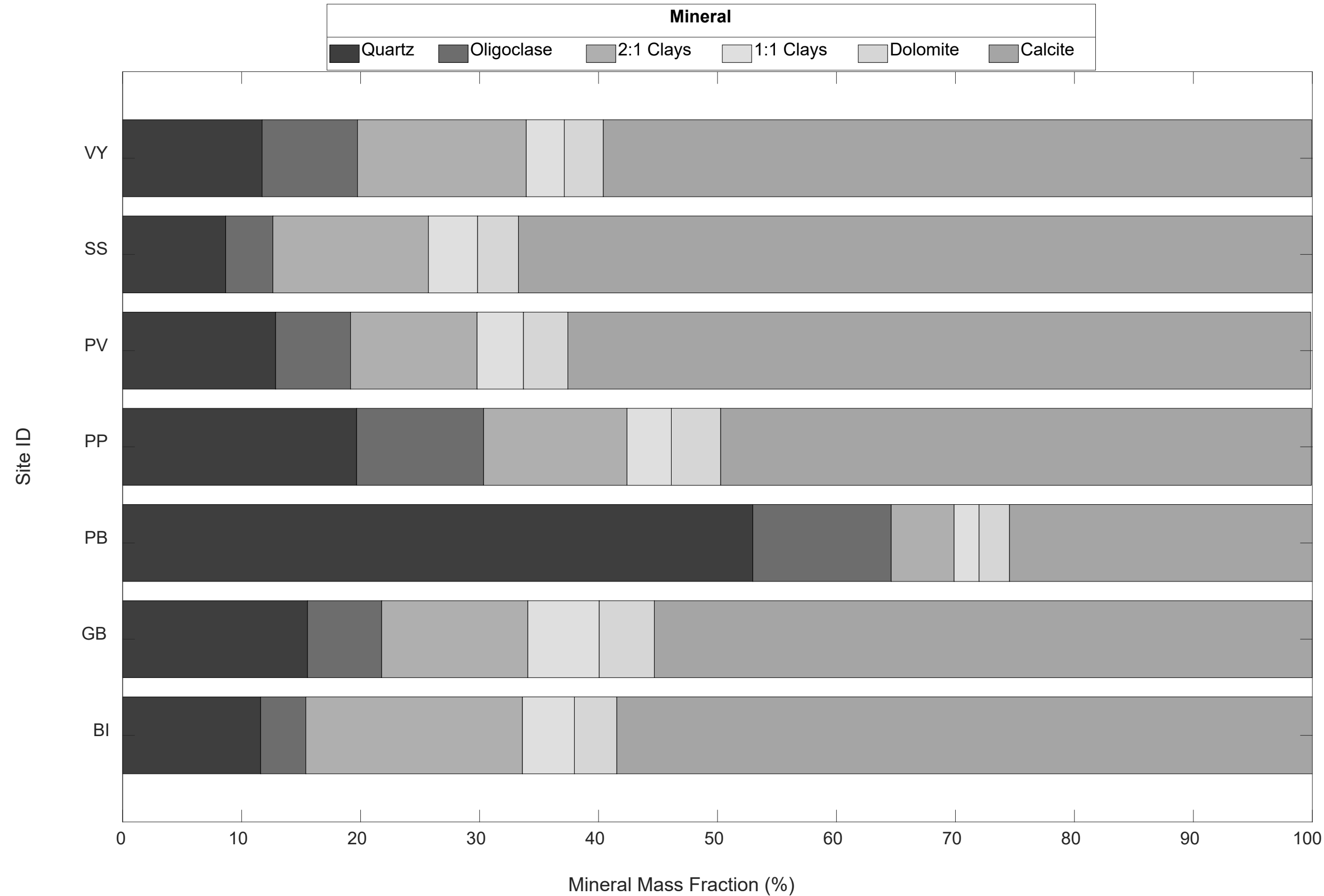


Figure 6. Mineral fractions across Utah Lake proper appear to be spatially consistent, excluding a significant enrichment of quartz found in PP. PB also significantly diverges from Utah Lake proper in terms of quartz and calcite content, being enriched with quartz but depleted of calcite. Clay content in terms of amount and type shows little variation across all Utah Lake sites, including PB. Given the lake's high alkalinity, most calcite found in the lakebed should originate from authigenic precipitation (Randall et al. 2019). However, without C and O isotope measurements from the sediment a specific amount of authigenic vs. alloigenic calcite cannot be given. The other detectable minerals, including dolomite, quartz, oligoclase, and clay, are detrital in origin, delivered via streams and rivers containing eroded materials from the mountains surrounding the lake. Additionally, Utah Lake sediment might contain authigenic metal hydroxides, however low concentrations yield the secondary minerals imperceptible using ^aXRD. Trends found in mineral fractions identified by ^aXRD follow the trends identified by particle size distributions and carbonate/OM digestions.

Notes: Ca = Calcium; Mn = Manganese; P = Phosphorus; OM = Organic matter; XRD = X-ray Diffraction; PB = Provo Bay; PV = Provo; VY = Vineyard; BI = Bird Island; GB = Goshen Bay; SS = Saratoga Springs; PP = Pelican Point; ^a = Chemical Composition by Acid-Digestion of Sediments (EPA 2007); ^b = Mineralogy by X-ray Diffraction and Rietveld fitting method (Bish & Post, 1993); ^c = Hydrochloric-Acid removal of carbonates (Dhillon et al. 2015)

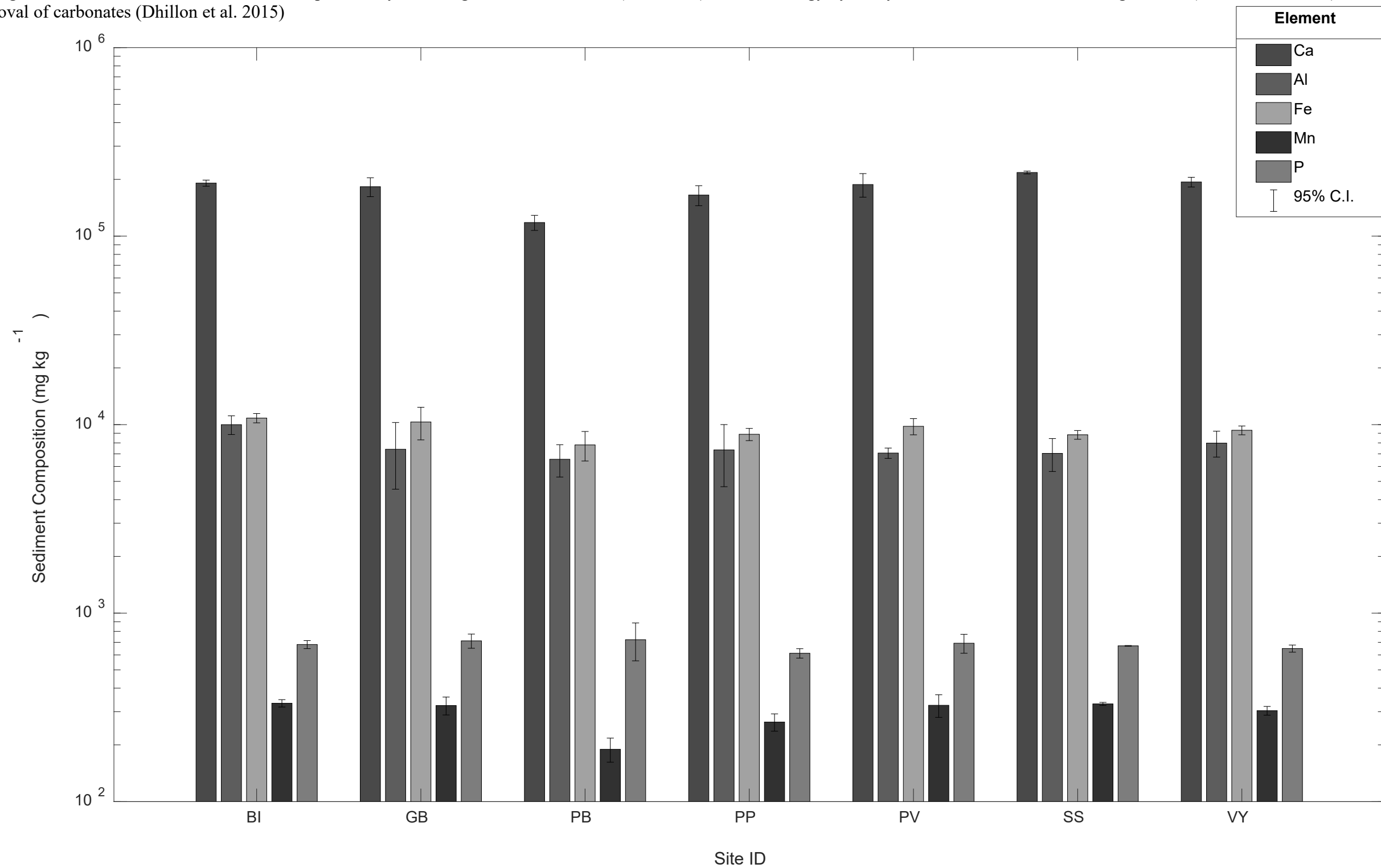


Figure 7. ^aAverage chemical compositions with their respective 95% confidence intervals as determined by acid-digestion of Utah Lake sediment do not vary greatly from site to site except for in a few notable instances. One, PB has significantly less Ca and Mn when compared to the main lake. Two, PP holds significantly less P on average when compared with GB, BI, and SS. The relative absence of Ca in PB concurs with ^bXRD and ^cHCl carbonate digestions which reveal the region to be depleted in calcite. Low P-content in PP could be due to low OM percentages within the sediment. This assumption seems especially reasonable when considering that PB has the highest average of P-content and OM content, while PP has the lowest of both.

Notes: P = Phosphorus; BSI = Batch sorption Isotherm; XRD = X-ray Diffraction; PB = Provo Bay; PV = Provo; VY = Vineyard; BI = Bird Island; GB = Goshen Bay; SS = Saratoga Springs; PP = Pelican Point; NH₄Cl = Ammonium Chloride extracted P, loosely adsorbed P; BD = Bicarbonate/Dithionite extracted P, redox-sensitive P bound to Fe and Mn compounds; NaOH = Sodium Hydroxide extracted P, P exchangeable against OH- ions and bound in organic matter; HCl = Hydrochloric-acid extracted P, carbonate bound P; Residual = Acid-Digestion extracted P, refractory organic P and hyper-stable mineral P; ^a= Sequential P-fractionation in sediments (Hupfer et al. 2009 and Gu et al. 2020)

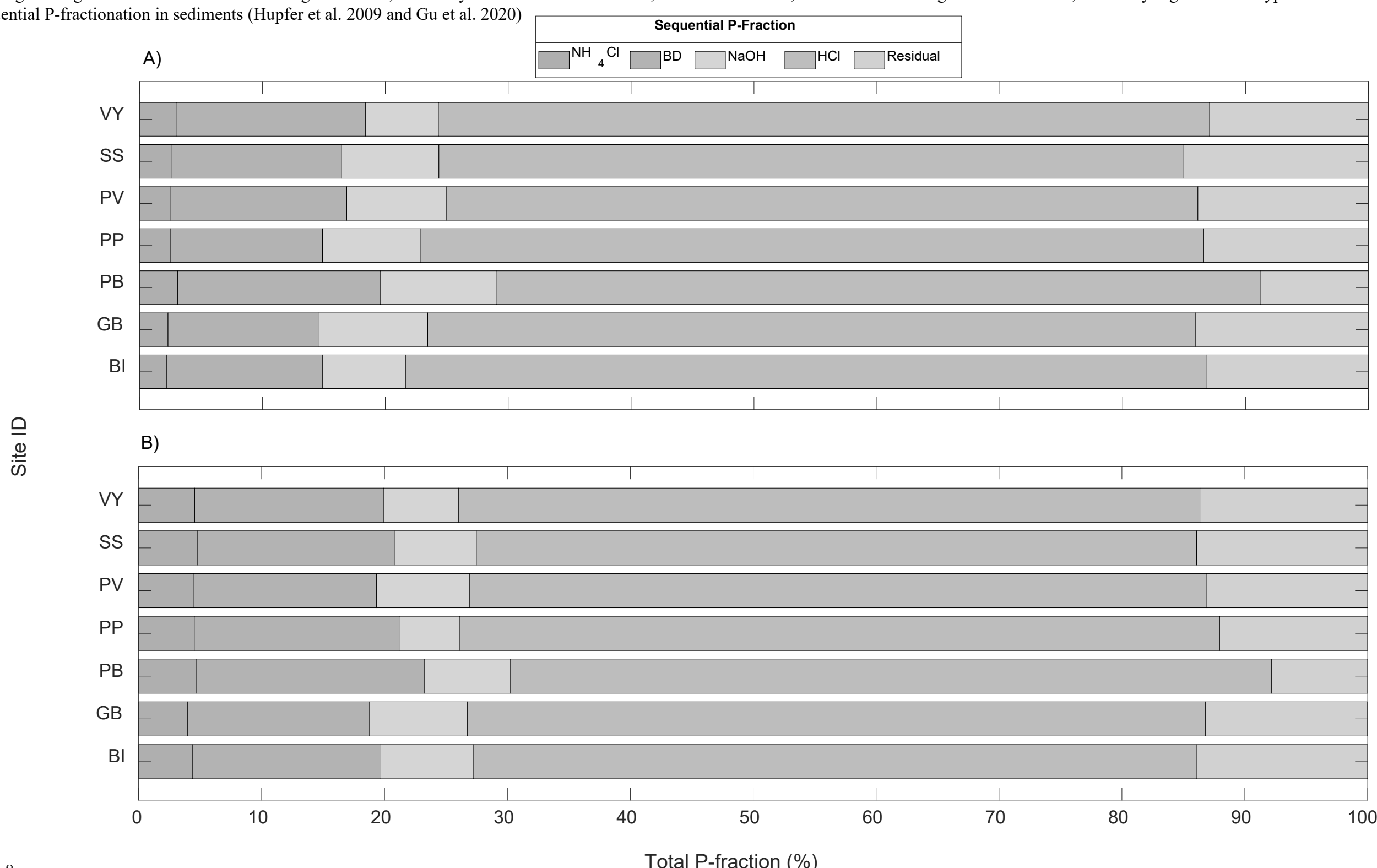


Figure 8.

A) P-fractions obtained through ^asequential extractions of Utah Lake sediment reveal that lakebed-P is primarily held by carbonate minerals (HCl), followed by redox-sensitive Fe and Mn compounds (BD), hyper-stable minerals and refractory OM (Residual), OM and OH- exchangeable compounds (NaOH), and loosely binding compounds most likely associated with clays and OM (NH₄Cl). Individual P-fraction amounts do not significantly vary from site-to-site, though we note that PB has the highest average of NaOH associated P.

B) Like unreacted sediments, individual P-fraction percentages do not significantly vary from site-to-site following sorption experimentation except for in a few instances, which are not particularly notable. However, hyper-stable minerals and refractory OM associated P is statistically lower in PB following experimentation when compared to every other sites. Sediment P-fraction percentages associated with loosely binding compounds significantly increase (2x) for every site following experimentation minus PB (avg. 4.45%-Total P).

Notes: DNA = Deoxyribonucleic-acid; PB = Provo Bay; PV = Provo; VY = Vineyard; BI = Bird Island; GB = Goshen Bay; SS = Saratoga Springs; PP = Pelican Point

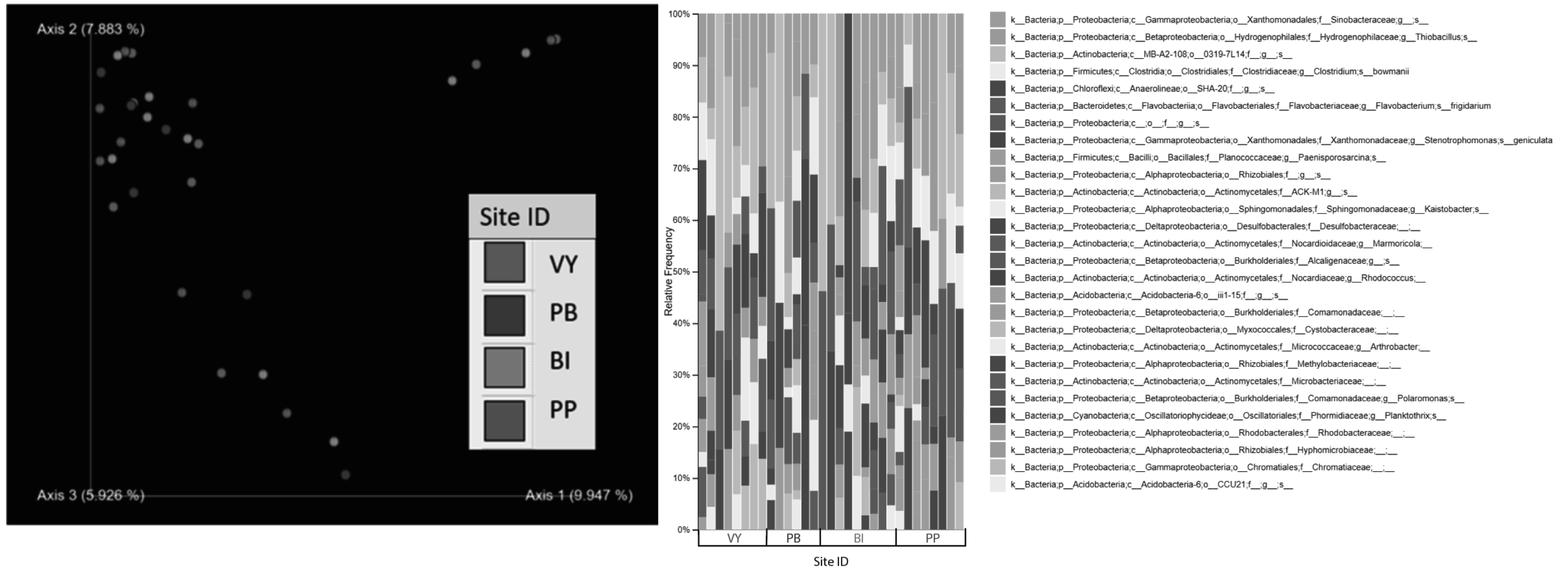


Figure 9. Sequences obtained from DNA extractions from lakebed sediments collected near VY, PB, BI, and PP reveal the microbiome of Utah Lake sediment to be taxonomically diverse. Filtering species by 1% abundance and 10% prevalence across all sequenced samples, the sediment microbiome is mostly composed of bacterial species in the proteobacteria, actinobacteria, chloroflexi, and firmicutes kingdoms. Despite the diversity of species housed within Utah Lake sediment, an emperor analysis of the sequences from each site suggests microbiome uniformity across the lake. DNA sequences were analyzed using Qiime2.

Notes: PB = Provo Bay; PV = Provo; VY = Vineyard; BI = Bird Island; GB = Goshen Bay; SS = Saratoga Springs; PP = Pelican Point; ^a = Waters collected on November 15, 2021, and analyzed using a Los Gatos Research cavity ring-down Liquid Water Isotope Analyzer; Surface = Waters in row collected from ~4 cm below water surface

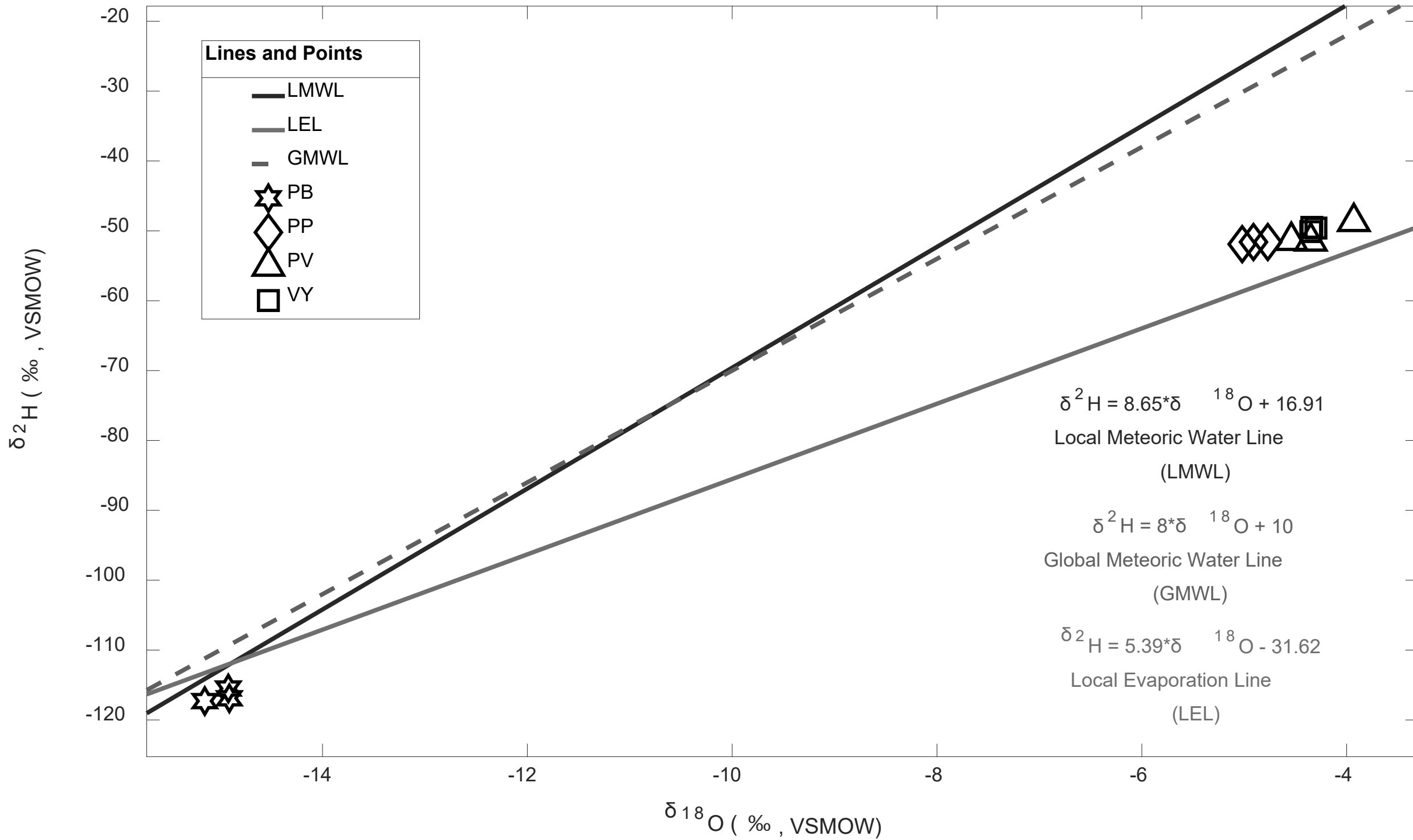


Figure 10. A plot of $\delta^2\text{H}$ vs. $\delta^{18}\text{O}$ values from surface waters of 4 locations across Utah Lake, including PB, PP, PV, and VY. ^aSurface waters were collected in November 2021 and are plotted against the global meteoric water line (GMWL, Craig 1961), a local meteoric water line (LMWL, Zanazzi et al. 2020), and a local evaporation line for Utah Lake (LEL, Zanazzi et al. 2020). Samples collected from the main body of Utah Lake (PV, VY, and PP) follow the LEL for Utah Lake, demonstrating significant enrichment from evaporation. Samples collected from PB plot at the intersection of the LMWL and LEL, showing PB to be an inlet point from which local meteoric waters enter the lake and subsequently evolve into enriched evaporated waters.

Notes: P = Phosphorus; PB = Provo Bay; PV = Provo; VY = Vineyard; BI = Bird Island; GB = Goshen Bay; SS = Saratoga Springs; PP = Pelican Point; Surface = Waters in row collected from ~4 cm below water surface; Middle = Waters in row collected from ~1-2 m below water surface; Bottom = Waters in row collected from ~3-4 m below water surface

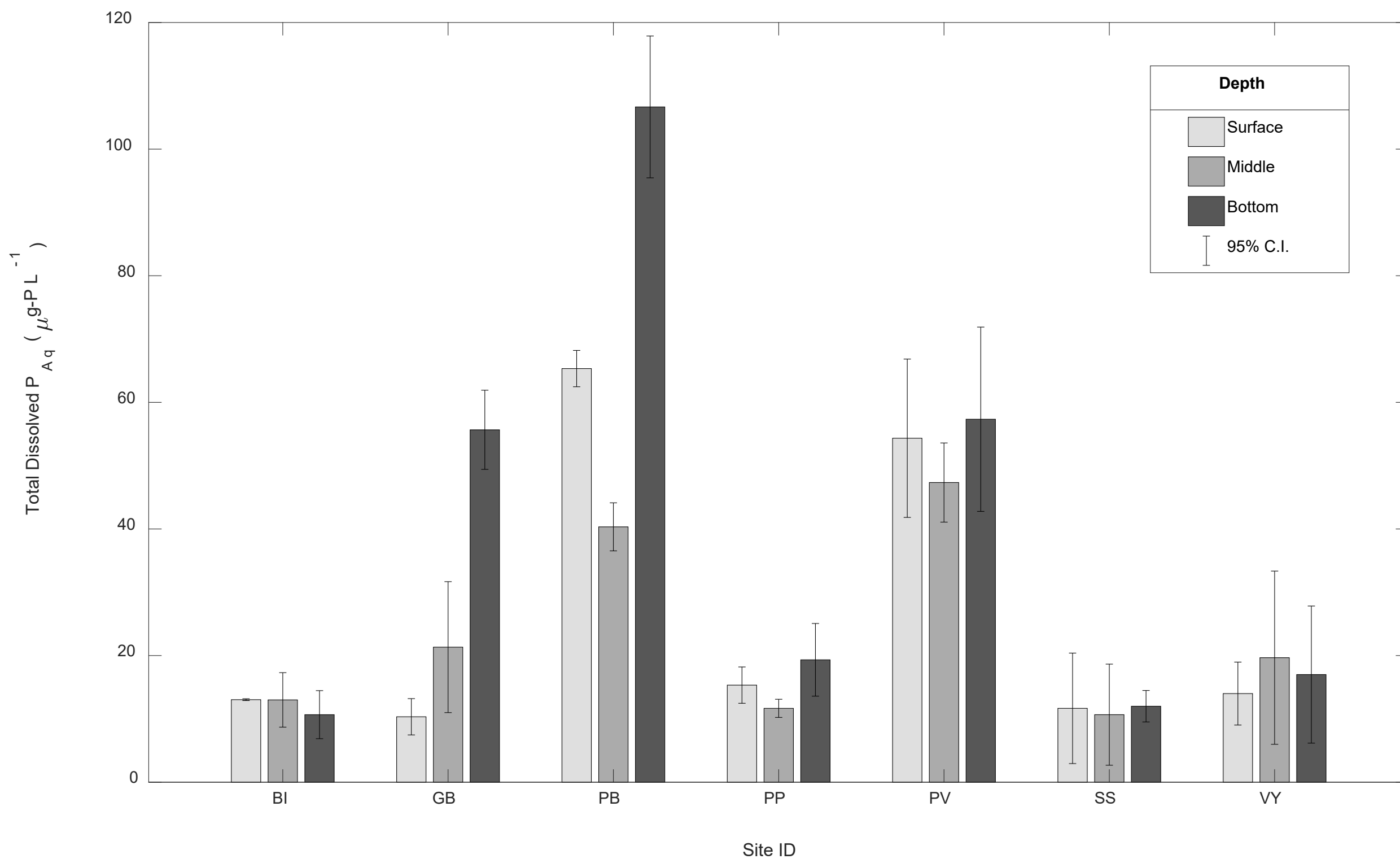


Figure 11. Average concentrations of P and other elements—with their respective 95% confidence intervals—found in the column water of an individual site do not significantly differ across depth in almost all instances, suggesting Utah Lake to be well mixed vertically (Zanazzi et al. 2020). A notable exception to this rule is PB, which appears to have poor vertical mixing (see Table 3). Furthermore, most sites share similar water-column P-concentrations, excluding PV and PB. PB and PV water-column P-concentrations are more like each other than to other sites in the lake with an average $61.9 \mu\text{g-P L}^{-1}$ compared $18.5 \mu\text{g-P L}^{-1}$ for the remainder of the lake. Elevated P-concentrations found in the column water of PB are probably tied to increased sediment P-concentrations and enhanced P-mobility in the area due to microbial activity.

Notes: DWQ = Data derived using the Utah Department of Water Quality (DWQ) Utah Lake Data Explorer (ULDE) for August 2021; OM = Organic matter; _{org} = Organic; PB = Provo Bay; PV = Provo; VY = Vineyard; BI = Bird Island; GB = Goshen Bay; SS = Saratoga Springs; PP = Pelican Point

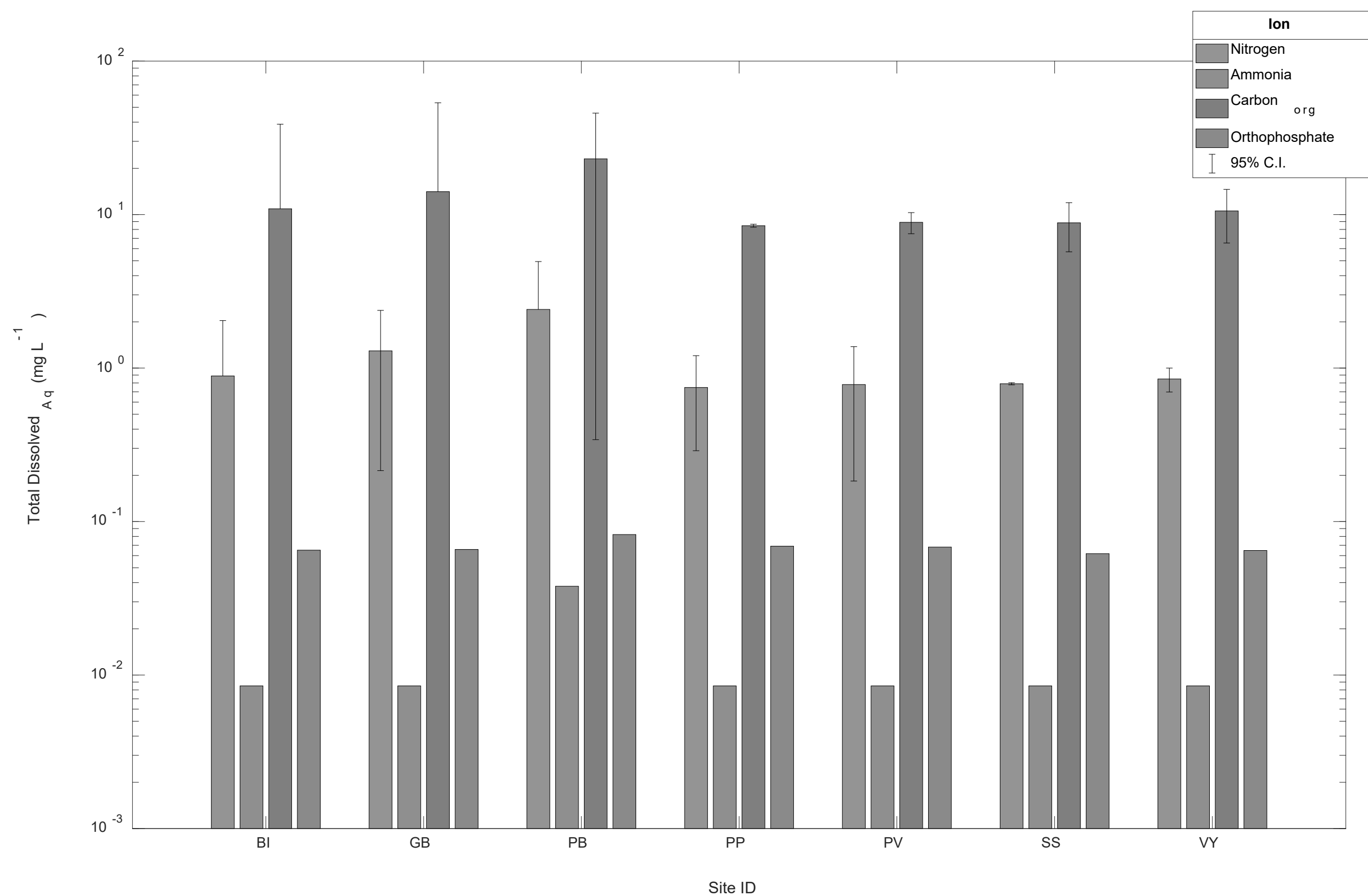


Figure 12. Average concentrations of ^{DWQ}nutrient species—with their respective 95% confidence intervals—found in the water column of Utah Lake appear to be horizontally consistent across the lake from site-to-site. However, the mean concentration of nitrogen, ammonia, carbon_{org}, orthophosphate, chlorophyll-a, and pheophytin-a is clearly greatest in PB (see Table 3). Elevated mean concentrations of nutrient species, chlorophyll-a, and pheophytin-a in PB suggest enhanced microbial activity in the area, which may be tied to increased OM percentages found in the sediment there.

Notes: BSI = Batch isotherm experiment; P = Phosphorus; Surface = Waters in row collected from ~4 cm below water surface; R^2 = R-squared; T = Temperature; I = Ionic strength; X = Sorption Origin or x-intercept of models, minimum aqueous P-concentration required for sediment P-sequestration; K_d = Linear partition coefficient; K_f = Freundlich partition coefficient; n = Freundlich correction factor; K_l = Langmuir relative binding strength; S_{max} = Sorption maximum of sorbent; $b_{d,f,l}$ = y-intercept of Linear, Freundlich, or Langmuir models

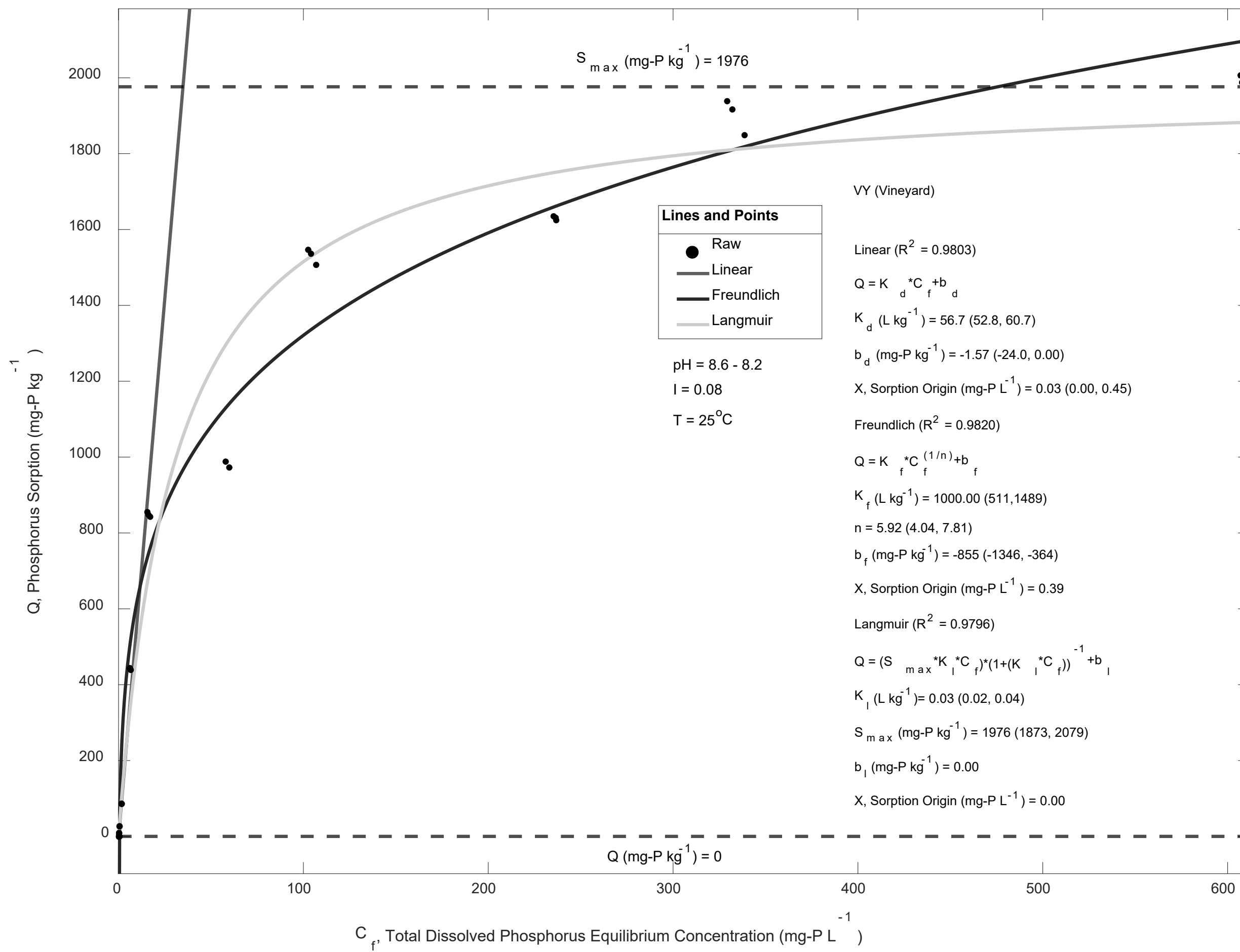


Figure 13. A plot of Q (P-sorption; mg-P kg^{-1}) vs. C_f (Total Dissolved Equilibrium P; mg-P L^{-1}) obtained from a BSI experiment which reacted surface lakebed sediments collected from Vineyard (VY) and surface waters collected from Saratoga Springs (SS) spiked to various P-concentrations (0, 0.5, 1, 3, 10, 50, 76, 100, 152, 250, 381, 500, and 762 mg-P L^{-1}) for 24 hours at a 1:10 sediment-to-water ratio, pH 8.5, and 25°C. Waters prepped for batch experimentation were buffered to a predetermined pH using 50 mM of a zwitterionic buffer (CHES or HEPPS) to maintain constant pH throughout the 24-hour period, without inhibiting sorption. Raw trends in Q vs. C_f were fitted Linear, Freundlich, and Langmuir models in MATLAB 2022b using least squares regression lines. R^2 values for fitted models across all BSI experiments performed were greater than 0.73, with a mean value of 0.98.

Notes: PB = Provo Bay; PV = Provo; VY = Vineyard; BI = Bird Island; GB = Goshen Bay; SS = Saratoga Springs; PP = Pelican Point; TDP = Total dissolved phosphorus; P = Phosphorus; X = Sorption Origin or x-intercept of models, minimum aqueous P-concentration required for sediment P-sequestration; $b_{d,f,l}$ = y-intercept of Linear, Freundlich, or Langmuir models

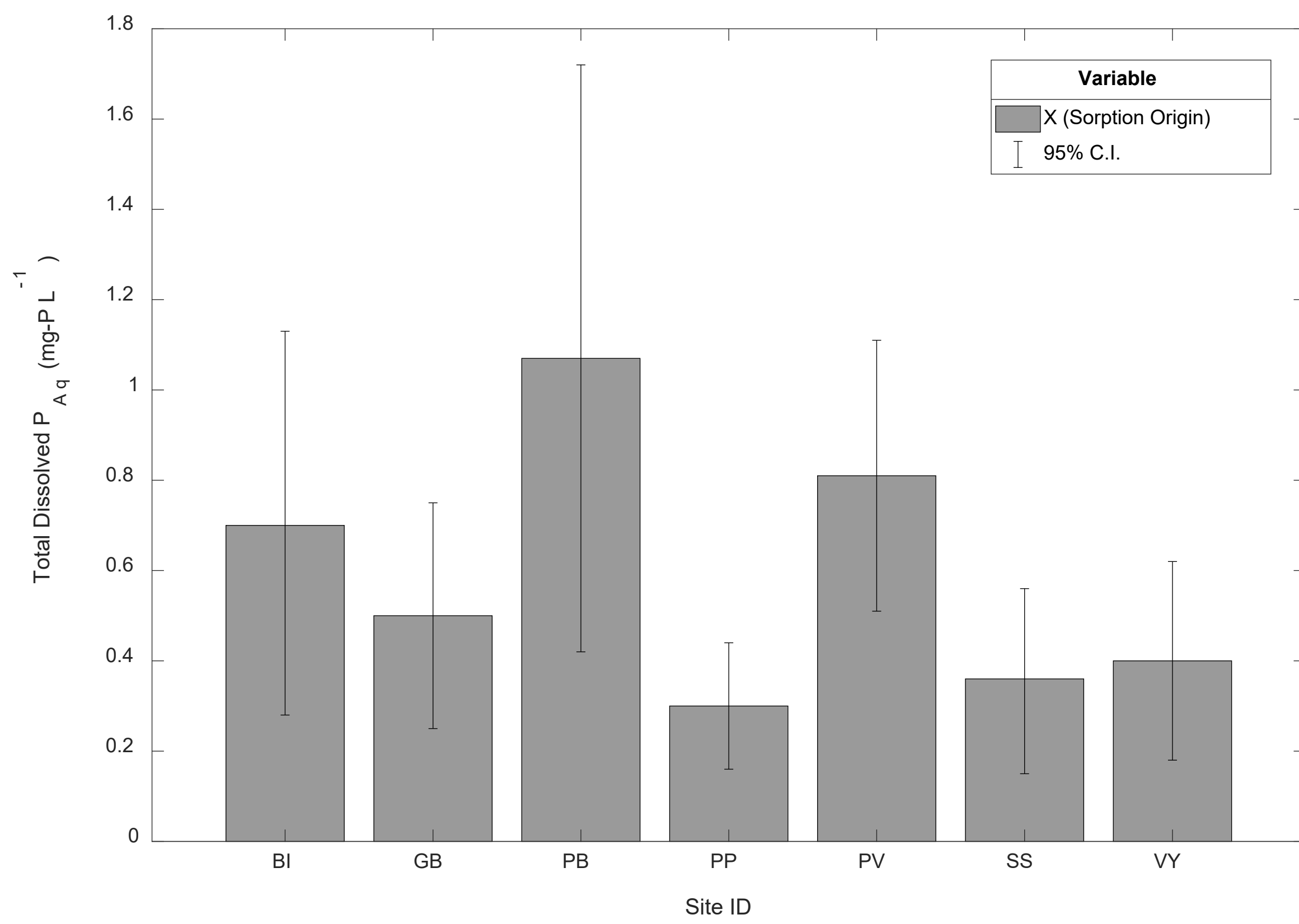


Figure 14. X, or sorption origin, represents the x-intercept of Linear, Freundlich, and Langmuir models. It is the minimum concentration of TDP required in the water column above a given lakebed sediment before P-sorption behavior can be observed. Aqueous TDP-concentrations below X tend to show desorption behavior instead of sorption behavior for a given sediment. X values derived from y-intercepts ($b_{d,f,l}$) for each site appear to be constant across pH (see Figure 19), thus the X values in this figure—with their respective 95% confidence intervals—represent the average X from all models for a given location. Average X values do not significantly differ from site-to-site except between PV (0.81 mg-P L⁻¹) and PP (0.30 mg-P L⁻¹). PP has the lowest average X of any site as well as the lowest average sediment P-content (612 mg-P kg⁻¹). Lower concentrations of sediment P in PP may assist P-sorption at lower concentrations of aqueous-P in the area by decreasing P-diffusion from the sediment.

Notes: PB = Provo Bay; PV = Provo; VY = Vineyard; BI = Bird Island; GB = Goshen Bay; SS = Saratoga Springs; PP = Pelican Point; K_d = Linear partition coefficient; K_f = Freundlich partition coefficient; K_l = Langmuir relative binding strength

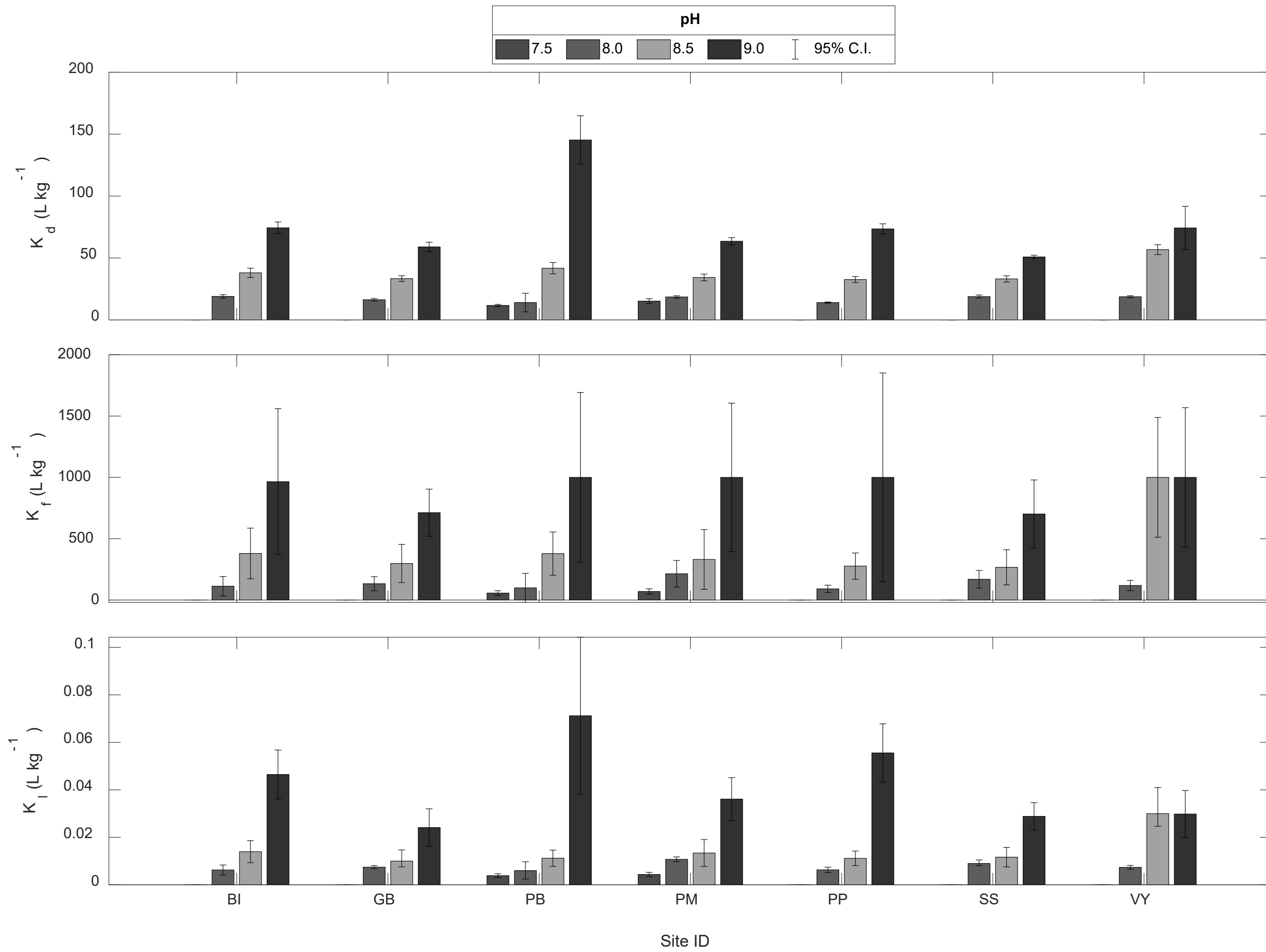


Figure 15. K_d has relatively tight 95% confidence intervals, suggesting sorption behavior to be more site-specific. Therefore, when using K_d in models, it is advisable to use site-specific K_d values for most cases. However, groups may be formed to simplify the lake when the 95% confidence intervals of K_d overlap between sites (see Table 4). K_f values differ from K_d values in that they are statistically more uniform across sites, covering a wider range of possible partitioning when compared to K_d . Freundlich models cover a broader range of concentrations in a sorption system for a given pH, redox, and temperature. Consequently, it may not be so that odd K_f appears more generalized for sediments of similar composition, like in Utah Lake. However, at pH 8.5 we do observe that VY exhibits significantly increased sorption when compared directly with GB, SS, and PP. K_l seems to be a mix of K_f and K_d in terms of variation across sites. At pH 7.5, PB and PV have similar sorption trends. At pH 8.0, all sites exhibit similar sorption partitioning to PB. At pH 8.5, all sites exhibit similar sorption behavior to each other except for VY, which shows significantly increased sorption to all other sites. At pH 9.0, all sites exhibit similar sorption partitioning to PV. Overall, it is advisable to use $K_{d,f,l}$ partition values in accordance with the pH from which they were obtained.

Notes: C.I. = Confidence interval; PB = Provo Bay; PV = Provo; VY = Vineyard; BI = Bird Island; GB = Goshen Bay; SS = Saratoga Springs; PP = Pelican Point; K_d = Linear partition coefficient; K_f = Freundlich partition coefficient; K_l = Langmuir relative binding strength

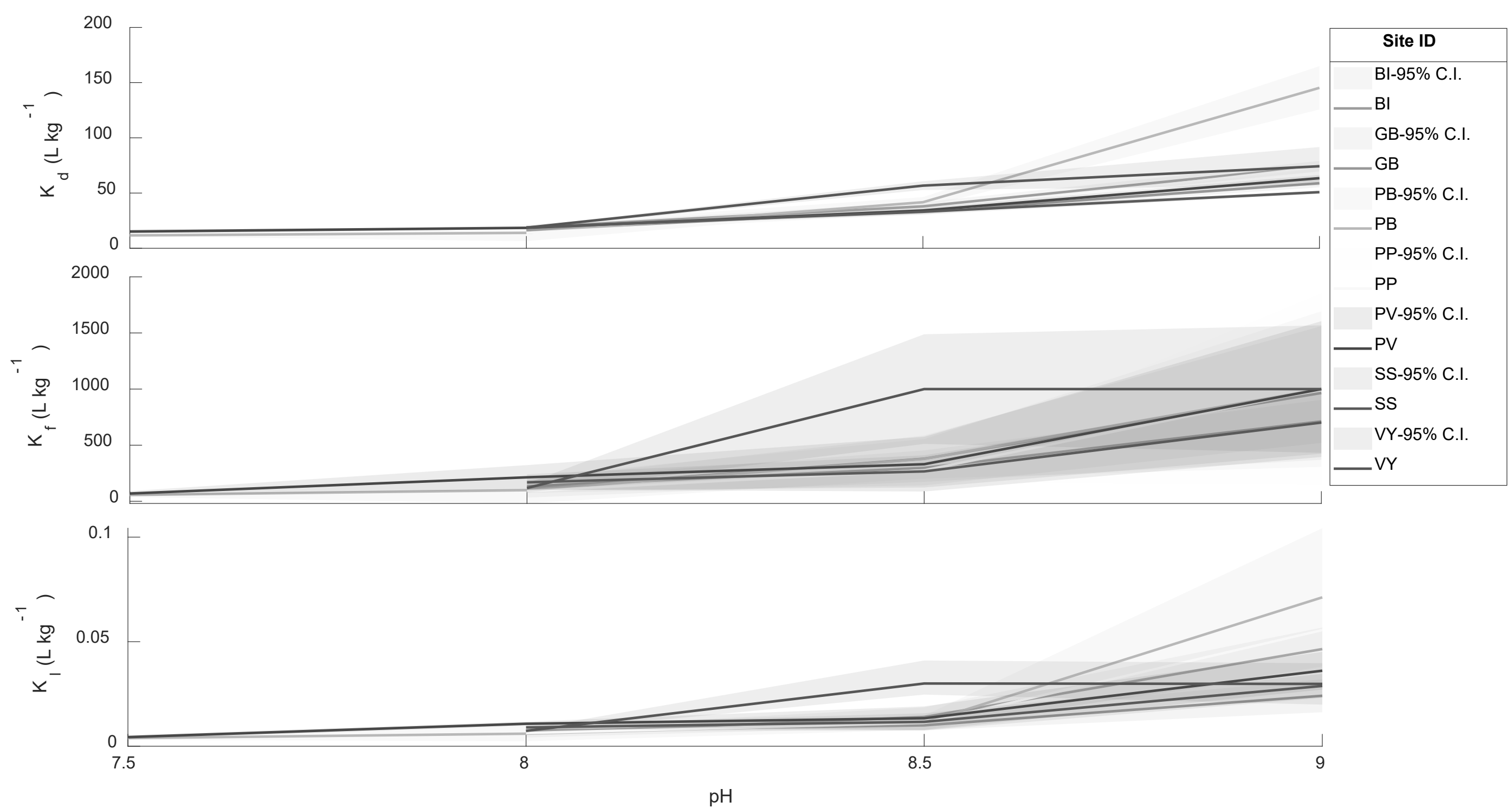


Figure 16. K_d , K_f , and K_l coefficients from Linear, Freundlich, and Langmuir models, respectively, all significantly increase from pH 8 to 9 for all locations taken from Utah Lake.

Notes: P = Phosphorus; PB = Provo Bay; PV = Provo; VY = Vineyard; BI = Bird Island; GB = Goshen Bay; SS = Saratoga Springs; PP = Pelican Point; n = Freundlich correction factor; S_{\max} = Sorption maximum of sorbent

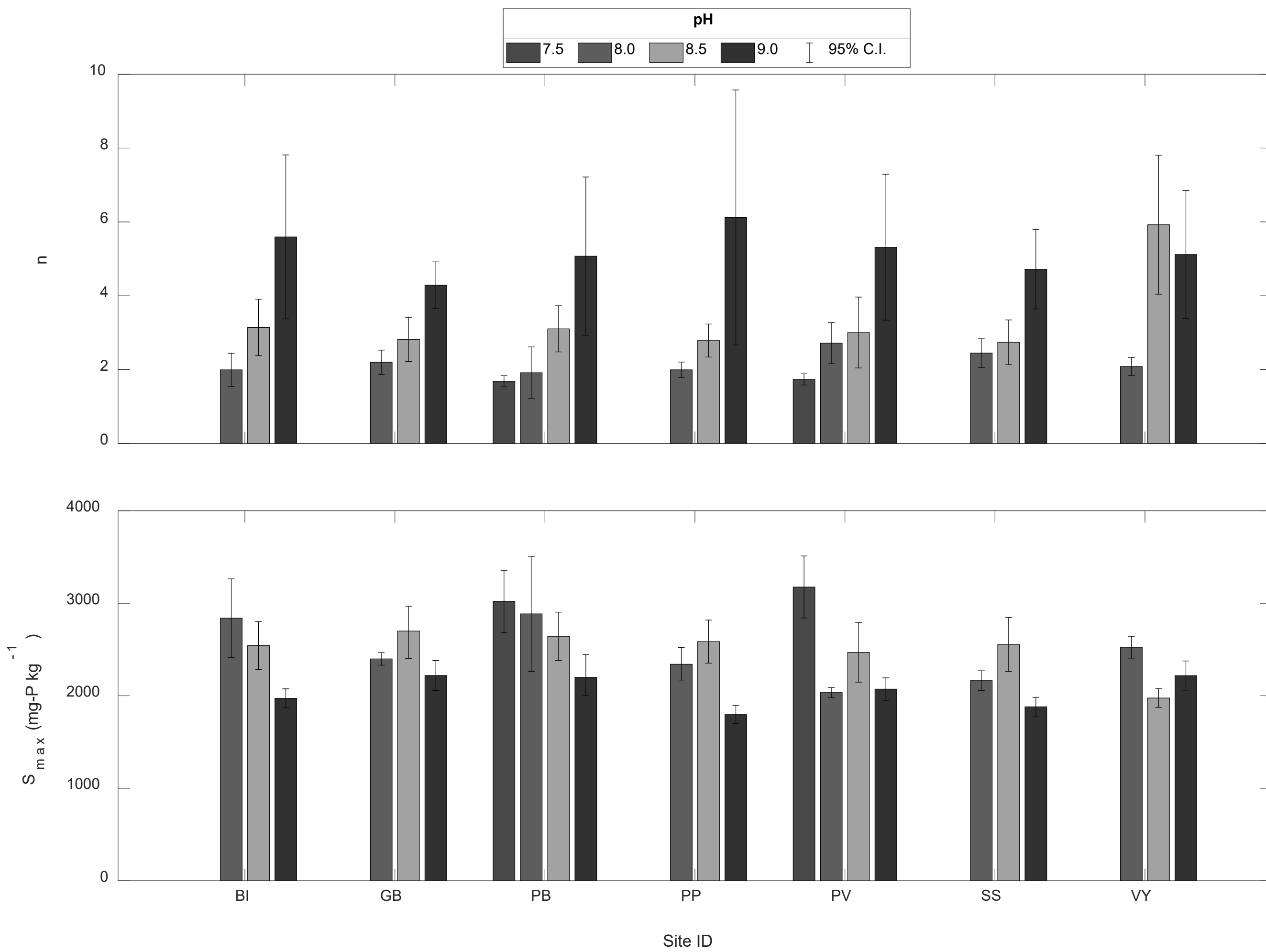


Figure 17. Freundlich values of n—with their respective 95% confidence intervals—do not statistically vary from site-to-site for a given pH, excluding VY which has a significantly higher n (5.92) at pH 8.5 (see Table 4). Langmuir values of S_{\max} —with their respective 95% confidence intervals—appear to be consistent from site-to-site for a given pH in most instances. There are three exceptions to this rule. First, at pH 8 S_{\max} for PV is significantly lower than every other site minus SS, together they form an average S_{\max} of 2099 mg-P kg⁻¹ compared to 2598 mg-P kg⁻¹ for the rest of the lake. Second, at pH 8.5 S_{\max} for VY is significantly lower than any other site at 1976 mg-P kg⁻¹ compared to an average 2580 mg-P kg⁻¹ for the other sites. Third, at pH 9 S_{\max} for SS is significantly lower than PB, VY, and GB while PP is significantly lower than PB, PV, VY, and GB, together PP and SS have an average S_{\max} of 1839 mg-P kg⁻¹ and the other parts of the lake average 2141 mg-P kg⁻¹.

Notes: C.I. = Confidence interval; P = Phosphorus; PB = Provo Bay; PV = Provo; VY = Vineyard; BI = Bird Island; GB = Goshen Bay; SS = Saratoga Springs; PP = Pelican Point; n = Freundlich correction factor; S_{max} = Sorption maximum of sorbent

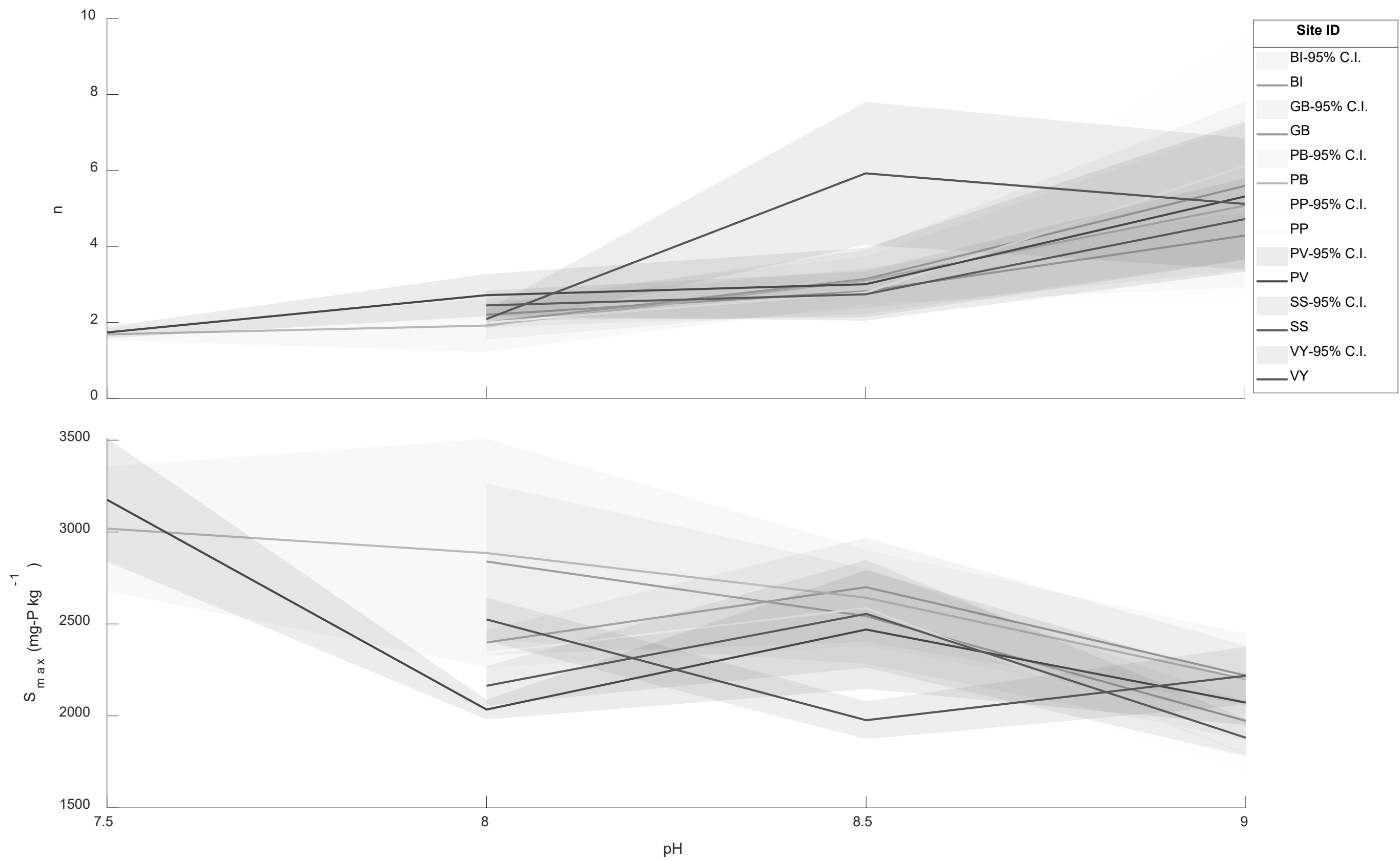


Figure 18. From pH 8 to 9, n values significantly increase for each individual site. S_{max} values observed at pH 9 for a given location are significantly lower than S_{max} values observed at pH's 7.5, 8, or 8.5 in at least one circumstance for each site. Basically, S_{max} decreases for each site as pH increases.

Notes: P = Phosphorus; PB = Provo Bay; PV = Provo; VY = Vineyard; BI = Bird Island; GB = Goshen Bay; SS = Saratoga Springs; PP = Pelican Point; $b_{d,f,l}$ = y-intercept of Linear, Freundlich, or Langmuir models

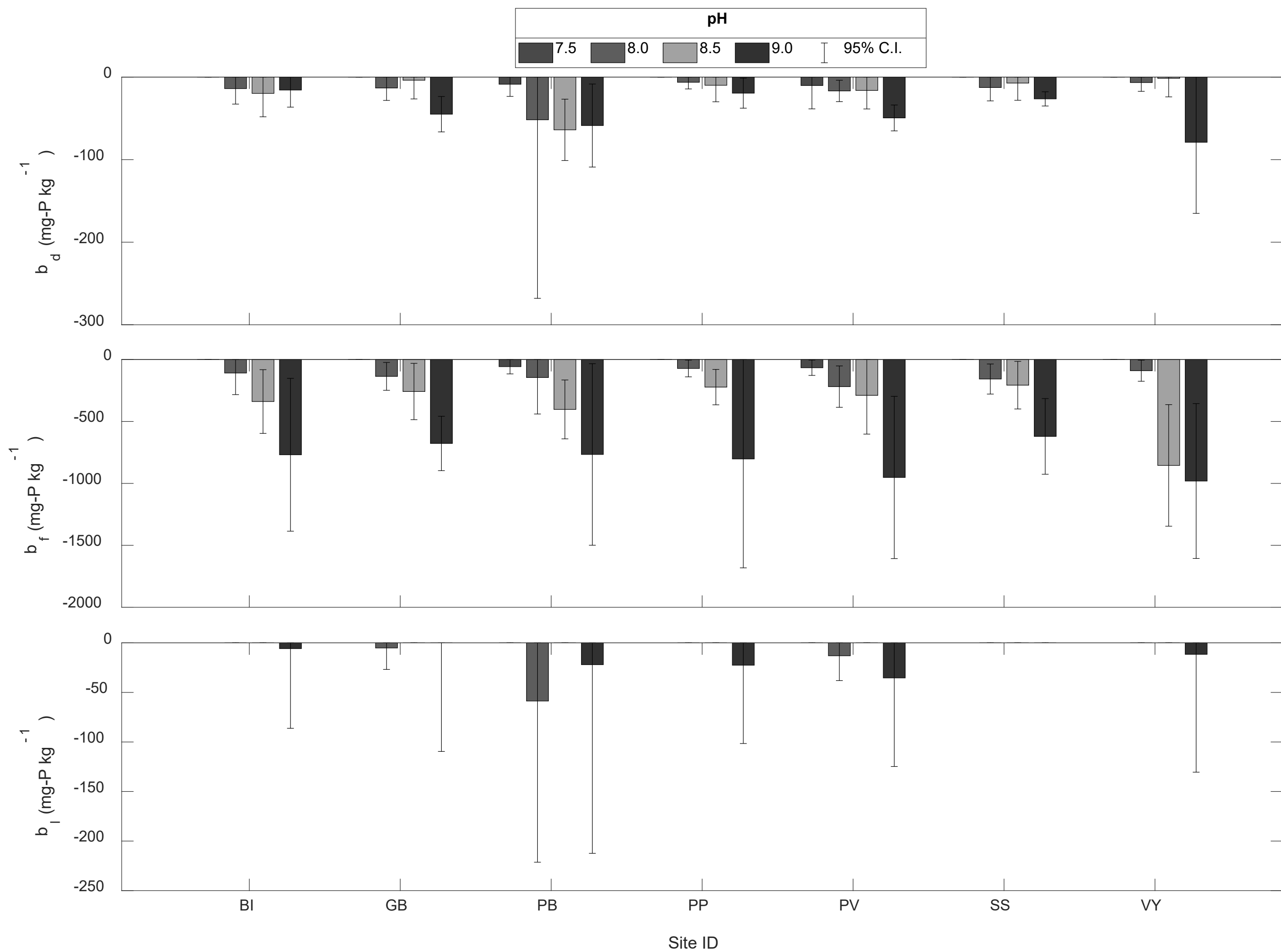


Figure 19. The application of a y-intercept ($b_{d,f,l}$) into Linear (b_d), Freundlich (b_f), and Langmuir (b_l) models only has precedence if the soil or sediment considered has been previously exposed to the contaminant of study (Chappell et al. 2020). Trends show values of b_d , b_f , and b_l —with their respective 95% confidence intervals—do not vary with site for a given pH. There is only one exception, which exists for b_d at pH 8.5 between PB with VY and GB, however at 97.2% confidence the intervals of these locations do overlap.

Notes: C.I. = Confidence interval; P = Phosphorus; PB = Provo Bay; PV = Provo; VY = Vineyard; BI = Bird Island; GB = Goshen Bay; SS = Saratoga Springs; PP = Pelican Point; $b_{d,f,l}$ = y-intercept of Linear, Freundlich, or Langmuir models

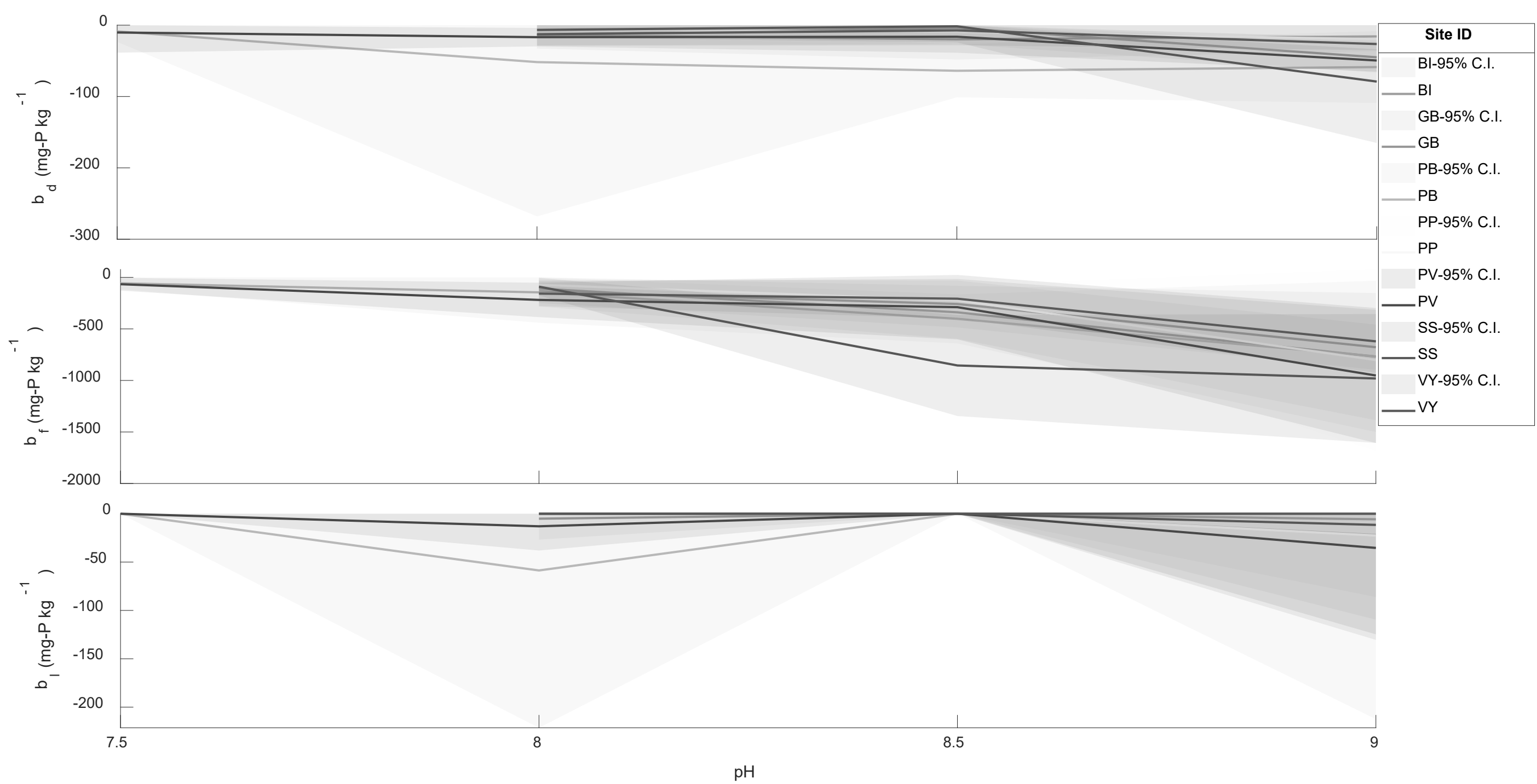


Figure 20. Linear values of b_d do not statistically vary across pH for a given location and exceptions to this are negligible. Langmuir values of b_l do not significantly vary across pH for a given site. Freundlich values of b_f across pH do not significantly vary from b_f values observed at pH 8.5 for a given site, excluding for PB at pH 7.5 and for VY at pH 8.

Notes: BSI = Batch sorption isotherm; UV = Ultra-violet; PB = Provo Bay; PV = Provo; VY = Vineyard; BI = Bird Island; GB = Goshen Bay; SS = Saratoga Springs; PP = Pelican Point; K_d = Linear partition coefficient; K_f = Freundlich partition coefficient; K_l = Langmuir relative binding strength

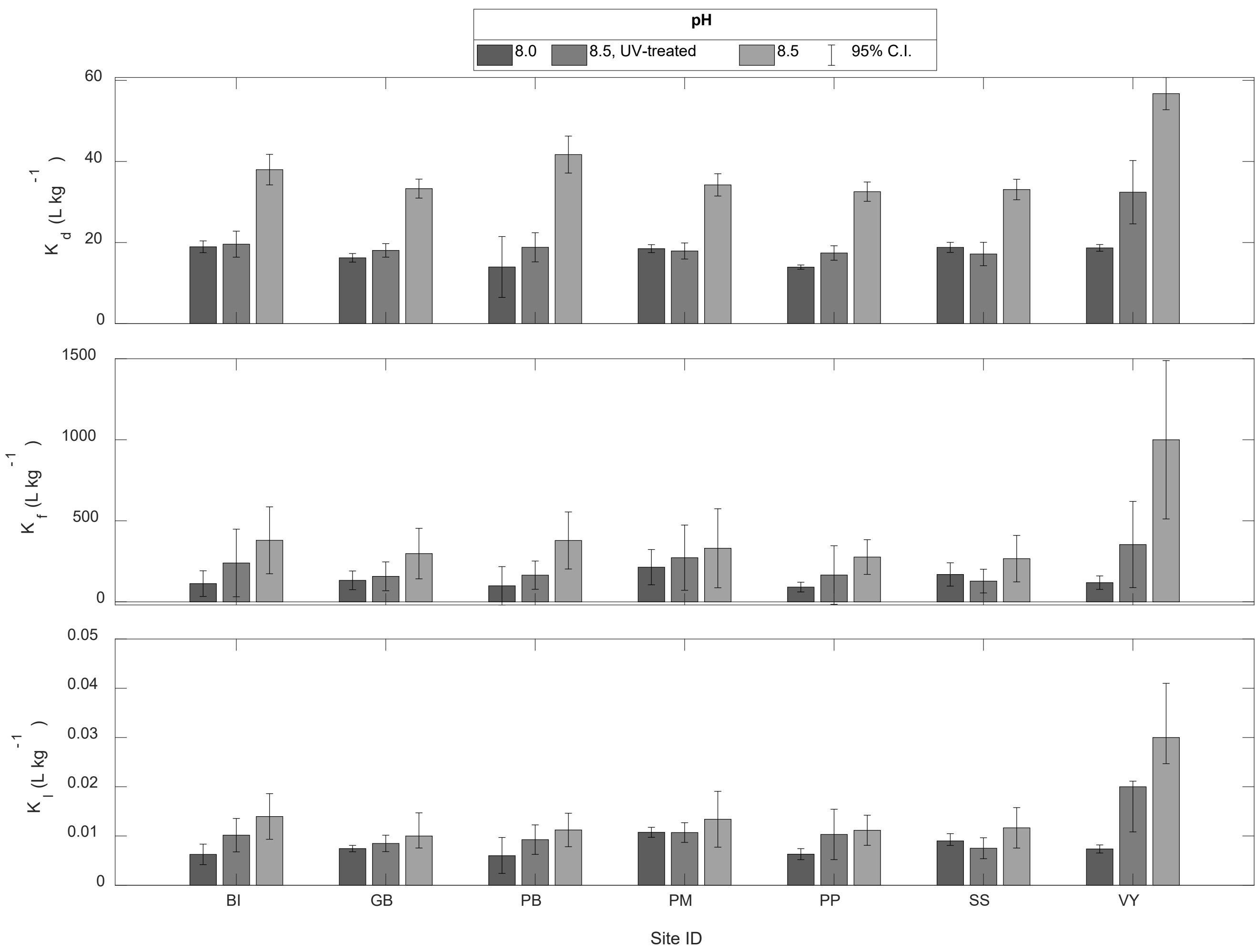


Figure 21. Average values of $K_{d,f,l}$ —with their respective 95% confidence intervals—sorted by site. Values of $K_{d,f,l}$ were calculated from three sorption experiments performed at pH 8.0 and 8.5. One of these sorption experiments was performed at pH 8.5 using UV-treated sediments. UV-treatment of Utah Lake sediments significantly decreases K_d for every site. Despite this, K_f and K_l do not significantly decrease for a given location following UV-treatment (excluding K_l for VY). Comparing across sites, all UV-treated sediments exhibit like $K_{d,f,l}$ values except for VY. For UV-treated sediments, K_d for VY averages 32.4 L kg^{-1} while the rest of the lake averages 18.2 L kg^{-1} . For UV-treated sediments, K_f does not differ across sites, including VY, creating an average of 199 L kg^{-1} . For UV-treated sediments, K_l for VY averages 0.016 L kg^{-1} while the rest of the lake averages 0.009 L kg^{-1} .

Given these trends, UV-treatment of Utah Lake sediments tends to homogenize sediment compositions or characteristics which contribute to P-sorption between sites.

Notes: P = Phosphorus; BSI = Batch sorption isotherm; UV = Ultra-violet; PB = Provo Bay; PV = Provo; VY = Vineyard; BI = Bird Island; GB = Goshen Bay; SS = Saratoga Springs; PP = Pelican Point; n = Freundlich correction factor; S_{\max} = Langmuir sorption maximum of sorbent

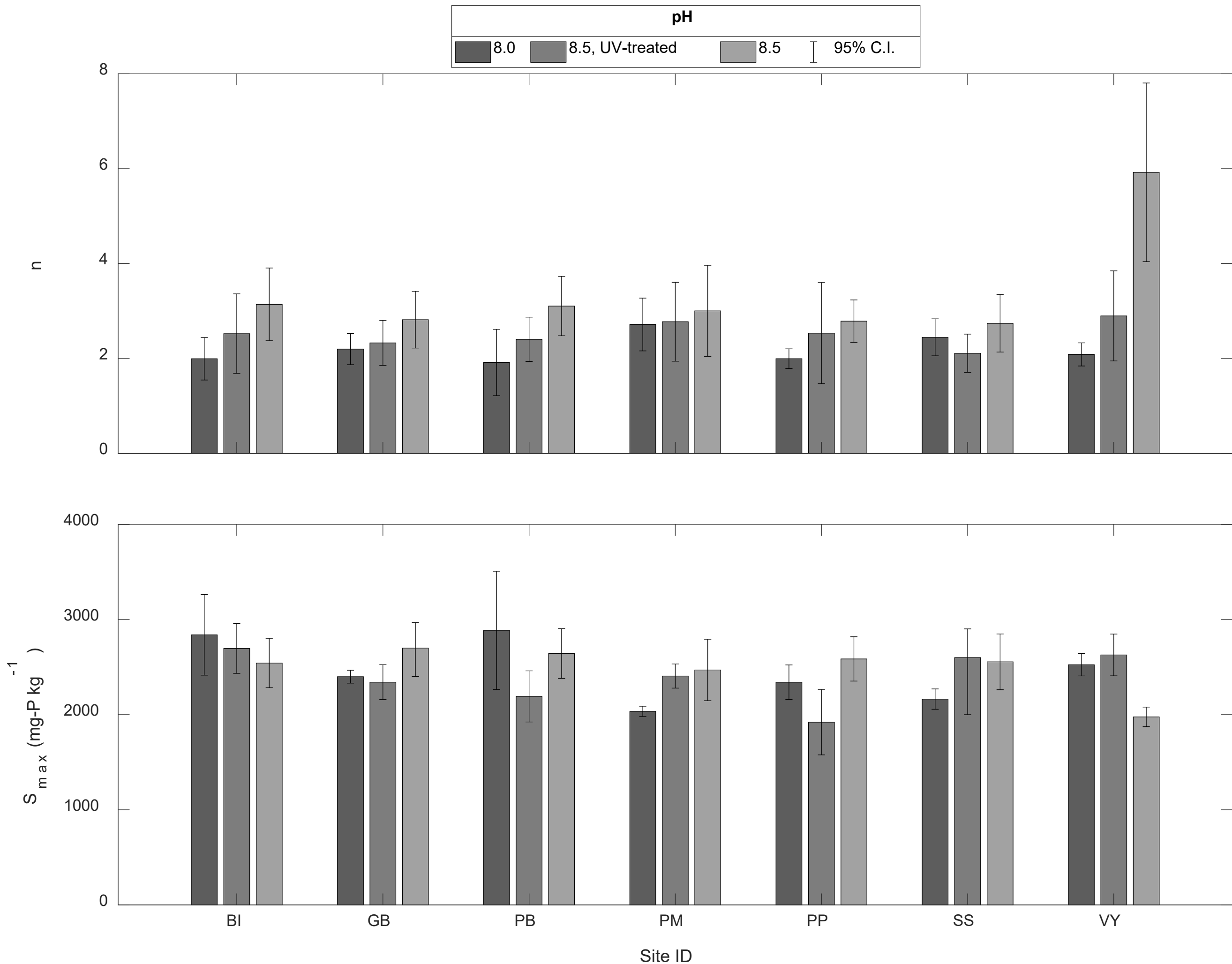


Figure 22. Average values of n and S_{\max} —with their respective 95% confidence intervals—sorted by site. Values of n and S_{\max} were calculated from three sorption experiments performed at pH 8.0 and 8.5. One of these sorption experiments was performed at pH 8.5 using UV-treated sediments. Sorption experiments performed at pH 8.5 using untreated and UV-treated sediments from Utah Lake do not significantly vary in terms n or S_{\max} for a particular location with few exceptions. For VY, UV-treated sediments yielded a significant decrease in n (^{UV}2.90 vs. ^{pH 8.5}5.92) and an increase in S_{\max} (^{UV}2628 vs. ^{pH 8.5}1976 mg-P kg⁻¹). For PP, UV-treated sediments yielded a significant decrease in S_{\max} (1921^{UV} vs. 2586 mg-P kg⁻¹). Values of n do not significantly differ from site-to-site following UV-treatment. Meanwhile, S_{\max} does not significantly differ from site-to-site following UV-treatment, except PP (1921 mg-P kg⁻¹) is less than PV, VY, and BI (avg. 2577 mg-P kg⁻¹). Given these trends, UV-treatment of Utah Lake sediments tends to homogenize sediment compositions or characteristics which contribute to P-sorption between sites in most cases.

Notes: SF = Stirred-flow; P = Phosphorus; S = the amount of P-sorbed to sediment inside SF reactor; dS/dt = P-sorption over time; C = Effluent concentration of aqueous-P from SF reactor; C_0 = Influent concentrations of aqueous-P into SF reactor; t = time in min; PB = Provo Bay; PV = Provo

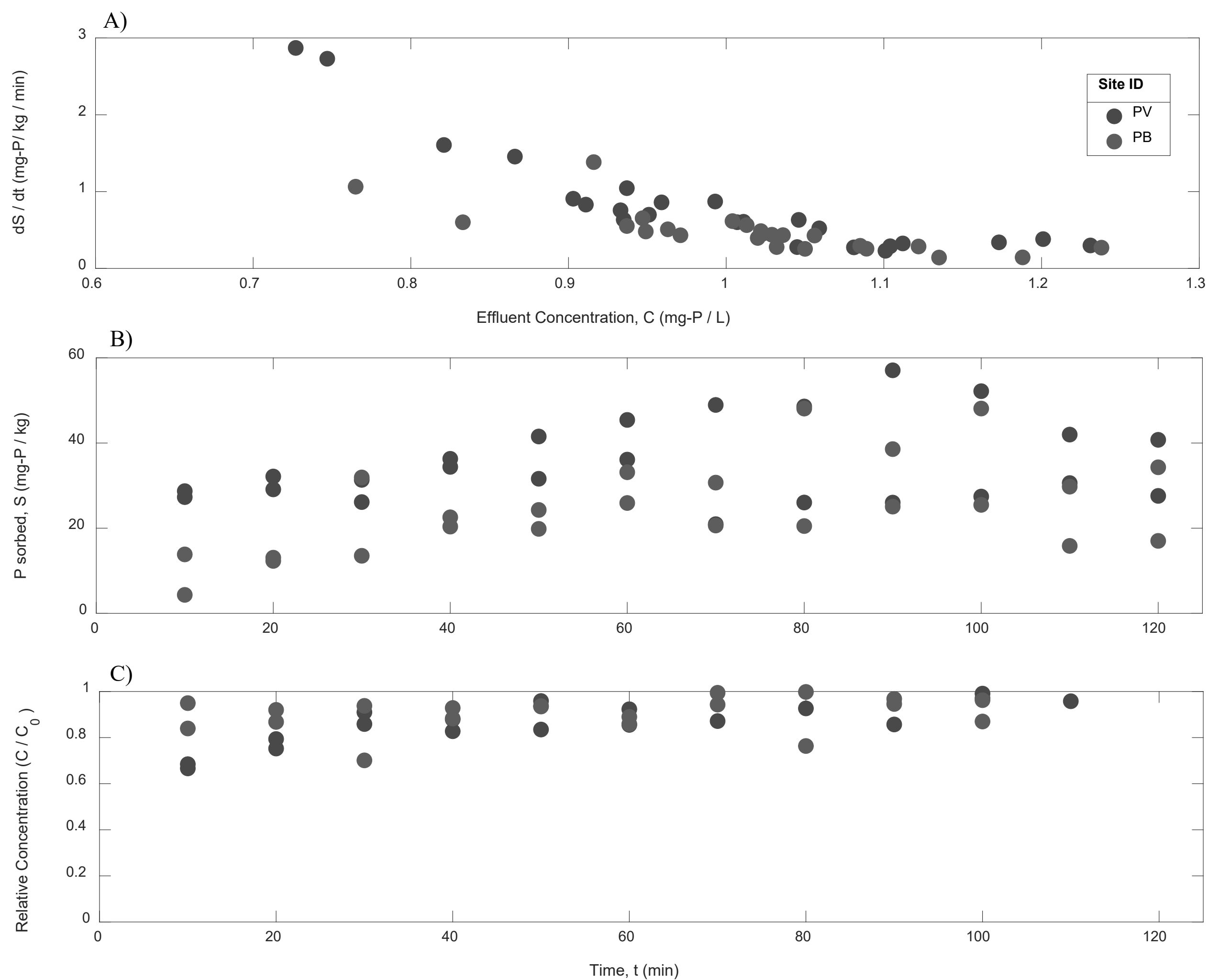


Figure 23. Changes in output solution and P-sorption from SF experiments using PV and PB sediment (~0.32 g).

A) Changes in the rate of sorption (dS/dt) indicate that as effluent P-concentrations (C) trend toward influent P-concentrations (C_0) the rate of P-sorption slows for PV and PB, indicating saturation of P-binding sites.

B) P-sorption (S) increases with time for both locations, reaching peak sorption between 80 - 100 min, average $37.8 \text{ mg-P kg}^{-1}$ for PV and $30.3 \text{ mg-P kg}^{-1}$ for PB. After reaching peak sorption, P seems to exchange evenly between sediment and solution phases.

C) Effluent P-concentrations (C) reach influent concentrations (C_0) at about 80 - 100 min and with comparable paces between PV and PB.

Notes: SF = Stirred-flow; P = Phosphorus; S = the amount of P-sorbed to sediment inside SF reactor; dS/dt = P-sorption over time; C = Effluent concentration of aqueous-P from SF reactor; C_0 = Influent concentrations of aqueous-P into SF reactor; t = time in min; ρ = Bulk density; θ = Volumetric Water Content; k_f = Forward retention rate; k_b = Backward retention rate; b = order of retention reaction; R^2 = R-squared; PB = Provo Bay; PV = Provo

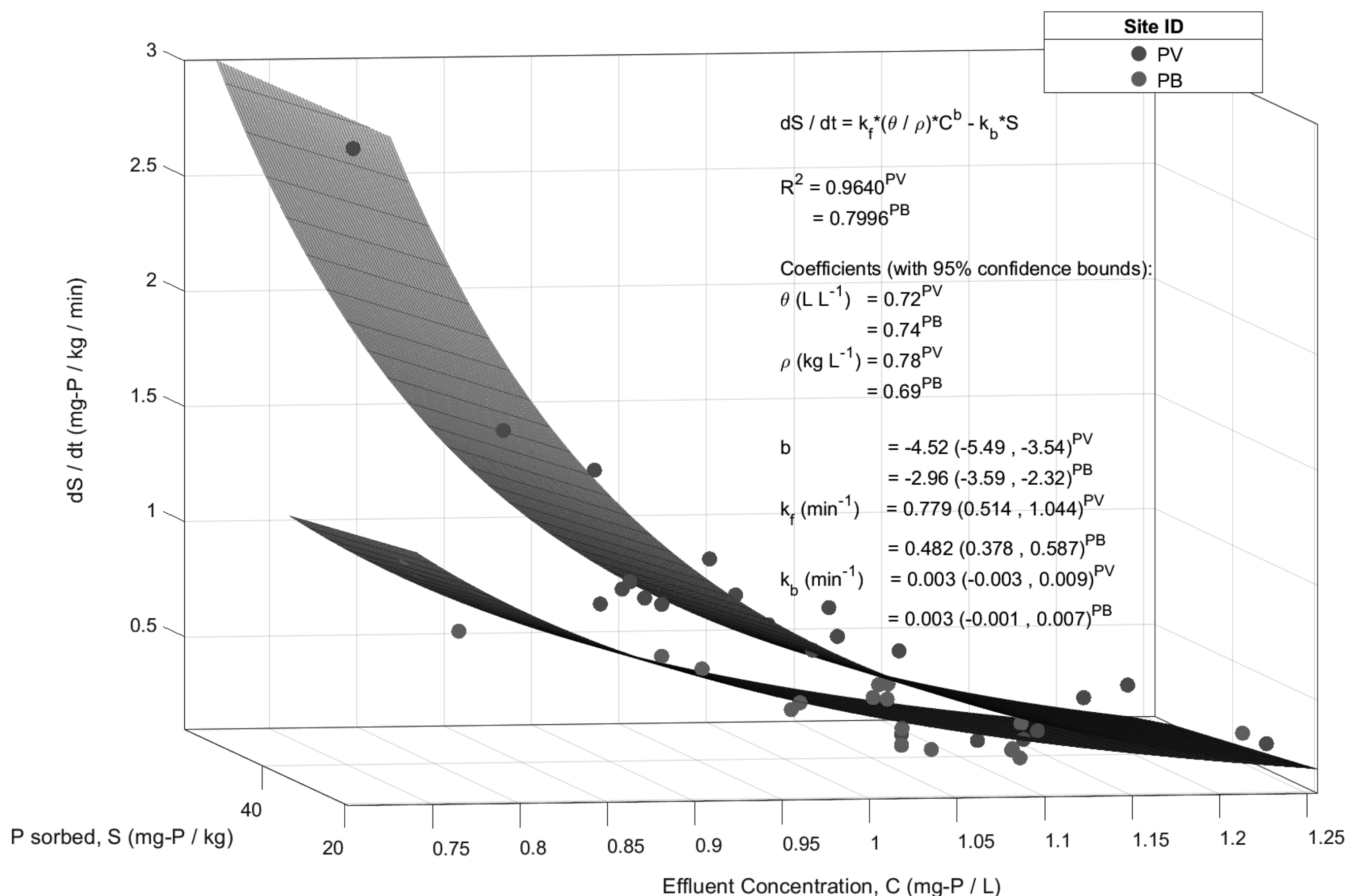


Figure 24. Nonlinear retention behavior of SF experiments showcasing nonlinear kinetics of P-sorption for PV and PB sediments. Raw trends in dS/dt (P-sorption over time) vs. C, S were fitted to a single-reaction nonlinear kinetic model (Selim 1992) in MATLAB 2022b using a least squares regression. Parameter b is dimensionless and represents the order of the retention reaction, illustrating the heterogeneity of sorption processes (Selim 2014). For PV ($b = -4.52$), b seems to suggest more heterogeneity of sorption processes than PB ($b = -2.96$).

Forward ($k_f^{PV} 0.78 \text{ min}^{-1}$ vs. $k_f^{PB} 0.48 \text{ min}^{-1}$) and backward ($k_b^{PV} 0.003 \text{ min}^{-1}$ vs. $k_b^{PB} 0.003 \text{ min}^{-1}$) retention rates suggest that PV experiences faster initial P-retention than PB, however as time progresses the retention maintained at both sites is comparable.